Aus dem Institut für Pharmakologie und Toxikologie
Direktor: Herr Prof. Dr. med. Ali El-Armouche

In vivo FLIM-FRET as a novel technique to assess cAMP and cGMP in the intact zebrafish heart

Dissertationsschrift

zur Erlangung des akademischen Grades

Doktor der Medizin

Doctor medicinae (Dr. med.)

vorgelegt

der Medizinischen Fakultät Carl Gustav Carus

der Technischen Universität Dresden

von

Julia Annika Janßen
aus München

Dresden 2017

1. Gutachter: _____

2. Gutachter: _____

Tag der mündlichen Prüfung (Verteidigungstermin):

gez.: _____
(Vorsitzender der Promotionskommission)

1 Summary of contents

1. SUMMARY OF CONTENTS I

2. LIST OF ABBREVIATIONS III

3. LIST OF FIGURES IV

4. LIST OF TABLES V

5. INTRODUCTION 1

5.1 The zebrafish as a model 1

5.2 cAMP in cardiac physiology 2

5.3 cGMP in cardiac physiology 2

5.4 cAMP/cGMP compartmentalization 3

5.4.1 The role of specific membrane structures 4

5.4.2 The role of PDEs 4

5.4.3 cAMP/cGMP compartmentalization in cardiac disease 5

5.5 Fluorescence Resonance Energy Transfer (FRET) 5

5.5.1 The cAMP FRET sensor EPAC1-camps 7

5.5.2 The cGMP FRET sensor cGi500 8

5.5.3 Fluorescence Lifetime Imaging (FLIM) -FRET 8

5.6 The use of blebbistatin, forskolin and SNAP 9

5.7 Calcium 10

5.7.1 The calcium sensors GCaMP6 and Fluo-4 AM 11

6. AIM OF THE STUDY 13

7. MATERIAL 14

7.1 Devices 14

7.2 Software 15

7.3 Laboratory equipment 15

7.4 Bacterial strains 19

7.5 Plasmids 19

7.6 Zebrafish lines 20

7.7 Primers 20

8. METHODS 22

8.1 Cloning 22

8.2 Zebrafish maintenance and transgenesis 25

8.3 Mounting and imaging 28

8.4 Statistical analysis 29

1 Summary of contents

9. RESULTS 30
9.1 The cloning results 30
9.2 Transgenesis in the zebrafish: injection concentrations 32
9.3 The selection of zebrafish for FLIM-FRET 33
9.4 The incubation and mounting for FLIM-FRET 34
9.5 The analysis of the FLIM-FRET data with SPCImage 36
9.6 The effect of DMSO on the fluorescent lifetime Ti 38
9.7 The localization of the cAMP/cGMP sensor in cardiomyocytes 39
9.8 Changes in cAMP/cGMP concentrations 41
9.9 Compartmentalization 44
9.10 Calcium 47
9.10.1 GCaMP6F 48
9.10.2 Fluo-4 AM 48

10. DISCUSSION 51
10.1 The advantages of FLIM-FRET 51
10.2 cAMP/cGMP sensor characterization 52
10.3 Scientific context 54
10.3.1 Regeneration 54
10.4 Improving the measurements 55
10.5 Including Calcium 57
10.6 Transfer of results derived from the zebrafish to humans 58
10.7 Open questions and conclusion 58

11. SUMMARY 60

12. ZUSAMMENFASSUNG 61

13. REFERENCES 63

14. ERKLÄRUNGEN VII
14.1 Eröffnung des Promotionsverfahrens VII
14.2 Einhaltung der aktuellen gesetzlichen Vorgaben im Rahmen der Dissertation IX

15. DANKSAGUNG X

16. LEBENSLAUF XI

17. SUPPLEMENT XII
17.1 EPAC1-camps cloning XII
17.2 cGi500 cloning XV
17.3 GCaMP6F cloning XVIII
17.4 The different DNA injection concentrations and their effect on the fish XX

2. LIST OF ABBREVIATIONS

AKAPs	A Kinase Anchoring Proteins
AN	Annealing Temperature
ANOVA	Analysis Of Variation
ANP	Atrial Natriuretic Peptide
BNP	Brain Natriuretic Peptide
bp	Basepairs
CA	Catecholamines
Ca^{2+}	Calcium
CaM	Calmodulin
cAMP	cyclic Adenosine 3', 5' Monophosphate
CFP	Cyan Fluorescent Protein
cGKI	cGMP-dependent protein Kinase type 1
cGMP	cyclic Guanosine 3', 5' Monophosphate
cmlc2	cardiac myosin light chain 2
cpGFP	circularly permuted Green Fluorescent Protein
CRTD	Center for Regenerative Therapies Technische Universität Dresden
Cx43	Connexin 43
DNA	Deoxyribonucleic Acid
dNTP	Deoxyribonucleotide Triphosphate
ET	Extension Time
FLIM	Fluorescence Lifetime Imaging
FRET	Förster Resonance Energy Transfer
hpf	Hours post fertilization
HPSF	High Purity Salt Free
NA	Noradrenaline
NP	Natriuretic Peptide
PCR	Polymerase-Chain-Reaction
PDEs	Phosphodiesterases
PKA	cAMP-dependent Protein Kinase A
PKG	cGMP-dependent Protein Kinase G
RNA	Ribonucleic Acid
rpm	Rotations per minute
RyR2	Ryanodine Receptor type 2
SEM	Standard Error of Mean
SNAP	S-Nitroso-N-Acetyl-Penicillamine
SOC	Super Optimal Broth with 20mM Glucose
WT	Wild Type
YFP	Yellow Fluorescent Protein
βARs	β-Adrenergic Receptors

3. LIST OF FIGURES

Figure 5.1 The zebrafish as a model 1
Figure 5.2 The FRET-based sensor 6
Figure 5.3 Intensity-based FRET 7
Figure 5.4 The principle of FLIM 9
Figure 5.5 The principle of Fluo-4 AM 12
Figure 8.1 The cloning strategy 22
Figure 8.2 The beveller 26
Figure 8.3 The injection setup 27
Figure 8.4 The mounting of the zebrafish embryo 28
Figure 9.1 The plasmid cmlc2/Tol2 restricted with SbfI and AscI 30
Figure 9.2 The control reaction for the EPAC1-camps ligation 31
Figure 9.3 The different DNA injection concentrations and their effect on the zebrafish 33
Figure 9.4 The zebrafish at 48 hpf and malformations 34
Figure 9.5 An immobilized and a moving zebrafish heart under the confocal microscope 35
Figure 9.6 The threshold in SPCImage 36
Figure 9.7 The region of interest in SPCImage 36
Figure 9.8 Autofluorescence in a zebrafish heart 37
Figure 9.9 The detection of artificial fluorescence 38
Figure 9.10 The effect of DMSO on the fluorescent lifetime Ti 38
Figure 9.11 EPAC expressed in one cardiomyocyte 39
Figure 9.12 cGi500 expressed in cardiomyocytes 40
Figure 9.13 A Z-stack of EPAC1-camps expressed in one cardiomyocyte 40
Figure 9.14 EPAC1-camps response to increasing forskolin concentrations 41
Figure 9.15 cGi500 response to increasing SNAP concentrations 42
Figure 9.16 The influence of forskolin/SNAP on the fluorescent lifetime Ti 43
Figure 9.17 The distribution of the lifetimes of control EPAC1-camps expressing cells around the mean 44
Figure 9.18 EPAC1-camps expressing cells in different conditions 45
Figure 9.19 The distribution of the lifetimes of control cGi500 expressing cells around the mean 46
Figure 9.20 cGi500 expressing cells in different conditions 47
Figure 9.21 GCaMP6F expressed in cardiomyocytes 48
Figure 9.22 Oversaturation and edema caused by Fluo-4 AM treatment 49
Figure 9.23 Ca^{2+} release detected with Fluo-4 AM during contraction in the sequence of a heart cycle 50
Figure 9.24 Pericardial perfusion with Fluo-4 AM in a 48 hpf embryo 50

Figure 10.1 Different studies using FRET-based sensors.....53
Figure 17.1 The EPAC1-camps gene in the Tol2 vector..... XII
Figure 17.2 The DNA sequence of the EPAC1-camps gene in the Tol2 vector.....XIV
Figure 17.3 The cGi500 gene in the Tol2 vector.....XV
Figure 17.4 The DNA sequence of the cGi500 gene in the Tol2 vector.....XVII
Figure 17.5 The GCaMP6F gene in the Tol2 vector XVIII
Figure 17.6 The DNA sequence of the GCaMP6F gene in the Tol2 vector XIX

4. LIST OF TABLES

Table 9.1 The sequencing results 32
Table 9.2 Summary of different approaches for introducing Fluo-4 AM into zebrafish cardiomyocytes *in vivo*.....49

5. INTRODUCTION

Heart failure is known as a condition in which heart action is insufficient to meet the needs of the body (Oni-Orisan and Lanfear, 2014). Fatigue and shortness of breath are one of several symptoms reducing the quality of life of over 23 million patients worldwide suffering from heart failure (Bui, et al., 2011). Thus, it is important to promote the research on heart failure to improve treatments and to find new therapeutical targets. Comparing the signaling pathways that are involved in the compartmentalization of cAMP and cGMP between the healthy and failing heart revealed differences (Mika, et al., 2012b). This observation has left many questions about the (patho-) physiological significance of cAMP/cGMP compartmentalization open. Therefore, this study was aimed to develop a method to answer these questions.

5.1 THE ZEBRAFISH AS A MODEL

The localization and thus compartmentalization of intracellular messengers such as cAMP and cGMP can best be investigated using fluorescent microscopy. Therefore, the zebrafish (*Danio rerio*) was a good animal model to use, because the transparency of the larvae enabled *in vivo* imaging of fluorescence (see Fig 5.1), which is difficult in animals such as mice, because skin and other tissue mask fluorescence underneath.

Figure 5.1 The zebrafish as a model

A 48 hour post fertilization (hpf) zebrafish embryo. The two-chambered heart is shown by the fluorescent marker Green Fluorescent Protein (GFP). (zebrafish line: Tg(tbx6l:Cre,myl7:EGFP)). 1. Atrium 2. Ventricle. Scale bar 100 µM.

Previous studies with fluorescent sensors in zebrafish larvae (which involved assessments of sensors for gene expression, ion fluctuations and enzyme activity that are introduced into the zebrafish germline by transgenes (Nemtsas, et al., 2010; Weber and Huisken, 2015)) confirmed that fluorescent *in vivo* imaging was possible in the zebrafish. Unlike the four-chambered heart of humans, zebrafish only have an atrium and a ventricle (see Fig. 5.1).

However, the zebrafish has a high genetic and organ system homology to humans, which increases the probability that conclusions of this study about cAMP and cGMP can be transferred to human (patho-) physiology (Brand, et al., 2002).

Furthermore, the quick development of zebrafish enables experiments shortly after fertilization. The heart, for example, develops after two days, which allows high numbers of experiments and thus results (Brand, et al., 2002). Additionally, zebrafish have the ability to sufficiently regenerate multiple organs, also the heart (Konantz and Antos, 2014). This makes the zebrafish a good model for future investigations, which include regeneration (see 10.3.1).

5.2 cAMP IN CARDIAC PHYSIOLOGY

The heart is a muscular organ that pumps blood through the body to supply all organs with oxygen and nutrients and to remove metabolic waste products. The speed of this supply and removal is defined by the contraction force (inotropy) and heart rate (chronotropy). Because the needs of the body continuously change, inotropy and chronotropy are precisely regulated to fill the needs. During stress, the body requires an increased inotropy and chronotropy to meet the higher demands for oxygen, nutrients and metabolic waste removal. On a molecular level, stress leads to the release of noradrenaline from intracardiac nerve terminals. Noradrenaline activates cardiac β-Adrenergic Receptors (βARs). Three subtypes of βARs exist. The β_3AR has mainly metabolic functions and does not regulate inotropy and chronotropy (Wachter and Gilbert, 2012). The β_1AR and β_2AR promote G_s protein activation of adenylyl cyclases. Adenylyl cyclases synthesize the downstream mediator cyclic Adenosine 3', 5' Monophosphate (cAMP) (Mika, et al., 2012a). cAMP activates the cAMP-dependent Protein Kinase A (PKA) which then phosphorylates the relevant target proteins, such as L-type Calcium (Ca^{2+}) channels and Ryanodine Receptors type 2 (RyR2) (Haj Slimane, et al., 2014; Wallukat, 2002). These target proteins implement the functional consequences of beta-adrenergic signaling for heart action. Mostly, this happens through changes in Ca^{2+} concentrations: L-type Ca^{2+} channels enable a Ca^{2+} influx from extracellular, RyR2 cause a Ca^{2+} influx from the sarcoplasmatic reticulum into the cytosol. Immediate responses of Ca^{2+} signaling include the regulation of inotropy and chronotropy (McConkey and Orrenius, 1997). Long lasting responses of Ca^{2+} signaling are changes in gene expression, such as the development of hypertrophy (Bers, 2008).

5.3 cGMP IN CARDIAC PHYSIOLOGY

The natriuretic peptides Atrial Natriuretic Peptide (ANP) and Brain Natriuretic Peptide (BNP) are released by atrial cardiomyocytes because of increased atrial elongation. Atrial elongation can occur in heart failure, when the heart insufficiently pumps blood and

congestion occurs. ANP and BNP mediate natriuresis, vasodilatation and renine-aldosteron inhibition (Hoffmann and Chen, 2014). Thus, direct effects of ANP/BNP signaling happen outside of the heart. In the heart, ANP and BNP are known to have indirect, inhibiting effects on inotropy and chronotropy mediated by cAMP (Feil, et al., 2003): ANP and BNP activate guanylyl cyclases in the sarcolemma, which then hydrolyze the second messenger cyclic Guanosine 3', 5' Monophosphate (cGMP). Nitric Oxide (NO) can also increase intracellular cGMP by activating soluble guanylyl cyclases. cGMP then influences βARs signaling by activating Phosphodiesterases (PDEs) (mainly PDE2, if cGMP concentrations are low/moderate) which hydrolyze cAMP (Götz, et al., 2014; Sperelakis, 1994; Zhao, et al., 2016). Some inhibiting effects of cGMP are also mediated through the cGMP-dependent Protein Kinase G (PKG) (Feil, et al., 2003). Because of the natriuretic, vasodilating and cAMP-inhibiting effects of natriuretic peptide signaling, ANP and BNP are suspected to have a protective effect on the heart during stress and in heart failure (Feil, et al., 2003; Nishikimi, et al., 2006).

While PDEs activated by cGMP hydrolyze cAMP, PDEs can also be activated by cAMP to hydrolyze cGMP (mainly PDE2, if cAMP concentrations are low/moderate, and PDE1, PDE3). The degradation of cyclic nucleotides by PDEs activated by cAMP and cGMP is referred to as cAMP/cGMP crosstalk. Consequently, PDEs communicate between the βARs and ANP/BNP/NO pathway, which regulates the synthesis of cAMP and cGMP, respectively (Fu, et al., 2014; Zhao, et al., 2016).

5.4 cAMP/cGMP COMPARTMENTALIZATION

Evidence indicates that cAMP is not uniformly distributed throughout cardiomyocytes (Leroy, et al., 2008; Mika, et al., 2012a; Nikolaev, et al., 2010; Vandecasteele, et al., 2006; Zaccolo, et al., 2002). Furthermore, Di Benedetto et al. indicated that the compartmentalization of cAMP signaling is necessary for specific responses to hormones. This theory about specific hormone response evolved out of the finding that different hormones using the same second messenger (cAMP) differentially regulate PKA targets (for PKA targets see 5.2) (Di Benedetto, et al., 2008). However, there are still many open questions about the mechanisms that cause this cAMP compartmentalization and hormone-specific responses (Mika, et al., 2012a; Mika, et al., 2012b). cGMP, too, shows a heterogeneous distribution in cardiomyocytes. Especially the crosstalk occurring between cAMP/cGMP varies in different subcellular compartments and under different conditions (Stangherlin, et al., 2011; Stangherlin and Zaccolo, 2012; Zhao, et al., 2016). In the end, the main factors determining the distinct compartmentalization of cAMP and cGMP are thought to be 1.) specific membrane structures 2.) the intracellular concentrations of the two cyclic nucleotides cAMP

and cGMP, which determines cAMP/cGMP hydrolyzing activity by PDEs (Zaccolo and Movsesian, 2007).

5.4.1 THE ROLE OF SPECIFIC MEMBRANE STRUCTURES

In mammalian ventricular cardiomyocytes, the sarcolemma folds into what is called a transverse tubular network (subsequently referred to as T-tubuli). Most importantly, T-tubuli ensure a synchronized Ca^{2+} release for contraction (Brette and Orchard, 2003). However, T-tubuli also generate subdivisions that are important for cAMP-compartmentalization: Nikolaev et al. showed that β_1AR are evenly distributed throughout the sarcolemma, whereas β_2AR are located in the T-tubuli. While β_1AR cAMP signals mediate responses through the whole cell, β_2AR mediated cAMP signaling remains localized to the T-tubuli (Nikolaev, et al., 2006; Nikolaev, et al., 2010). Actually, several members of the cAMP pathway were found to be localized specifically in the T-tubuli. One member is the adenylyl cyclase (Gao, et al., 1997; Zaccolo, et al., 2002). Furthermore, the cAMP-PDEs type 3 and 4 (Mongillo, et al., 2004) and PKA regulatory subunits (Yang, et al., 1998) are found primarily in T-tubuli. PKA isoforms are compartmentalized by A Kinase Anchoring Proteins (AKAPs) (Röder, et al., 2009), which are also localized in the T-tubuli. Consequently, T-tubuli are postulated to be a critical element in cAMP compartmentalization. It is most likely that T-tubuli play an important role in cGMP compartmentalization, too.

5.4.2 THE ROLE OF PDES

A PDE is an enzyme that can break the phosphodiester bond in the cyclic nucleotides cAMP and cGMP (Leroy, et al., 2008). Götz et al. described real-time cGMP dynamics in intact adult cardiomyocytes. Their results revealed the importance of well-established and also potentially novel PDE-dependent mechanisms that regulate cGMP under physiological and pathophysiological conditions (Götz, et al., 2014). Fu Q. et al. showed that PDEs play a significant role in desensitization effects of beta-adrenergic signaling (Fu, et al., 2014). Thus, the use of cAMP and cGMP sensors provided new insights in the role of PDEs mediating cAMP and cGMP crosstalk and pointed a different activity of PDEs in different tissues or cellular locations out. Furthermore, Nikolaev and Lohse showed that PDE2 hydrolysis of cAMP kinetically overcomes cAMP production (even in the continuous presence of adenylyl cyclase stimulation) in experiments with exclusive PDE2 isoform expression in adrenal zona glomerulosa cells. Therefore, PDE2 is an example of PDE-mediated compartmentalization that shapes the local pools of cAMP by hydrolysis (Nikolaev and Lohse, 2006). Additionally, PDEs maintain the specificity of the βARs response by decreasing the amount of cAMP diffusing from membrane to cytoplasm (Leroy, et al., 2008; Nikolaev and Lohse, 2006; Zaccolo, 2006; Zaccolo and Pozzan, 2002)

5.4.3 cAMP/cGMP COMPARTMENTALIZATION IN CARDIAC DISEASE

Nikolaev et al. found that β_2AR, who are mainly located in T-tubuli and contribute to cAMP compartmentalization, diffusely redistribute throughout the whole sarcolemma in heart failure (Nikolaev, et al., 2010). Furthermore, cAMP-PDEs showed malfunction in many cardiac diseases (Weber, et al., 2015) and they are downregulated during cardiac hypertrophy (Abi-Gerges, et al., 2009) and heart failure (Mika, et al., 2012b). Sprenger et al. uncovered the existence of a PDE-dependent receptor-microdomain communication. This microdomain communication is affected in hypertrophy and causes reduced βARs-cAMP signaling to the Sarcoplasmatic/Endoplasmatic Reticulum Calcium ATPase (SERCA) (Sprenger, et al., 2015), indicating a mishandling of Ca^{2+} caused by PDE-dependent mechanisms. However, it remains unclear whether the redistribution of β_2AR and the different activity of cAMP-PDEs leads to a disorganization of cAMP compartmentalization and whether this leads to cardiac disease (Mika, et al., 2012a).

5.5 FLUORESCENCE RESONANCE ENERGY TRANSFER (FRET)

Microscopic fluorescent techniques based on Fluorescence Resonance Energy Transfer (FRET) allow the observation of biochemical events and second messengers inside intact cells (Nikolaev and Lohse, 2006).

FRET occurs between a fluorescence donor and a fluorescence acceptor when they are in molecular proximity (typically 2-6nm) to each other and when the emission spectrum of the donor overlaps with the excitation spectrum of the acceptor (Nikolaev and Lohse, 2006). In this case, after excitation, the donor's emission can excite the acceptor by FRET. Consequently, FRET results in the quenching of the donor-emitted fluorescence and in the increase of the acceptor-emitted fluorescence. To use FRET for tracking molecules of interest, FRET-fluorophores can be linked to 5' and 3' to the binding site for the molecule (referred to as FRET sensor). A binding of the molecule to the FRET sensor causes a conformational change. The conformational change affects the distance between donor and acceptor. Thus, if the distance of the fluorophores increases, FRET decreases, and vice versa (see Fig. 5.2). Therefore, FRET can be used as a tool to monitor molecular interactions, such as the formation of amyloid plaques in Alzheimer's disease (Bacskai, et al., 2003), research on synaptic transmission (Bosch, et al., 2014) and ion-channel physiology (Mies, et al., 2007). The latest research on cAMP/cGMP crosstalk and PDEs by the researchers Nikolaev, Fu Q. and Götz (see 5.4.2) was derived from FRET sensors. I also used the FRET sensors in this study, because FRET sensors efficiently allow to monitor cAMP and cGMP. The sensors had a binding domain for cAMP or cGMP with the donor fluorophore Cyan Fluorescent Protein (CFP) and the acceptor fluorophore Yellow

Fluorescent Protein (YFP) attached at the N-terminus and C-terminus of the binding domain of the respective nucleotide. CFP and YFP are commonly used in FRET-applications, because their spectral properties allow FRET (Ponsioen, et al., 2004). As illustrated in Figure 5.2, in the absence of cAMP or cGMP FRET happens. This is referred to as a high FRET efficiency. The consequent conformational change after the binding of cAMP or cGMP increases the distance between the CFP and YFP, causing the FRET efficiency to decrease.

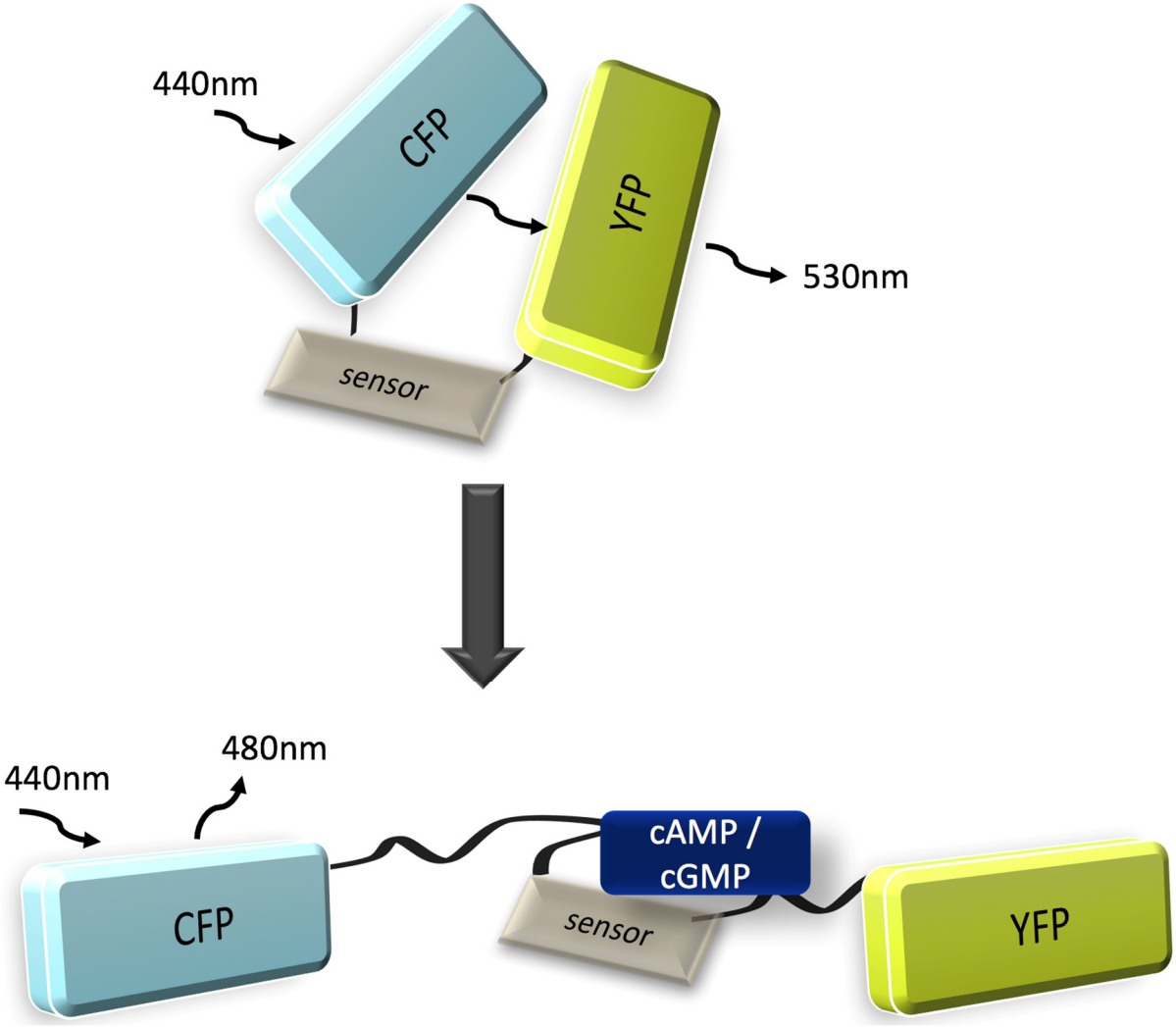

Figure 5.2 The FRET-based sensor

The FRET sensor has two fluorophores attached to a binding site that interacts with cAMP or cGMP. In the absence of cAMP or cGMP, the donor fluorophore and the acceptor fluorophore are in close proximity, so efficient FRET can happen. The presence of cAMP or cGMP causes a conformational change, which increases the distance between the fluorophores and causes a subsequent decreased FRET efficiency. For this thesis, two different sensors for cAMP and cGMP were used. However, the general principle applies to both sensors, which is why both cyclic nucleotides were both labelled in this figure.

The concentration of cAMP or cGMP can be evaluated by measuring the emitted light at 480 and 530nm in response to excitation at 440nm. An increase in concentration of the molecule is followed by a decrease of FRET and thus of 535nm emitted light together with an increase of 485nm emitted light. The ratio of the fluorescence intensity at 480 and 530nm represents

the concentration of cAMP or cGMP (Holz, et al., 2006; Landa, et al., 2005). Intensity-based FRET relies on this ratio for the analysis. An example is given in Fig. 5.3.

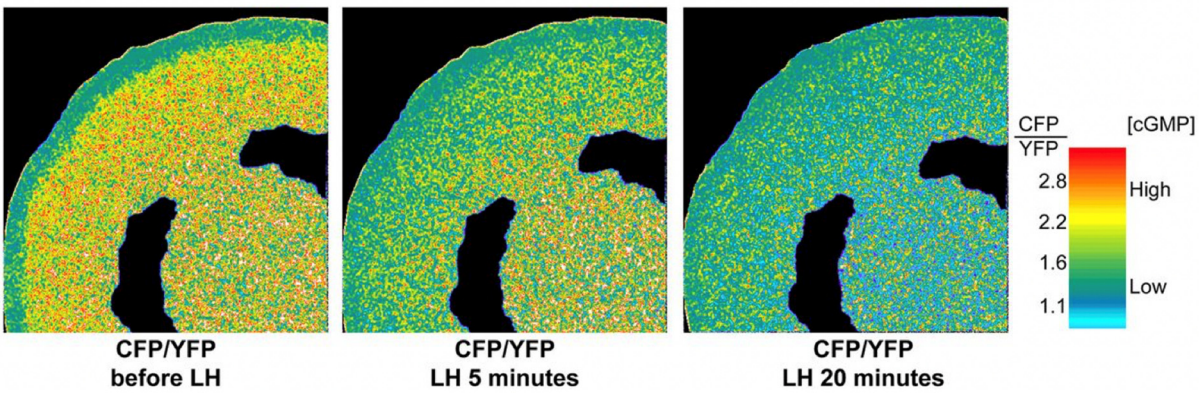

Figure 5.3 Intensity-based FRET

Shown is the diffusion of cGMP through gap junctions in real-time in live follicles from mice, tracked by a FRET sensor. Pictures from left to right are taken before, 5 minutes and 10 minutes after treatment with luteinizing hormone. Luteinizing hormone is involved in follicles whose effects on cGMP were investigated by Shuhaibar et al.. It is important to note that the pictures are pseudo-colored. The legend on the right shows each ratio of the fluorescent emission of the CFP over YFP (the fluorophores of the FRET sensor for cGMP) with a given a color, which are represented in the pictures on the left. Due to the conformation of the sensor, high concentrations of cGMP cause low FRET and a high emission in the CFP spectra. This is given a red color. It is clearly visible that cGMP diffuses over time from the cell surface the oocyte (Shuhaibar, et al., 2015).

5.5.1 THE CAMP FRET SENSOR EPAC1-CAMPS

In order to assess cytosolic cAMP in living cells, two types of FRET sensors were developed. The two FRET sensors differ in the binding domain that interacts with cAMP: PKA-based cAMP FRET sensors contain the binding domain for cAMP from the PKA (for explanation of PKA see 5.2), whereas EPAC-based sensors are derived from the cAMP-binding site of the guanine nucleotide exchange factor for Rap1, an enzyme that is activated by binding cAMP. PKA-based cAMP sensors have slow response times, because they have multiple subunits requiring four cAMP molecules to bind to four different sites before the dissociation of the catalytic subunits implement the change in FRET (Nikolaev and Lohse, 2006; Ponsioen, et al., 2004). EPAC-based sensors have a single cAMP-binding domain, allowing faster kinetics and making them more suitable for monitoring rapid intracellular cAMP changes (Mironov, et al., 2009). Moreover, the short cAMP-binding sequences in the EPAC-based sensors do not contain any catalytic or targeting domains that can interfere with cAMP measurements (Nikolaev, et al., 2004). Two isoforms of EPAC exist, EPAC1 and EPAC2. EPAC-based sensors derived from EPAC1 and EPAC2 are referred to as EPAC1-cAMP-sensor (EPAC1-camps) or EPAC2-camp-sensor (EPAC2-camps). In previous studies, the EPAC1-camps revealed a significantly larger signal amplitude and activation kinetics when compared to the EPAC2-camps (Nikolaev, et al., 2004), which is why I used the EPAC1-camps in this study.

The EPAC1-camps sensor has been successfully used in a number of studies. Nikolaev and Lohse used it to investigate cAMP and Ca^{2+} oscillations (with Fura-2-AM) in insulin producing cells and thereby revealed a PDE1-involved mechanism in this context (Nikolaev and Lohse, 2006). EPAC2-camps was used in the study from Leroy et al. to compare cAMP and Ca^{2+} kinetics in cardiomyocytes (results discussed in 5.7) (Leroy, et al., 2008). Subsequent studies using EPAC as a sensor for cAMP have shown that the second messenger increases under β-AR stimulation preferentially in discrete t-tubular microdomains, and that cAMP diffusion is limited by PDE activity (Nikolaev and Lohse, 2006; Zaccolo and Pozzan, 2002).

However, although recent developments include using the FRET sensors such as EPAC1-camps in intact cardiomyocytes and also in live samples (this includes follicles (Shuhaibar, et al., 2015) and skeletal muscle (Röder, et al., 2009)), there is no record of studies using a fluorescent FRET sensor for cAMP in an *in vivo* context of cardiomyocytes in the heart.

5.5.2 THE CGMP FRET SENSOR CGI500

The sensor cGi500 also uses the FRET principle. The sensor contains the tandem cGMP-binding sites of the bovine cGMP-dependent protein Kinase type 1 (cGKI). Compared to other cGMP-FRET sensors, the cGi500 sensor is particularly useful for cGMP imaging, because it provides a large fluorescent amplitude and fast reversibility of the cGMP-induced FRET change after activation by cGMP. Furthermore, the sensitivity to cGMP is high, while cAMP affinity is low, which limits cross-activation by cAMP. It is important to ensure that cross-activation by cAMP is not possible, because this alters the interpretation of the data (Thunemann, et al., 2013a). Thuneman et al. generated mouse lines carrying the cGMP sensor cGi500 in cardiovascular tissues. They visualized cGMP in primary cells and tissues isolated from mice, and in blood vessels of live animals. They found out that different types of smooth muscle cells had different sensitivities in their cGMP responses to cGMP-elevating drugs such as nitric oxide (NO) (Thunemann, et al., 2013b). Götz et al. visualized real-time cGMP dynamics and pharmacology in intact adult cardiomyocytes. Their results revealed the novel PDE-dependent mechanisms that regulate cGMP (see 5.4.2) (Götz, et al., 2014). However, as with cAMP, no studies have been performed using a fluorescent FRET sensor for cGMP *in vivo* in the heart.

5.5.3 FLUORESCENCE LIFETIME IMAGING (FLIM) -FRET

Fluorescence Lifetime Imaging (FLIM) was first introduced in 1989 by Bugiel, König and Wabnitz (Bugiel, et al., 1989) and is based on the fact that the lifetime of fluorophores in a fluorescent sample can vary. The first FLIM module for laser scanning microscopes was introduced in 1998 (Becker and Hickl, 2015). Thus, a sample can be repetitively scanned by a pulsed laser, while fluorescent decay parameters and the coordinates of each pixel are

collected and represented in a photon distribution array (see Fig 5.4). FLIM-FRET can be used for monitoring molecular interactions with FRET sensors, because the transfer of energy from the donor to the acceptor fluorophore during FRET decreases the lifetime of the donor. Therefore, in FLIM-FRET the donor's lifetime of a FRET sensor is determined.

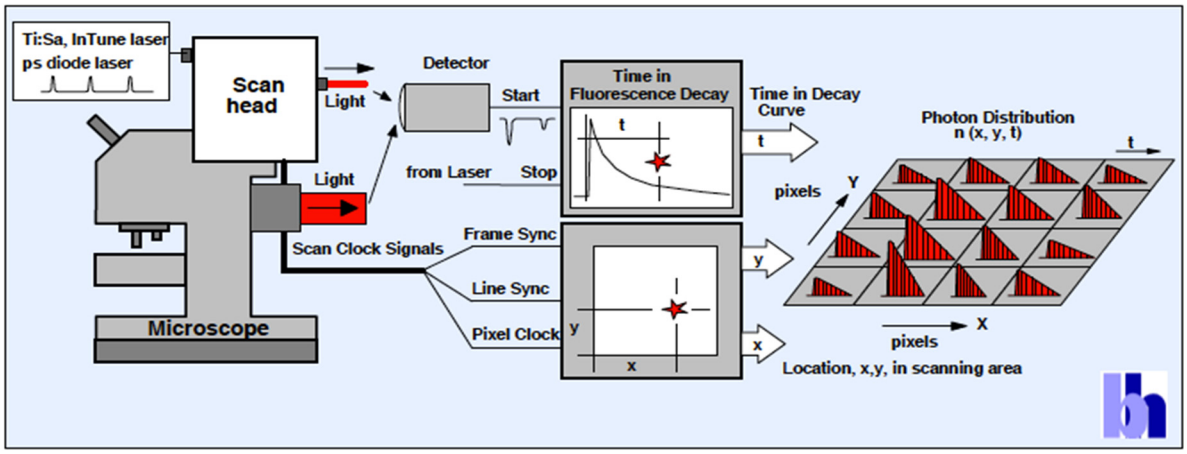

Figure 5.4 The principle of FLIM

For FLIM, a FLIM detector is connected to a confocal microscope. The sample is repetitively scanned by a pulsed laser. For each pixel fluorescent decay parameters and the coordinates are collected and represented in a photon distribution array (Becker and Hickl, 2015).

The analysis of the FLIM data includes complex mathematical calculations. The Becker and Hickl software, which I used in my study, provides the lifetimes of the donor fluorophore in certain areas of interest or pixels as numerical data. It is also possible to visualize these lifetimes by assigning each lifetime a color. The result is a pseudo-color-coded picture showing areas of high lifetimes (low FRET, low concentration of cAMP/cGMP) and areas of low lifetimes (high FRET, high concentration of cAMP/cGMP).

5.6 THE USE OF BLEBBISTATIN, FORSKOLIN AND SNAP

FLIM-FRET confocal microscopy requires immobile samples, because otherwise the image taken is blurred. To inhibit contraction of the zebrafish's heart, blebbistatin (dissolved in DMSO) is a good drug to use. It inhibits cell myosin cycling by binding to the ADP Pi complex of myosin. Thus, it uncouples excitation from contraction in the heart. Furthermore, it inhibits myocardial contraction without altering action potential morphology or intracellular Ca^{2+} transients (which would alter the results) (Jou, et al., 2010).

To find out whether under extreme situations compartmentalization events can be still observed, the cAMP or the cGMP pathway can be provoked by cAMP or cGMP-elevating drugs. For raising the intracellular cAMP levels, forskolin can be used. It activates the adenylate cyclase, which produces cAMP. Forskolin has been used to significantly increase intracellular cAMP levels in zebrafish larvae (Bovo, et al., 2013; Coutts, et al., 2009), showing

that the drug has an effect in zebrafish. For raising the intracellular cGMP levels, S-Nitroso-N-Acetyl-Penicillamine (SNAP) can be used. SNAP is a NO donor, which activates the NO-dependent guanylyl cyclase to produce cGMP. SNAP has, depending on the conditions, a half-life of 1-5h and is thus more suitable for imaging sessions, because other NO-donors decompensate much faster. Furthermore, SNAP has been successfully used in zebrafish (Westermann and Meissl, 2008).

5.7 CALCIUM

Ca^{2+} is an important intracellular messenger implementing the functional consequences of the βARs and βAR-inhibiting ANP/BNP/NO pathway that regulate intracellular Ca^{2+} handling: immediate responses of Ca^{2+} signaling regulate contraction and long lasting responses of Ca^{2+} signaling are changes in gene expression (see 5.2). Therefore, Ca^{2+} can be used as a functional readout of the βARs and ANP/BNP/NO pathway. However, only few studies compare cAMP as the mediator of the βARs- or cGMP as the mediator of the ANP/BNP/NO pathway with Ca^{2+}, and none combines the important crosstalk of cAMP/cGMP with Ca^{2+}. It is of great interest to investigate whether compartmentalized cAMP/cGMP also causes compartmentalized Ca^{2+} (and therefore local differences in contraction), or whether functional responses are homogeneous throughout the cell.

Comparing cAMP and Ca^{2+} kinetics, Leroy et al. found that L-type Ca^{2+} channel activation develops >2-fold slower than membrane cAMP responses, and its return to basal levels develops >7-fold slower membrane cAMP responses, suggesting that phosphorylation and dephosphorylation are rate-limiting in the β-AR cascade (and not cAMP concentrations). Furthermore, Leroy et al. found that in rats, PDE4 is the main PDE subtype modulating β-AR-induced-cAMP transients and, as a consequence, Ca^{2+} concentrations after β-AR stimulation. Including Ca^{2+} in the studies thus revealed important regulatory mechanisms for Ca^{2+} handling and indicate the significance of including Ca^{2+} in investigating cardiac regulators (Leroy, et al., 2008).

To track Ca^{2+}, the sensor GcAMP6 and its previous versions have been used in *in vivo* contexts in the zebrafish. Using light sheet microscopy, Weber and Huisken imaged Ca^{2+} currents in a developing heart in real-time, revealing differences in Ca^{2+} handling, cardiac output and contraction in different parts of the heart (Weber and Huisken, 2015). Weber and Huisken thus showed that the GcAMP6 sensor can be used to assess Ca^{2+}, which is why GcAMP6 was used in this study.

5.7.1 THE CALCIUM SENSORS GCAMP6 AND FLUO-4 AM

The genetic fluorescent Ca^{2+} sensor GCaMP6 has been successfully used in *in vivo* contexts by Huisken and Weber (see 5.7), which is why GCaMP6 was used in this study. The reporter genes of the GCaMP6 family consist of circularly permuted Green Fluorescent Protein (cpGFP), the calcium binding protein Calmodulin (CaM) and CaM-interacting M13 peptide. Calcium dependent conformational changes cause increased brightness (Chen, et al., 2013). The different variants of GCaMP6 vary in their fluorescent decay. The fluorescence of the GCaMP6S variant lasts much longer than the fluorescence of the GCaMP6F variant after Ca^{2+} binding. Thus, the GCaMP6F sensor allows the tracking of immediate changes in Ca^{2+} (implementing fast responses such as contraction, see 5.2, whereas the GCaMP6S sensor allows the tracking of changes in sustained Ca^{2+} levels (Badura, et al., 2014) (implementing long lasting responses such as changes in gene expression, see 5.2).

Additionally, the fluorescent dye Fluo-4 AM was used to track Ca^{2+}, because a dye can easily be combined with transgene sensors (such as FRET sensors for cAMP and cGMP) for simultaneous measurements if the fluorophores used do not spectrally overlap. Furthermore, a dye requires less preparation compared to genetic sensors, which have to be introduced into the animal by a time-consuming process (including cloning and microinjection of the construct into fertilized oocytes). Fluo-4 AM was used because the dye has been worked with extensively in *in vitro* studies in the past, which generated a large amount of experience that was benefitted from in this study.

Fluo-4 AM exhibits high fluorescent emission after intracellular cleavage of the AM ester and following Ca^{2+} binding (see Fig. 5.5). The AM ester is important for the dye to pass the plasma membrane. After cleavage, the dye is trapped into the cell. Because after incubation of the sample or injecting the dye into areas of interest the dye shows immediate fluorescent response, data analysis is immediately possible. Due to its excitation near 488nm, the fluorescence of Fluo-4 AM can be analyzed with an Argon-laser (Gee, et al., 2000). Argon-laser based fluorescent microscopes are easily accessible in most institutes. This easy access is important for experiments in which quick evaluations about fluorescence must be made, for example while establishing a new protocol, which is why Fluo-4 AM was used in this study.

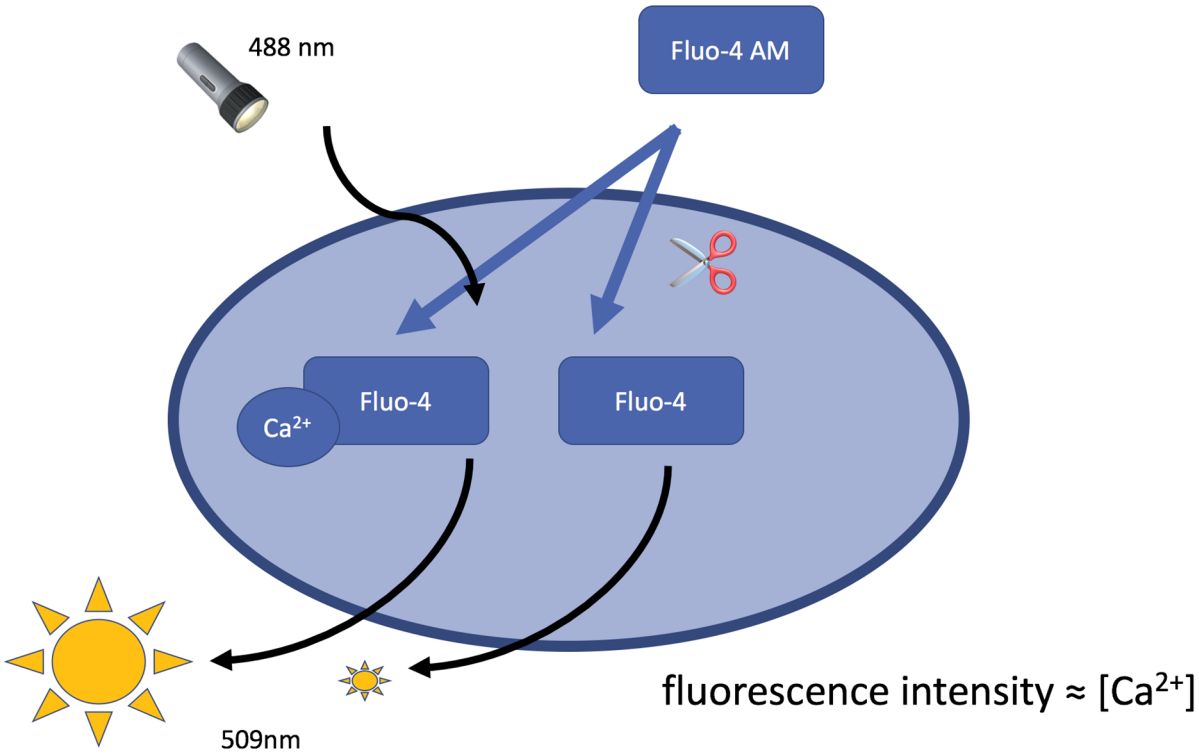

Figure 5.5 The principle of Fluo-4 AM

Fluo-4 AM diffuses into the cell, where intracellular esterases hydrolyze the AM ester, resulting in the Fluo-4 being membrane impermeable and trapped in the cytosol (notice Fluo-4 AM outside the cell and Fluo-4 without AM ester inside the cell). Upon excitation with an Argon laser (488nm), the dye Fluo-4 emits fluorescence at a wavelength of 509nm. The emitted fluorescence is significantly higher when Ca^{2+} is bound to the dye.

6. AIM OF THE STUDY

In cardiac research, the scientific community drives to understand the subcellular distribution patterns of cAMP and cGMP in cardiomyocytes, because many open questions remain in the context of why cAMP and cGMP show a distinct compartmentalization in cardiomyocytes and whether a distorted compartmentalization of cAMP and cGMP leads to the phenotypes of cardiac diseases. FRET-methods to track cAMP and cGMP have been used as a tool to learn about cAMP and cGMP in real-time and in high spatial resolution. However, the inability to optically penetrate the body of most of the animal models mask fluorescence in the heart, which significantly complicates *in vivo* analyses of cAMP and cGMP with FRET sensors (Lee, et al., 2012). Because zebrafish are transparent in early stages of development, the first aim of this study was to introduce FRET sensors for cAMP and cGMP into zebrafish via transgenesis. The second aim was to perform FLIM-FRET as a novel technique to assess cardiomyocyte cAMP and cGMP *in vivo*, because fluorescent lifetime imaging can provide accurate, subcellular high-resolution assessment of FRET sensors. It was also aimed to introduce the genetic sensor GCaMP6 for assessing Ca^{2+}, because Ca^{2+} is the intracellular messenger implementing the functional consequences (such as contraction) of cAMP/cGMP signaling and can therefore be used as a functional readout of these pathways. With the data collected, the third aim was to find out whether the same compartmentalization of cAMP and cGMP signaling, to which T-tubuli are attributed to significantly contribute in mammals, can be observed in zebrafish (which lack T-Tubuli). Also, the cAMP and the cGMP pathway were planned to be provoked by cAMP and cGMP-elevating drugs to find out whether under extreme conditions compartmentalization events can be still observed.

7. MATERIAL

7.1 DEVICES

All light microscopy applications were performed on devices of the Light Microscopy Facility, a core facility of BIOTEC/CRTD at Technische Universität Dresden.

Name	**Product name**	**Producer**
Analytical balance	MC BA 100	Sartorius
Autoclave	Vakulab HP	MMM
Beveller	Kapillarenschleifgerät Typ 462	Bachhofer GmbH
Centrifuge	Mini Centrifuge MCF-2360 Micro centrifuge I R Heraeus Centrifuge Fresco 21 Heraeus Megafuge 8R Multifuge 4 KS-R	LMS Co., LTD Carl Roth Thermo Fisher Scientific Thermo Fisher Scientific Heraeus
Clean water supply	Milli-Q G-Pod	Merck Millipore
Gas burner	06F125, Gas Lock System C 206 GLS Super	Campingaz
Gel analyzer	Fusion FX	Vilber Lourmat
Gel electrophoresis chamber	SGU-020T-02	C.B.S Scientific Co.
Gel electrophoresis power supply	PowerPac™ Basic	Bio-Rad
Incubator	Unitwist	Uniequip
Micromanipulator	Pneumatic PicoPump PV820	World Presicion Instruments, Inc.
Microscope, Laser Scanning Confocal Microscope	Axio Observer LSM 780/FLIM Objective: Zeiss C-Apochromat 40X 1,2W, Illumination: Laser Argon Multiline 458,488,514nm, Laser Diode 475nm (pulsed), Transmitted light (Halogen)	Zeiss FLIM dual channel unit from B&H
Microscope, stereo	Olympus MVX10 (Fluorescence) Olympus SZX10 (Injections) Olympus SZX16 (Dechorionation)	Olympus Corporation
Microwave	HF 22023	Siemens
Needle puller	Flaming/Brown P-97 Micropipette Puller Settings: Heat 537, Pull 250, Vel 150, Time 80	Sutter Instrument Co.
PCR cycler	Mastercycler nexus (gradient)	Eppendorf
Pipette	2, 20, 200, 1000µl	VWR, Eppendorf
Pipetting helper electric	Multipette® plus	Eppendorf
Sonicator	Sonorex RK100H	Bandelin
Spectrophotometer	NanoDrop® 1000	Peqlab

Speed vac	Concentrator 5301	Eppendorf
Suction	CVC 2000	Vacuubrand
Thermomix	Thermomixer comfort Thermomixer compact	Eppendorf Eppendorf
Vortexer	Vortex-Genie2	Scientific Industries

7.2 SOFTWARE

Function	**Name**	**Provider**
Analysis Olympus MVX10	cellSens Dimension	Olympus Corporation
Computer operating system	macOS Windows 2000, Vista, 8	Apple Microsoft Corporation
Control and analysis gel analyzer	Fusion-Capt	Vilber-Lourmat
FLIM	SPCImage SPCM	B&H
Laser Scanning Confocal Microscope	Zen Black 2011	Zeiss
Nanodrop	NanoDrop 100 3.7.1	Thermo Fisher
Organization fish database	File Maker Pro Advanced	FileMaker, Inc.
Plasmid handling, sequence analysis and design	APE	M. Wayne Davis
Statistical analysis	GraphPad Prism 7.0b	GraphPad Software, Inc.

7.3 LABORATORY EQUIPMENT

7.3.1 REUSABLE LABORATORY EQUIPMENT

Name	**Product name**	**Producer**	**Catalog Number**
Beaker	FisherBrand® 100, 400ml	Thermo Fisher Scientific	FB33110, FB33113
Falcons	Jena Therm 100ml	Jena Therm	Unknown
Microinjection mold templates	TU-1 (for Ca^{2+} dye injections, 48 hpf), PT-1 (for Ribonucleic Acid (RNA)/DNA injections)	Adaptive Science Tools	(774) 239-6133
Mouse cage for temporary fish collection and net inserts for spawning	Own production: redesigned aqua box 24,5*15*13,5 cm with PVC cover, net 21*10,5*8,5cm with a grid distance of 2mm		
Tweezers	Tweezers Dumont #5 11cm Dumoxel	World Presicion Instruments, Inc.	14099

7.3.2 CONSUMABLES

Name	Product name	Producer	Catalog Number
Lysogeny broth plates (100 µg/ml Ampicillin)	Ampicillin 100	CRTD (Center for Regenerative Therapies Technische Universität Dresden) Dresden	Ampicillin 100
Cover slip glued under object plate with hole for microscopy	24x60mm, own production		
Disposable pipette Tips	10µl, 20µl, 100µl, 200µl, 1250µl extra long 20µl microloader for injections 5ml, 10ml, 50ml	Sarstedt Eppendorf Corning Incorporated	Various 0030 001.222 4487, 4488, 4490
Eppendorf tubes	1,5ml 2ml 1,5ml brown PCR tubes	Sarstedt Sarstedt Sarstedt Eppendorf	72.706 72.695.500 72.706.001 0030 121.023
Glass capillaries	Glass thin 1.0 mm	World Precision Instruments, Inc.	TW100 F-3
Pasteur pipette	Pastette®	Alpha Laboratories Limited	LW4111
Petri dish	Petri dish	Greiner bio-one	633180
Petri dish nunc	nunclonTM Delta Surface	Thermo Fisher Scientific	150318
Well plates	6, 24, 96 well plates	Corning Incorporated	3506, 3527, 3598

7.3.3 CHEMICALS

Unless otherwise stated, all chemicals have a per analysis level of purity.

Name	Producer	Catalog Number
agarose	Serva	11404.07
Blebbistatin (sonicated before use)	Sigma	B0560
Boric acid	VWR chemicals	20185.297
Calcium chloride	Sigma	C5670-100G
DEPC Diethylpyrocarbonat	Carl Roth	K028.2
Disodium hydrogen orthophosphate dehydrate ($Na_2HPO_4x2H_2O$)	Merck	106576
DMSO Dimethyl sulfoxide	Sigma	D8418-250ML
EDTA	Merck	K35265018601

Ethanol absolute	VWR chemicals	20821.310
Ethyl 3-aminobenzoate methanesulfonate salt	Sigma	A5040-250G
Isopropanol	VWR chemicals	20842.330
Magnesiumsulfate heptahydrate	Merck	1.05886.1000
Methyl cellulose	Sigma	M0387-100G
Methylene blue	Sigma	03978-250ML
Potassium chloride	Merck	1.04933.0500
Propan-2-ol	VWR	20842.330
Rnase free H2O	Promega	P119E
SNAP (S)-Nitroso-N-acetylpenicillamine	Tocris	0598
Sodium chlorate	Sigma	403016-100G
Tris base	Carl Roth	9090.2

7.3.4 BUFFER AND SOLUTIONS

Name	**Composition**
10X TBE	For 1l 121,1g Tris base 61,8g boric acid 7,4g EDTA Fill up with Milli-Q H_2O
E3	5 mM Sodium chloride, 0.17 mM Potassium chloride, 0.33 mM Calcium chloride, 0.33 mM Magnesiumsulfate heptahydrate, 0.0002 % Methylene blue pH 6.5
Mesab solution for anesthetization	For 100ml: 0,4g Ethyl 3-aminobenzoate methanesulfonate salt 1g Disodium hydrogen orthophosphate dehydrate ($Na_2HPO_4x2H_2O$) 100ml DEPC water Application: Add 3ml into petri dish with E3 water
Phenolred	0.2% in 0.25M KCl

7.3.5 REAGENTS

Function	**Name**	**Producer**	**Catalog Number**
DNA Ladder	GeneRuler 1kb Plus DNA ladder	Thermo Fisher Scientific	SM1331

DNA Loading dye	6X DNA loading dye	Thermo Fisher Scientific	R0611
DNA Stain	HDGreen Plus	Intas	ISII-HDGreen
Dye, Ca^{2+} sensor	Fluo-4, AM	Molecular probes life technologies	F14201

7.3.6 KITS

Function	**Product Name**	**Producer**	**Catalog Number**
Gel Extraction	QIAquick® Gel Extraction Kit (250)	Qiagen	28706
Gel extraction/DNA purification	NucleoSpin® Gel and PCR Clean-up	Macherey-Nagel	740609.250
In vitro transcription	mMESSAGE mMachine™ T7 mMESSAGE® SP6 mMACHINE	Thermo Fisher Scientific Ambion	AM1344 AM1340
Plasmid Minis/Midis	QIAGEN® Plasmid Midi Kit (25)	Qiagen	12143
	SOC Medium for the QIAGEN® Plasmid Midi Kit (25)	CRTD (Center for Regenerative Therapies Technische Universität Dresden) Dresden	SOC Medium

7.3.7 ENZYMES

Funktion	**Name**	**Product name**	**Producer**	**Catalog Number**
Restriction enzyme	AatII	Anza™ 46 AatII	Thermo Fisher Scientific	IVGN0464
	AscI	Anza™ 21 SgsI	Thermo Fisher Scientific	IVGN021-4
	BamHI	Anza™ 1 BamHI	Thermo Fisher Scientific	IVGN0056
	BglII	Anza™ 19 BglII	Thermo Fisher Scientific	IVGN0196
	ClaI	Bsu15I(ClaI)	Fermentas	ER0141
	HindIII	Anza™ 16 HindIII	Thermo Fisher Scientific	IVGN0166
	KpnI	Anza™ 17 KpnI	Thermo Fisher	IVGN0176

			Scientific	
	NheI	Anza™ 6 NheI	Thermo Fisher Scientific	IVGN0066
	NotI	Anza™ 1 NotI	Thermo Fisher Scientific	IVGN0014
	SalI	SalI	Fermentas life sciences	ER0641
	SbfI	FastDigest SdaI	Thermo Fisher Scientific	FD1194
	SmaI	Anza™ 22 SmaI		IVGN0226
	XbaI	XbaI	Thermo Fisher Scientific	ER0681
	XhoI	XhoI	Thermo Fisher Scientific	ER0691
Polymerase	DNA Polymerase for PCR	Pfu DNA Polymerase	Thermo Fisher Scientific	EP0502
Ligase	DNA Ligase	T4 DNA Ligase	New England BioLabs®$_{GmbH}$	M0202S
Phosphatase	Alkaline Phosphatase	Alkaline Phosphatase, Calf Intestinal (CIP)	New England BioLabs®$_{GmbH}$	M0290S

7.4 BACTERIAL STRAINS

Competent cells for bacterial transfection (DH5α strain) were provided by Dr. Antos.

7.5 PLASMIDS

Name used in this thesis	**Name in database**	**Origin**
cGi500	CAG cGi500	Dr. Nikolaev (Institute of Experimental Cardiovascular Research)
EPAC1-camps	EPAC-camps	
EPAC1-camps	564 pcDNA6-YFP-EPAC-CFP-myc-His B for FRET	Dr. Antos (Institute of Pharmacology and Toxicology)
GcAMP6 M/F/S	565 pTol_ubi_gCampMedi-lensgreen 566 pTol_ubi_gCampFast-lensgreen, 567 pTol_ubi_gCampSlow-lensgreen	Dr. Kizil (CRTD)
PCS2	30.pCS2gfpN1	Dr. Antos (Institute of Pharmacology and Toxicology)
miniTol2cmlc2	263. miniTol2cmlc2 TetAGBD P2A GFP_final construct	Dr. Antos (Institute of Pharmacology and Toxicology)

Transposase	100.pCS-TP	Dr. Antos (Institute of Pharmacology and Toxicology)

7.6 ZEBRAFISH LINES

Name	Date of birth	Tank number	Origin
615 – 4 Wild Type (WT) WIK	8.10.15	4140 CRTD	Dr. Antos (Institute of Pharmacology and Toxicology)
615 – 5 WT WIK	8.10.15	4141 CRTD	Dr. Antos (Institute of Pharmacology and Toxicology)
615 – 6 WT WIK	8.10.15	4142 CRTD	Dr. Antos (Institute of Pharmacology and Toxicology)
615 – 8 WT WIK	8.10.15	4143 CRTD	Dr. Antos (Institute of Pharmacology and Toxicology)
615 – 9 WT WIK	8.10.15	4144 CRTD	Dr. Antos (Institute of Pharmacology and Toxicology)
615 – 10 WT WIK	8.10.15	4145 CRTD	Dr. Antos (Institute of Pharmacology and Toxicology)
405 – WT AB	8.3.16	5440 CRTD	CRTD
405 – WT AB	9.2.16	5441 CRTD	CRTD
405 – WT AB	8.3.16	5442 CRTD	CRTD
405 – WT AB	1.12.15	5443 CRTD	CRTD
405 – WT AB	8.3.16	5444 CRTD	CRTD

7.7 PRIMERS

All Primers were synthesized by the company Eurofins Genomics and cleaned in High Purity Salt Free (HPSF) quality.

Function	Name of Primer	Sequence 5´-3
Cloning of EPAC1 into TOL2 forward	epacYFPfretsbfl	ATACCTGCAGGAAGCGCAAAGATGCTAGCATG
Cloning of EPAC into TOL2 reverse	epacCFPfretAscl	ATAGGCGCGCCCCGGTATGCATATTCAGATCC
Cloning of cGi500 into TOL2 forward	CGI500Tol2sbf3’	TATCCTGCCAGGAGATATCTGCAGCGCCACCAT
Cloning of cGi500 into TOL2 reverse	CGI500Tol2Asc3’	TATGGCGCGCCAGTTACTTGTACAGCTCGTCC
Cloning of GCaMP6 into Tol2 forward	GCamP6forTol2for	GGTCCTGCAGGAGTTATATGGGTTCTCATCAT
Cloning of GCaMP6 into Tol2	GCamP6forTol2rev	AAAGGCGCGCCGTTGATTTACTTCGCTG

reverse		TCAT
Cloning of GCaMP6 into PCS2 forward	GCamP6forPCS2for	TGTAAGCTTAGTTATATGGGTTCTCATCAT
Cloning of GCaMP6 into PCS2 reverse	GCamP6forPCS2rev	TTTTCTAGAGTTGATTTACTTCGCTGTCAT
Sequencing EPAC forward	EPACcampSbf1Forw	CATACCTGCAGGTAGGGAGACCCAAGCTTATGG
Sequencing EPAC reverse	EPACcamAsclrev	CATTAGGCGGCGCGCCGGTGACACTATAGAATAGGGC
Sequencing GCaMP6 forward	UbiPromoter3’	GGCTAGAACATTGTAGT
Sequencing GCaMP6 reverse	lengreenNtermRev	GTTCAGGGGGAGGTGTGG
Sequencing Tol2 clones forward	cmlc2forseqprim	GGGACGAACAGAAACACTGC
Sequencing Tol2 clones reverse	Nr. 820 SV40_Seq_1	GCAGCTTATAATGTTACAA

8. METHODS

Unless otherwise stated, molecular biology methods were performed according to Sambrook&Russel (Molecular cloning, 3rd edition) or according to the instructions provided with the enzymes, reagents and kits provided.

8.1 CLONING

Each plasmid which contained the fluorescent sensor EPAC1-camps, cGi500 and GCaMP6 (see 5.5.1,5.5.2 and 5.7.1)), respectively, was merged with a vector backbone that had all the features that were needed for molecular cloning: the Ampicillin resistance (see step 7. on page 24), the SV40 Poly A Signal that is necessary for transcription when the cloned gene is incorporated into the fish (Li, et al., 2012), the Tol2 transposable element (see 8.2) and the *cmlc2* promoter (see 8.2). The cloning strategy used is shown in Fig. 8.1. and will be further explained in the following.

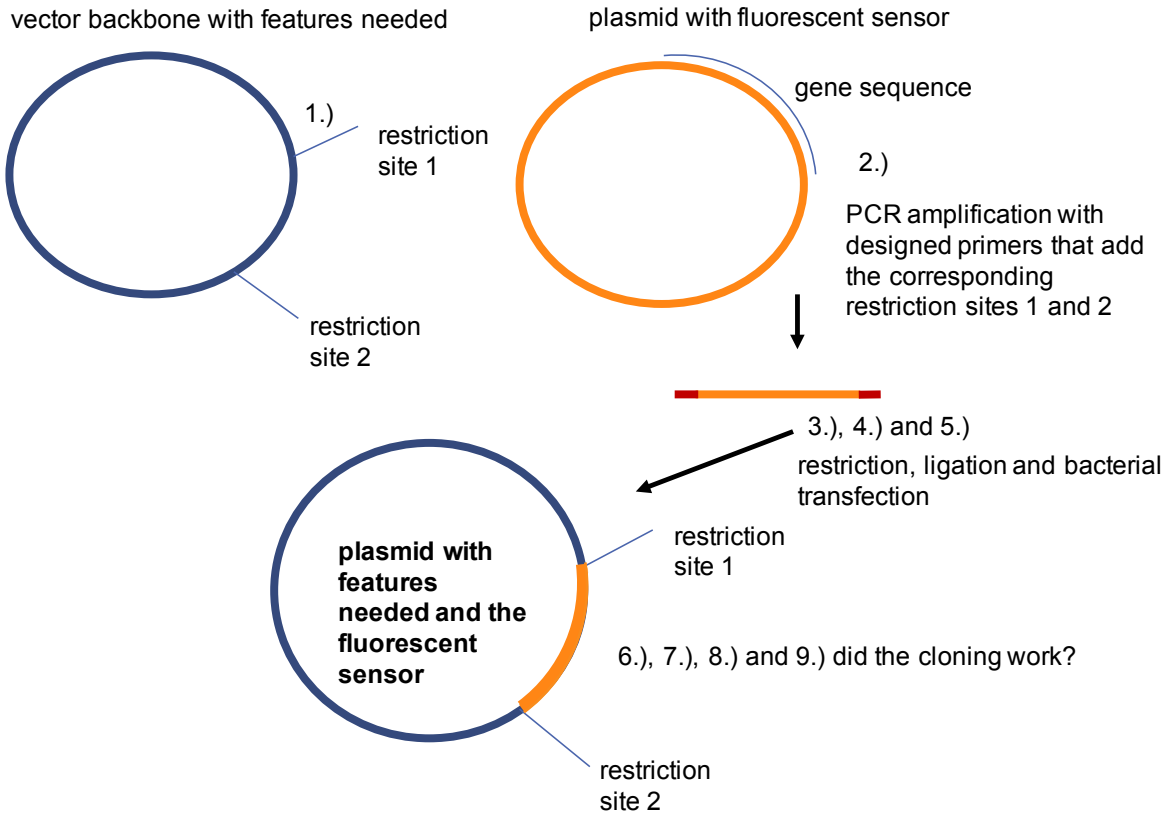

Figure 8.1 The cloning strategy

1.) Identification of two unique restriction sites in the vector backbone in between the fluorescent sensor was cloned **2.)** PCR for gene amplification with designed primers that added the restriction sites identified in **1.)** to the PCR product. **3.), 4.)** and **5.)** Restriction of the vector backbone plasmid and the PCR products with the restriction enzymes cutting at the restrictions sites identified in **1.),** ligation reaction to insert the PCR product into the backbone vector and transfection of bacteria with the ligated plasmid. **6.), 7.), 8.)** and **9.)** bacterial preparation and check if cloning had worked.

Detailed explanation of steps in Fig.8.1:

1.) The two unique restriction sites in the vector backbone were SbfI and AscI.
2.) The primers listed in 7.7 were designed to add the restriction sites identified in **1.)** to the gene sequence of each fluorescent sensor. Using these primers, a standard Polymerase-Chain-Reaction (PCR) (Cline, et al., 1996) was performed to amplify the gene. After the PCR, gel electrophoresis with 1% agarose gel (1g agarose per 100ml TBE1X) was performed with the PCR products (adding 10µl Thermo Fisher Scientific 6X loading dye to 50µl PCR product) and subsequently purified with the NucleoSpin® und PCR Clean-up gel purification kit.

PCR components	Volume
EPAC1-camps/cGi500/GCaMP6 10 ng/µl	1µl
Primer forward Sbf1 50 µM	1µl
Primer reverse Asc1 50 µM	1µl
Buffer Pfu Mg^+ Polymerase 10X	5µl
Deoxyribonucleotide Triphosphate (dNTP) 25mM	0,5µl
Nuclease free water	40,5µl
total	50µl

PCR cycle	Temperature	Duration	EPAC1-camps	cGi500	GCaMP6
1	95°C	120sec			
2	35 repeats				
	A.) 95°C	30sec			
	B.) Annealing Temperature (AN)	30sec	AN 58°C	AN 65°C	AN 63°C
	C.) 72°C	Extension Time (ET)	ET 120sec	ET 135sec	ET 135sec
3	72°C	600sec			

3.) The vector backbone plasmid and PCR products were restricted with the restriction enzymes cutting at the restriction sites identified in **1.)** All restrictions were performed according to the instructions provided with the enzymes. After the digestions, the samples run on a 1% agarose gel (1g agarose per 100ml TBE1X) to check if the restriction had worked. An example is shown in 9.1. Then the band was cut at the desired size and gel purified with the NucleoSpin® und PCR Clean-up gel purification kit.
4.) The ligation reaction was performed with the room temperature protocol of the T4 DNA ligase (see 7.3.7) to insert the PCR product of **2.)** into the backbone vector.

5.) Then, bacteria from the DH5α strain were transfected with the ligated plasmid.

Reaction	Volume	Control reaction	Volume
Insert Xng/µl	3µl	Insert Xng/µl	-
Backbone vector ½Xng/µl	2µl	Backbone vector ½Xng/µl	2µl
Nuclease free water	12µl	Nuclease free water	15µl
T4 DNA Ligase buffer 10X	2µl	T4 DNA Ligase buffer 10X	2µl
T4 DNA Ligase	1µl	T4 DNA Ligase	1µl
total	20µl	total	20µl

Ligation/Transfection protocol	
Incubate reaction mix at room temperature	10min
Take 5µl and add it to competent bacteria (see 7.4), then let chill on ice	10min
Heat shock at 42°C	30-40sec
Let chill on ice	2min
Add SOC Medium 250µl	
Incubate at 37°C at 950rpm	
Plate the bacteria (Ampicillin 100 plates)	

6.) After overnight culture (37°C), only bacteria with ampicillin resistance and therefore the ligated plasmid grew on the plate. Minipreps with the transfected bacteria were performed. The ligated plasmid was isolated according to the instructions provided with the QIAGEN® Plasmid Midi Kit.

7.) To check if the cloning had worked, the plasmids were incubated with restriction enzymes that gave specific band patterns when the insert was integrated into the backbone vector. The digestion reaction was run on a 1% agarose gel (1g agarose per 100ml TBE1X) (an example is shown in 9.1).

8.) Successfully cloned candidates were send for sequencing to Eurofins Genomics.

9.) After sequencing, midipreps were performed with the QIAGEN® Plasmid Midi Kit in order to generate a stock of purified new transgene plasmids that were ready to be injected (see 9.1 for detailed sequencing results and which clones were chosen for midipreps). *In vitro* transcription for mRNA synthesis of the Transposase, that needed to be co-injected with the transgene plasmids (see 8.2), was performed with the mMessage Kits from Ambion (see 7.3.6).

8.2 ZEBRAFISH MAINTENANCE AND TRANSGENESIS

The zebrafish were kept under a 14h light, 10h dark cycle at 28,5°C according to the standard conditions as explained in zebrafish: A practical approach (Brand, et al., 2002).

Several approaches are available for introducing transgenes into zebrafish, from the injection of naked DNA (Deoxyribonucleic Acid) to transposon-mediated integration. In particular, the Tol2 transposable element from the medaka fish has been shown to create chromosomal integrations in the zebrafish genome very efficiently, resulting in the development of transgene zebrafish (Kawakami, et al., 2000). Transgene approaches allow the use of tissue-specific promoters to limit gene expression to cells of interest, such as cardiomyocytes (Kawakami, et al., 2016; Suster, et al., 2009). Therefore, the cardiomyocyte-specific *cardiac myosin light chain 2 (cmlc2)* promoter was used in this study. To achieve the introduction of EPAC1-camps, cGi500 and GCaMP6 into the zebrafish, a DNA plasmid containing the fluorescent sensor was injected into the one-cell stage of a fertilized zebrafish embryo.

The sensor then was incorporated into the animal's genome with the help of the Tol2-Transposase, if transposase-mRNA was co-injected and the plasmid DNA was a transposon vector (a vector with two Tol2 sites that the transposase recognizes) (Kawakami, 2005). Integration normally happens after the one-cell-stage, because the cell of the zebrafish embryos divides rapidly. Therefore, the fish showed a mosaic expression and only a few cells expressed the transgene in the injected fish. Because isolated cells expressed the transgenic sensor, the evaluation of subcellular dynamics of cAMP, cGMP and Ca^{2+} in individual compartments of the cell could be done without additional marking of cell boundaries. If the transgene integrates into the genome of the germ cells, the transgene is in the genome of each cell of subsequent generations and a new transgenic line is established. The new transgenic line would express the transgene throughout the heart. A transgenic line allows the imaging of cAMP, cGMP and Ca^{2+} dynamics in multiple experiments under continuous timescales.

The Injections of the genetic fluorescent sensors EPAC1-camps, cGi500 and GCaMP6 into fertilized zebrafish embryos happened at two different developmental stages: at the one-cell stage in order to establish transgene fish lines and after 48 hpf for Fluo-4 AM injections into the pericardium. The injection needles were generated by pulling glass capillaries with a needle puller. The needles were then carefully broken at a point where their diameter was between 0,05mm and 0,15mm with Dumont tweezers under the microscope. This is a common protocol for the preparation of injection needles (Brand, et al., 2002). For the injections of the Fluo-4 AM dye at 2dpf, another step was added in the preparation of injection needles: the needles were beveled, because a bevel facilitated the entrance of the

needle into the tissue and reduces damage. The right amount of beveling was achieved when the needle starts to bend and water was sucked up by capillary action. The angle of the bevel was 50°.

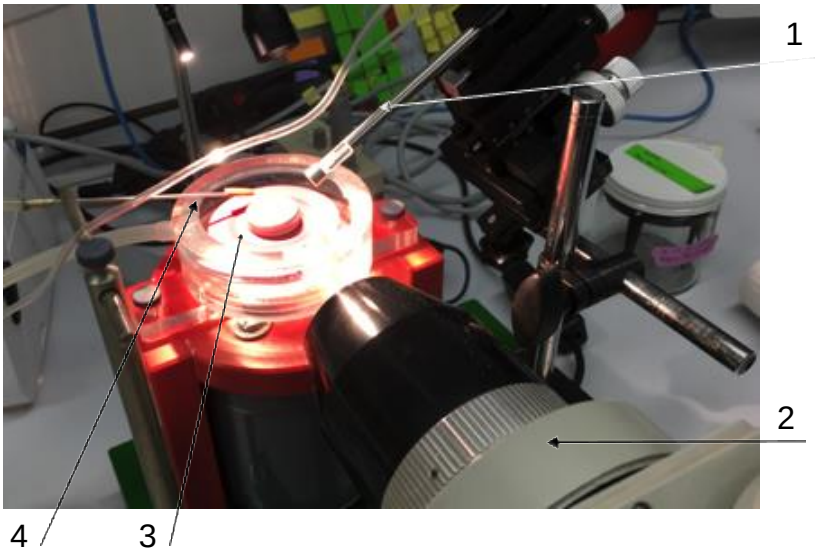

Figure 10.2 The beveller

1. The tube holding the needle. 2. The microscope through which the needle is shown with the appropriate magnification to follow the correct bevel of the needle. 3. The spinning rubber which is covered with water to smoothen and cool the surface and on which the tip of needle was positioned for beveling. 4. The pipe along which the water drops onto the rubber to smoothen and cool the surface.

Zebrafish varied in their quality of eggs and also in the amount of eggs that they laid. To maximize the probability to harvest good embryos for the injections, two different Wild Type (WT) fish strains for each injection- session were simultaneously used: AB from the WT-service from the CRTD and WIK type zebrafish from Christopher Antos stocks. The pairing and harvesting of embryos itself was carried out according to the protocols described in: Zebrafish: A practical approach (Brand, et al., 2002).

Injections into fertilized zebrafish embryos were easier to perform using a mold in which the embryos sunk in to prevent their free movement in the water (see Fig. 10.3, page 30). For one-cell injections, embryos were placed in a mold with 150 individual holes (see “B” in Fig. 10.3, page 30). For pericardial injections, a mold with six grooves was used. Both the grooves and the individual holes have steep walls on one side and flat walls on the other to facilitate needle approach. For preparing the molds, the following protocol provided by Brand et al. was used: 1% agarose in E3 was boiled, cooled for 3minutes, then poured into a petri dish with the template for the molds laid on top. If the agarose was solid, the template could be removed and the mold was ready to use (Brand, et al., 2002).

One-cell stage injections

In order to introduce the genetic fluorescent sensors EPAC1-camps, cGi500 and GCaMP6 into the zebrafish, the plasmid containing the sensor was injected into fertilized zebrafish embryos at one-cell stage. Maximum 60 embryos from each clutch (hold watery in E3) were placed onto the corresponding mold and distributed evenly with a long pipette tip. After putting the mold under the microscope and ensuring the right settings for the needle position,

DNA was injected from the side at the edge between cell and yolk targeting the cell with a volume of 1nl. The injection-setup is shown in Fig. 8.3.

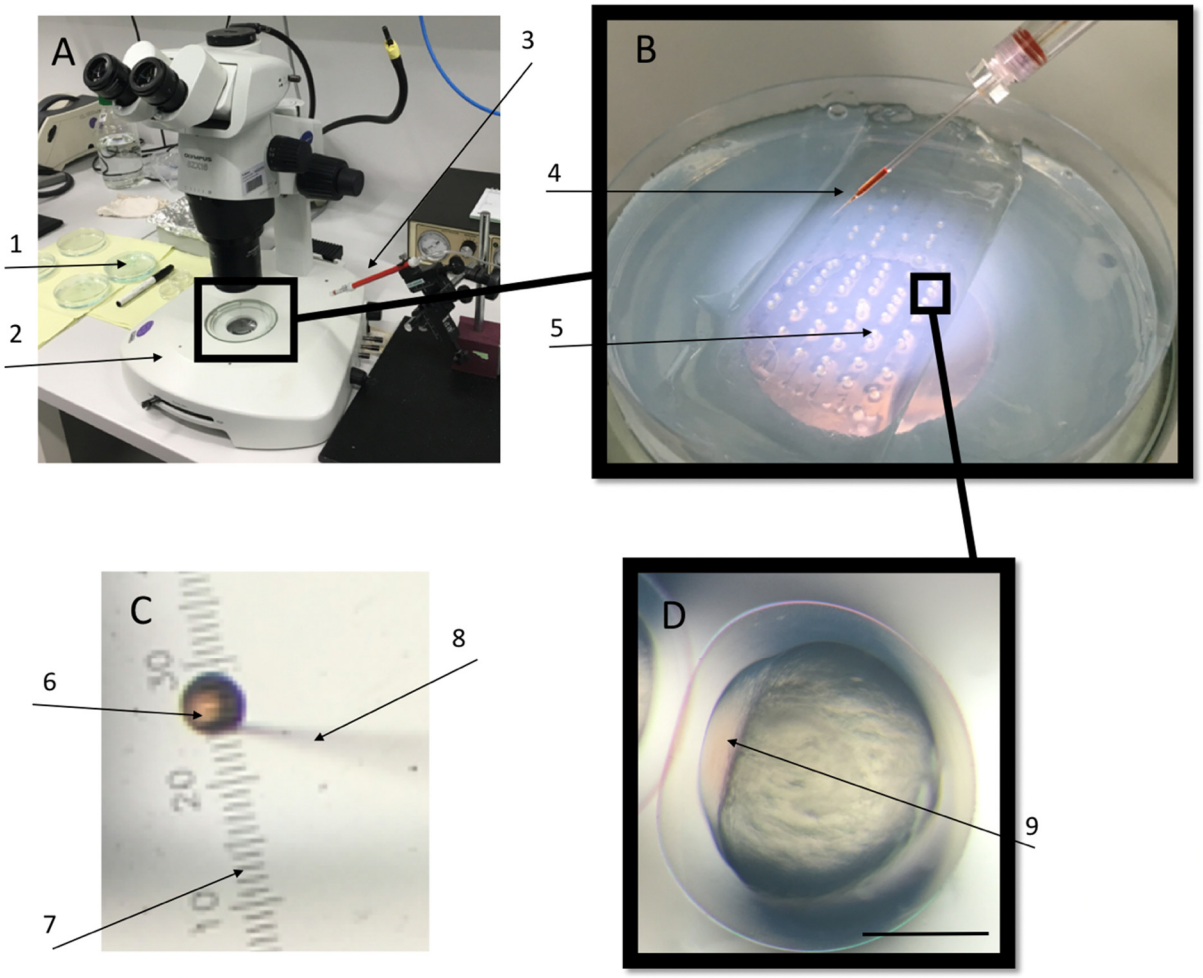

Figure 8.3 The injection setup

A. 1. Petri dish with fertilized embryos in E3 2. The microscope 3. The micromanipulator **B.** Magnified area depicted in A 4. The needle with the injection solution 5. Fertilized embryos on agarose mold **C.** Calibrating the injection volume as described by Brand et al.; A drop of solution at a magnification of 4 that covers 5units on the scale equals 1nl (Brand, et al., 2002) 6. 1nl drop 8. The needle (due to focus on the 1nl drop, only the shape of the needle is visible) 7. Scale of the microscope **D.** Magnified area from B shows a fertilized embryo (scale bar 0,5mm). 9. Injected cell, visible by reddish color. Rest is yolk.

DNA injections at one-cell stage
X µg DNA (concentration with best expressing/toxicity ration has to be found out for each individual construct)
300 µg RNA Transposase
1 µl Phenolred
Fill up with nuclease free water to 10 µl

A high concentration of the plasmid injected into the embryos is toxic for the fish and in low concentrations the gene is very poorly expressed. The optimum plasmid DNA concentration varies between each construct, has to be determined individually and will be explained in 9.2. From the protocol shown on the left, 1 nl DNA are injected into the cell of an one-cell stage fertilized embryo (see “D” in Fig 8.3). For RNA injections, 10 nl are injected into the yolk.

8.3 MOUNTING AND IMAGING

After the injections, genetic fluorescent sensor expression was checked at 48 hpf with a fluorescence light microscope (Olympus MVX10). Fish expressing the sensor in individual cardiomyocytes were then gently dechorionated (“D” in Fig. 8.3 shows cell and yolk, around is the chorion) by opening and then removing the chorion with Dumont tweezers under the stereo light microscope (Olympus SZX16). Dechorionation was important to facilitate Blebbistatin (dissolved in DMSO) (see 5.6) diffusion into the cardiomyocytes for immobilizing the heart for the FLIM-FRET-measurements. After blebbistatin and eventual forskolin/SNAP incubation (see 5.6), the fish were mounted onto the Laser Scanning Confocal Microscope, which was connected to the FLIM-detector. A zebrafish cardiomyocyte is 5 µM long and confocal microscopy enabled a spatial resolution up to individual compartments in the cell. For mounting, the fish were placed in an aqueous drop (0,05ml) containing the incubation solution (blebbistatin with or without forskolin/SNAP) onto a coverslip that was glued underneath an object slide with a hole in the middle (see B in Fig 8.4). Then the object slide was put onto the mount of the inverse confocal microscope. The objective was a 40X water objective. If drifting of the fish within the water droplet occurred, 2% methylcellulose in E3 solution was used to gently fix the tail of the fish onto the cover slip.

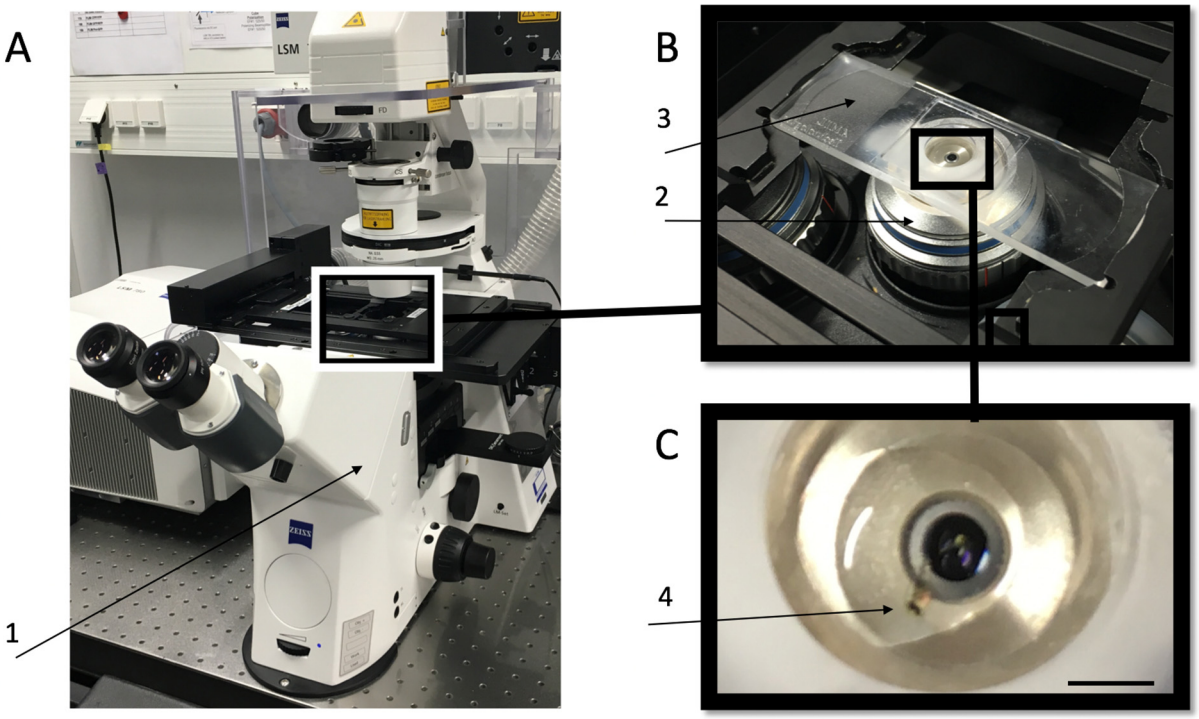

Figure 8.4 The mounting of the zebrafish embryo

A: 1. The inverse laser scanning confocal microscope. B is the magnified area out of A. 2.) the 40X water objective. 3. The coverslip. The black box marks an area that is shown magnified in C. It also indicates the hole under which the cover slip is glued. 4. A zebrafish embryo in an aqueous drop on the cover slip. Scale bar 3mm.

The confocal microscope was controlled by the Zen Black 2011 software. The excitation wavelength was 475nm (Laser Diode, pulsed), and for the detection a dichroic beamsplitter matching the spectral properties of the FRET sensors (CFP/YFP) was installed. The zoom was fixed to 5, the resolution was 528*528 pixels and the bidirectional scan was used. After adjusting the focus to a single sensor expressing cardiomyocyte, FLIM was activated. The FLIM software run on a separate computer. The fluorescent probe subsequently appeared on the screen of the separate computer with the FLIM-SPCM software. To analyze the donor fluorophore, the short wavelength analysis window was selected and the data sent to SPCImage. Settings in SPCImage: The Chi value (X^2) is the result of a statistical hypothesis test performed by SPCImage and represents the accuracy of the fit curve. The best accuracy was achieved if X^2 equaled 1 (Becker and Hickl, 2015). The shift is a mathematical consideration of the instrumental response function, which is the function the FLIM system would record when it detects the laser pulse directly. In order to achieve the most accurate X^2, the shift had to be changed until the closest X^2 to 1 is reached (Becker and Hickl, 2015).

The scatter indicates the amount of scattered excitation light detected and is used to fit data in which scattering plays a role, such as second harmonic components in multiphoton FLIM. Scattering did not play a role in this study, so the scatter was kept at 0 as recommended by Becker and Hickl (Becker and Hickl, 2015).

8.4 STATISTICAL ANALYSIS

The data was processed with Microsoft Excel. Graphs and the statistical analysis were performed with GraphPad Prism 7.

Gaussian distribution was checked with the Shapiro-Wilk normality test. The appropriate unpaired student T-test was used for evaluating the significance of the means of two samples and the one-way Analysis of Variation (ANOVA) Newman-Keuls multiple comparisons test for evaluating the significance of the means of more than two samples.

In the figures depicted in this thesis, the significance is indicated by the p-value according to the New England Journal of Medicine style ranging from not significant (n.s) to significant (*: $p < 0.05$, **: $p < 0.01$, ***: $p < 0.001$). Numerical data is expressed as mean ± SEM.

9. RESULTS

In this study, I cloned the fluorescent sensors EPAC1-camps, cGi500 and GCaMP6 into a backbone vector allowing the introduction of these sensors into zebrafish. Using transparent zebrafish larvae expressing the sensors in individual cardiomyocytes, I established a protocol to use confocal microscopy combined with FLIM to analyze the subcellular distribution of cAMP and cGMP. Moreover, I established a protocol to analyze subcellular Ca^{2+}. I concluded with a functional characterization of the sensors and scientific results.

9.1 THE CLONING RESULTS

In order to merge the gene for each fluorescent sensor with the vector backbone carrying the features needed (see 8.1), I restricted both the vector backbone and the PCR-amplified sensor genes with SbfI and AscI. Figure 9.1 shows the restriction reaction for the vector backbone *cmlc2*/Tol2.

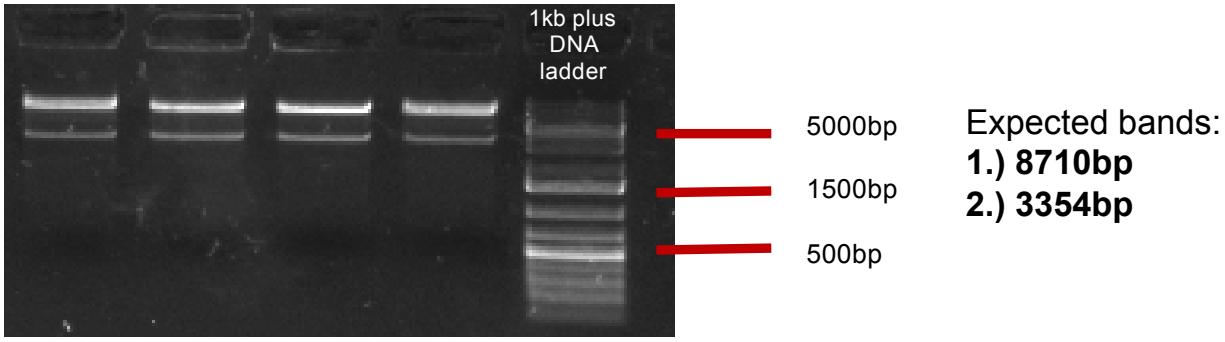

Figure 9.1 The plasmid *cmlc2*/Tol2 restricted with SbfI and AscI

All band patterns match the expected bands as indicated on the right. Expected bands were determined by the bp and subsequent calculation of how many bp lay in between the two restriction sites.

After the ligation reaction of vector backbone and each of the fluorescent sensor, transfection and Minipreps (step 4-6 in 8.1), I incubated the cloned plasmids with restriction enzymes that gave specific band patterns when the insert was integrated into the backbone vector: SmaI and AatII were unique cutters in the Tol2 + EPAC1-camps construct; SmaI cut in the EPAC1-camps sequence and AatII in the Tol2 vector backbone region. Run on an agarose gel showed

- a simply linearized plasmid, if EPAC1-camps was not integrated into the vector (as SmaI could not cut) or
- two bands, one at 8568bp and one at 2076bp (together 10644bp, the expected lengths of the Tol2 vector plus integration of EPAC1-camps), if EPAC1-camps was successfully integrated into the Tol2 vector (see Fig. 9.2).

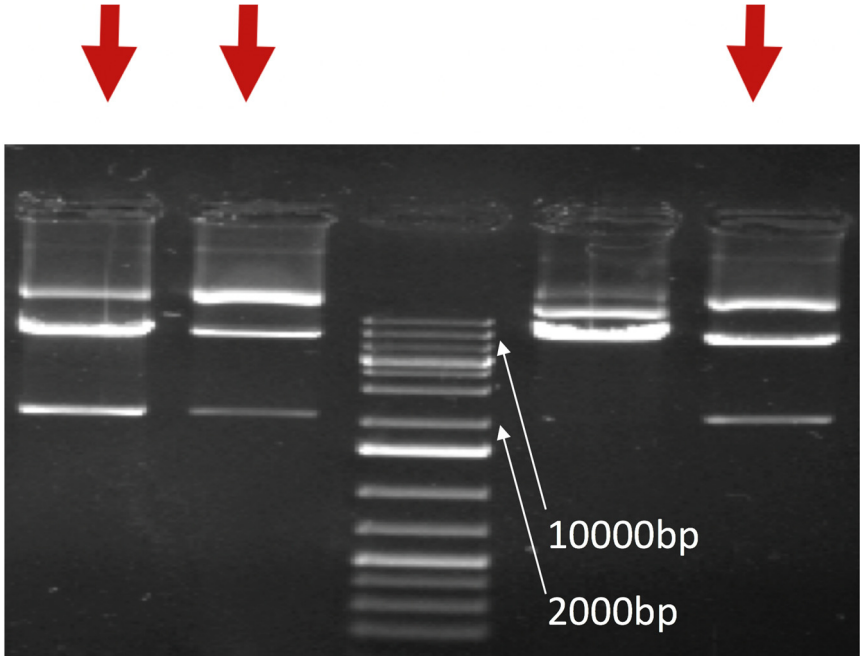

Figure 9.2 The control reaction for the EPAC1-camps ligation

Four clones are shown in separate lanes of the agarose gel, in the middle DNA ladder. Red arrows mark the clones showing a band pattern that indicates successful cloning (one band at 8568bp and one at 2076bp).

For cGi500 cloning I used EcoRI (2 cutting sites). For GCaMP6 cloning I used NHEI and SalI.

After the cloning, the plasmids were sequenced by Eurofins genomics. Then, I blasted the nucleotide sequence provided by Eurofins genomics with the nucleotide sequence of the genetic sensors in the original plasmids that I used for cloning (see 7.5). Table 9.1 shows the clones of each construct that I sent for sequencing, the number of sense mutations I found during the blast and the type of sense mutations. All EPAC1-camps clones showed the same three sense mutations that were already present in the original plasmid. I chose to inject Clone number 4, because it showed no additional mutations to these three sense mutations. From the cGi500 and GCaMP6F clones, I chose to proceed with the clones that did not show any mutations (Clone 4B for cGi500 and Clone1 for GCaMP6F). In this study, I focused on GCaMP6F, because GCaMP6F enables the tracking of fast responses of Ca^{2+} signaling, such as contraction (see 5.7.1). For the investigation of long lasting responses of Ca^{2+} signaling, such as changes in gene expression, GCaMP6M/S can be used in future studies (see 10.5).

Table 9.1 The sequencing results

Each of the sensors, EPAC1-camps, cGi500 and GCaMP6 were cloned into the miniTol2cmlc2 vector backbone. The table shows each individual clone and number and type of sense mutations. The grey marked clones are the ones used for injections.

construct	Sense mutations: number and type
EPAC1-camps Clone 1	**5** = Deletion of glutamic acid, Asparagine to Histidine, Lysine to Arginine (+ Tryptophan to Tyrosine, Valine to Glycine)
EPAC1-camps Clone 3	**4** = Deletion of glutamic acid, Asparagine to Histidine, Lysine to Arginine, (+ Proline to Alanine)
EPAC1-camps Clone 4	**3** = Deletion of glutamic acid, Asparagine to Histidine, Lysine to Arginine
cGi500 Clone 4A	**2** = Alanine to Threonine, Deletion of Cysteine → frameshift
cGi500 Clone 4B	none
cGi500 Clone 7	**1** = Deletion of Threonine → frameshift!
GCaMP6F Clone 1	none
GCaMP6M Clone 1	**1** = Lysine to Glutamic acid
GCaMP6M Clone 2	**3** = Lysine to Glutamic acid (+ Glutaminc acid to Lysine, Deletion: of Histidine)
GCaMP6M Clone 4	**2** = Lysine to Glutamic acid (+Threonine to Proline)
GCaMP6S Clone 1	**1** = Lysine to Histidine
GCaMP6S Clone 2	**3** = Lysine to Histidine (+ Arginine to Glutamine, Glutamic acid to Lysine)
GCaMP6S Clone 3	**4** = Lysine to Histidine (+M to Glycine, Lysine to Serine, Lysine to Glutamic acid)

Each of the marked clones is shown graphically and by the sequence of their sensor basepairs in the supplement.

9.2 TRANSGENESIS IN THE ZEBRAFISH: INJECTION CONCENTRATIONS

In order to introduce the fluorescent sensor into the zebrafish, I injected them into fertilized zebrafish embryos (see 8.2). I did an analysis with increasing concentrations of DNA to find out how much I should optimally use in order to have a minimal toxic effect and maximal gene expression. These experiments revealed that 200 ng should be used for the EPAC1-camps, 250 ng for the cGi500 and 300 ng for the GCaMP6 constructs (see Figure 9.3, for numerical data see 17.4 (supplement)). The protocol, which I used for the injections, is shown in 8.2, with “200 ng” for Epac1-camps and the other concentrations, respectively, representing “X”. It is a standard protocol that was kindly provided to me by the lab of Dr. Caghan Kizil.

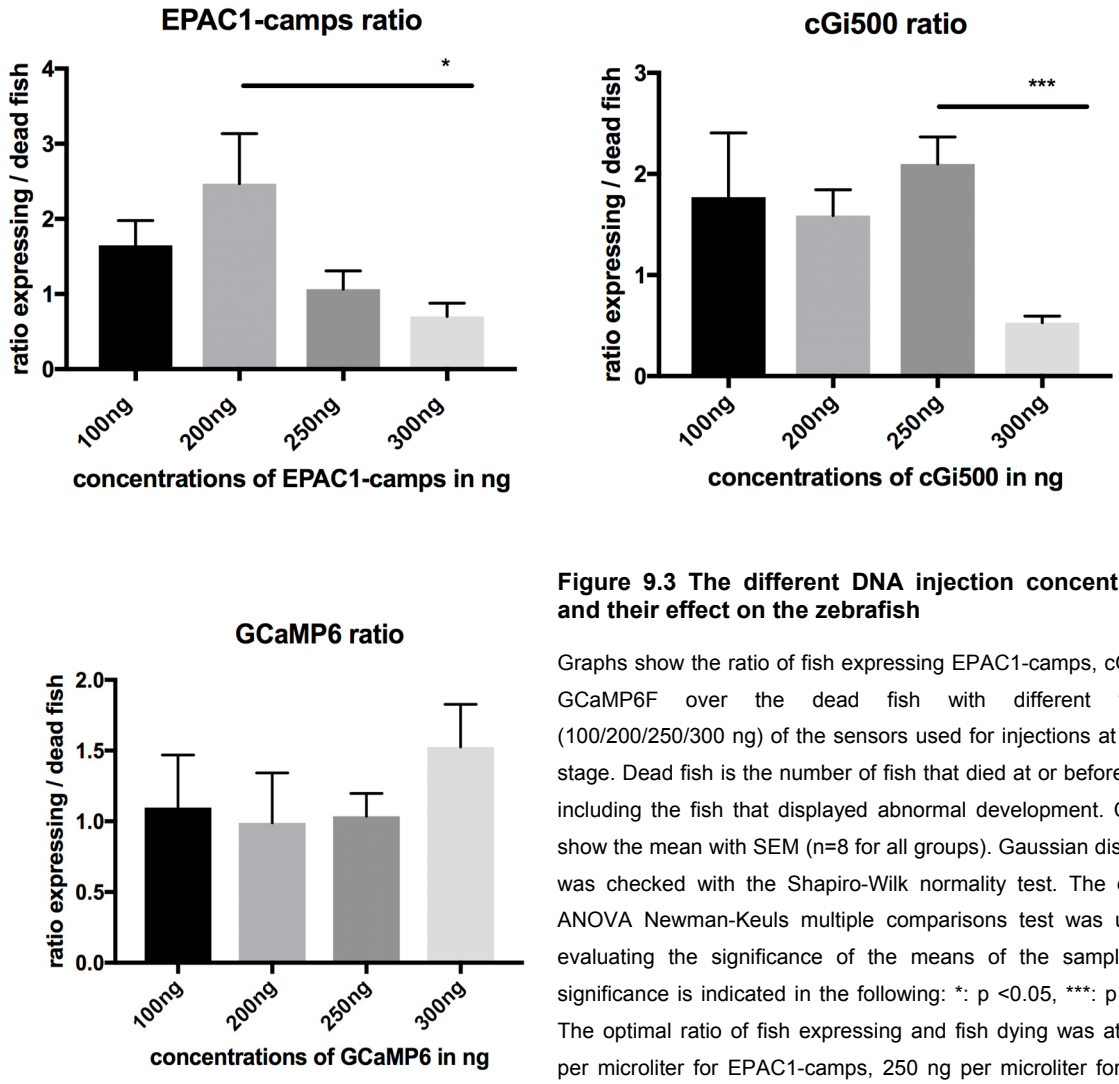

Figure 9.3 The different DNA injection concentrations and their effect on the zebrafish

Graphs show the ratio of fish expressing EPAC1-camps, cGi500 or GCaMP6F over the dead fish with different volumes (100/200/250/300 ng) of the sensors used for injections at one-cell stage. Dead fish is the number of fish that died at or before 48 hpf, including the fish that displayed abnormal development. Columns show the mean with SEM (n=8 for all groups). Gaussian distribution was checked with the Shapiro-Wilk normality test. The one-way ANOVA Newman-Keuls multiple comparisons test was used for evaluating the significance of the means of the samples. The significance is indicated in the following: *: $p < 0.05$, ***: $p < 0.001$) The optimal ratio of fish expressing and fish dying was at 200 ng per microliter for EPAC1-camps, 250 ng per microliter for cGi500 and 300 ng per microliter for GCaMP6F. For the data tables see 17.4 (Supplement).

9.3 THE SELECTION OF ZEBRAFISH FOR FLIM-FRET

After the injections, I performed FLIM-FRET at 48 hpf. However, before performing FLIM-FRET, I checked the fish with a stereo light microscope (Olympus SZX16). Fish that were trembling or did not swim actively were excluded from the measurements. Fish were also excluded that showed malformations (see Fig. 9.4).

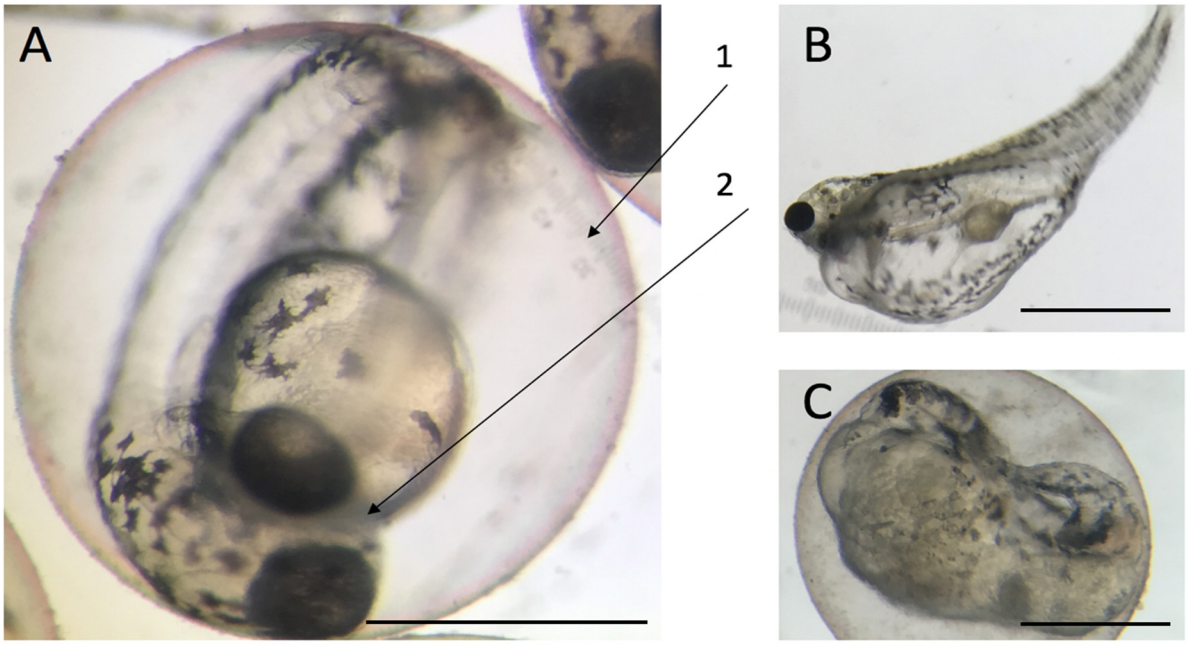

Figure 9.4 The zebrafish at 48 hpf and malformations

A: A healthy 48 hpf zebrafish. 1: the chorion protecting the embryo, 2: the location of the heart, B: A 48 hpf zebrafish suffering edema, C: a malformed zebrafish at 48 hpf. The lives of animals showing malformations or sickness as in B/C were humanely ended immediately to end potential suffering according to the current protocols available for euthanasia in zebrafish (Murray, et al., 2011; Wilson, et al., 2009). Scale bar A,B,C 1mm.

Then I took the zebrafish with sensor expression in individual cells to perform FLIM-FRET.

9.4 THE INCUBATION AND MOUNTING FOR FLIM-FRET

Because heart movement prevented good resolution during the confocal imaging, I used blebbistatin to stop the embryo`s heart (see 5.6) for the imaging. Unfortunately, I could not use the protocols as described by Jou et al. (Jou, et al., 2010). Jou et al. used a 1-10 µM concentration of blebbistatin in their perfused zebrafish hearts. This concentration showed no effect in zebrafish 48 hpf embryos *in vivo*. Instead, the heart rate did not change. I performed an experiment treating the zebrafish embryos with an increasing concentration of blebbistatin and identified the time it took for the fish until the contraction of the heart was completely blocked. I confirmed the immobilization of the heart visually using a stereo light microscope (Olympus SZX10). Interestingly, a concentration above 200 µM did not affect the time it took for heart immobilization. Thus, I worked with a concentration of 200 µM. However, the time it took for each individual embryo to stop heart movement varies significantly. Consequently, I applied the following standard: I waited for complete heart immobilization before performing the measurements.

Blebbistatin is deactivated by light-exposure. This information is provided with the instruction manual from Sigma (see blebbistatin in chemicals in 7.3). In my experiments, the laser power used by the microscope apparently also deactivated blebbistatin, resulting in a decreased time window in which I could perform the measurements. Consequently, I took images only for a short period of time until the heart was moving again and then took the next fish. Figure 9.5 shows an example of how movement of the heart interfered with the measurements.

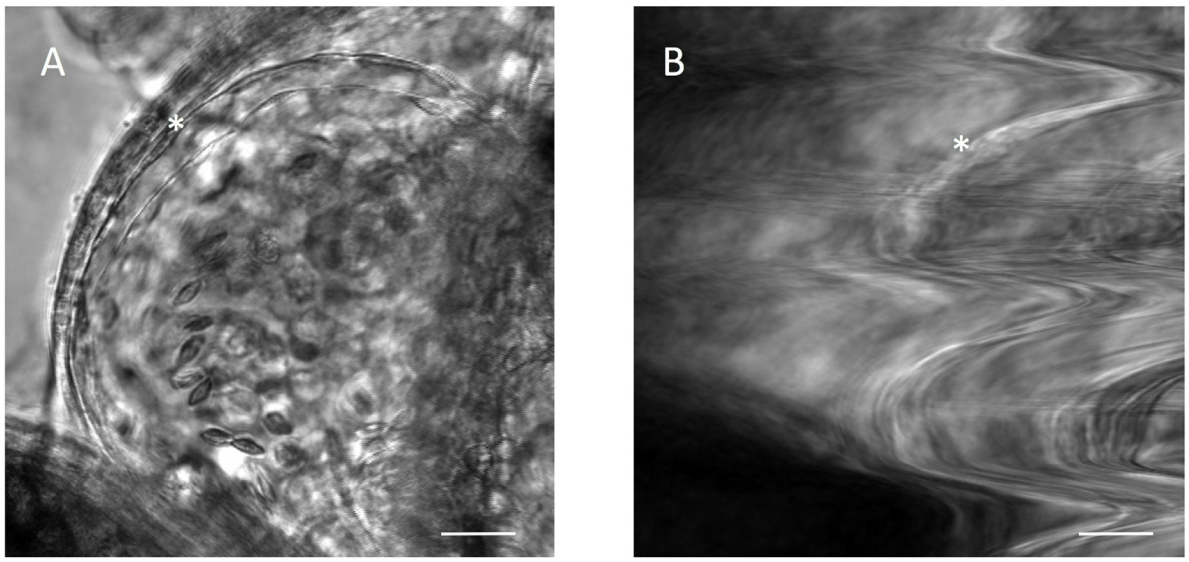

Figure 9.5 An immobilized and a moving zebrafish heart under the confocal microscope

A: The atrium of a 48 hpf zebrafish embryo. A cardiomyocyte is labeled through a star (*). It is in the outer layer, the myocardium. The inner layer, the endocardium is also clearly visible. Erythrocytes fill the atrium. B shows the same fish and atrium as in A, but inactivation of blebbistatin led to significant movement of the heart. Individual cardiomyocytes appear blurry. Scale bar 5 µM.

A standardized protocol must be applied to compare results from different measurements. However, the zebrafish organism is very complex and varies between individual organisms. To give an example, eight minutes of incubation time with blebbistatin might immobilized the heart in one zebrafish, but in another fish heart immobilization takes 25min. Furthermore, hatches from different parents vary in terms of egg- and embryo quality, and individual fish responded differently to microinjection. Evidently, criteria must be found that ensured the well-being of the embryo for data analysis. Fish must not be used for measurements if they showed signs of abnormality, because these fish might have had an altered physiology (and therefore altered levels of intracellular cAMP and cGMP). Finally, this was the protocol that worked best for me:

I first incubated the fish in a 200 µM blebbistatin in E3 solution. After 8min of blebbistatin incubation, I checked in a 5min distance on the microscope if the heart was immobilized. If drugs were applied (forskolin for raising cAMP or SNAP for raising cGMP), I added the drugs

(for the concentration see 9.8) after the heart was immobilized and then had a two-minute incubation time.

9.5 THE ANALYSIS OF THE FLIM-FRET DATA WITH SPCIMAGE

The more photons were collected by FLIM-FRET for the measurements, the better was the quality of the analysis. The threshold defines a minimum number of photons that are used for the decay analysis. This is used to suppress dark pixels and improves the analysis. I used a threshold of 5, because data drawn from below 5 photons per pixel is not likely to be accurate (Becker and Hickl, 2015). Everything below the threshold was not taken into the measurement calculation. This is shown in Fig. 9.6.

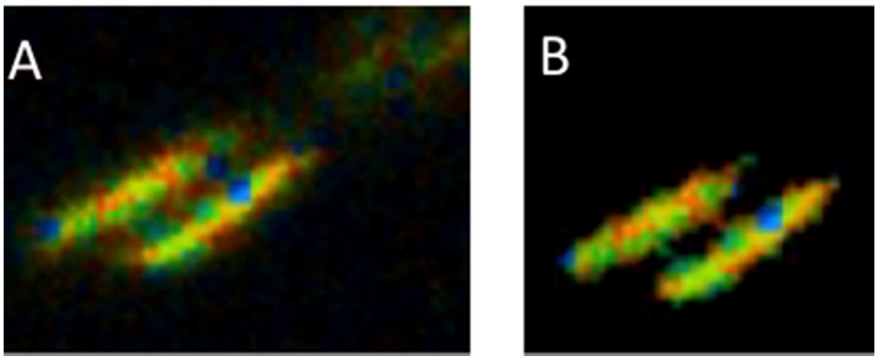

Figure 9.6 The threshold in SPCImage

A: cardiomyocytes before applying the threshold B: threshold eliminates pixels with non sufficient number of photons for the analysis

I defined a region of Interest (one cardiomyocyte), because data from single cardiomyocytes were aimed to be generated (see Fig 9.7). I set the legend for the pseudo-colored representation of the fluorescent lifetime to cover exactly all values (min-max) collected during the experiments but not to exceed this min/max range, because that would dilute individual differences in the lifetimes in the pseudo-colored matrix. Subsequently, a range of 700-200 ps as fluorescent lifetimes for EPAC1-camps and 1200-220 ps for cGi500 was used (see Fig. 9.7).

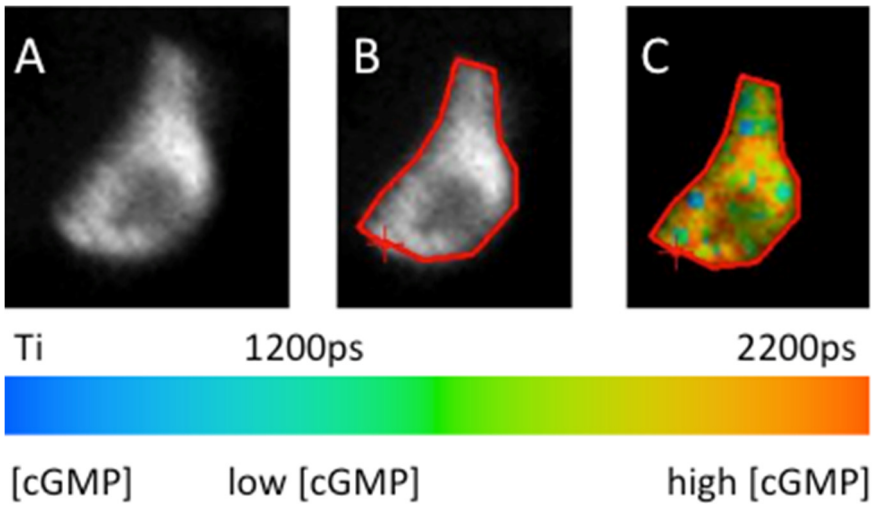

Figure 9.7 The region of interest in SPCImage

A. One cardiomyocyte (confocal microscopy, analysis with SPCImage) **B.** Drawing around the cardiomyocyte **C.** The pseudo-colored image (legend underneath) within the region of interest.

I then performed another check with the confocal microscope used for FLIM-FRET: fish with malformations that did not show in the stereo microscope (see Fig. 9.4) were excluded. Malformations correlated with increased (auto) fluorescence (see Fig. 9.8), which was also detectable with the confocal microscope.

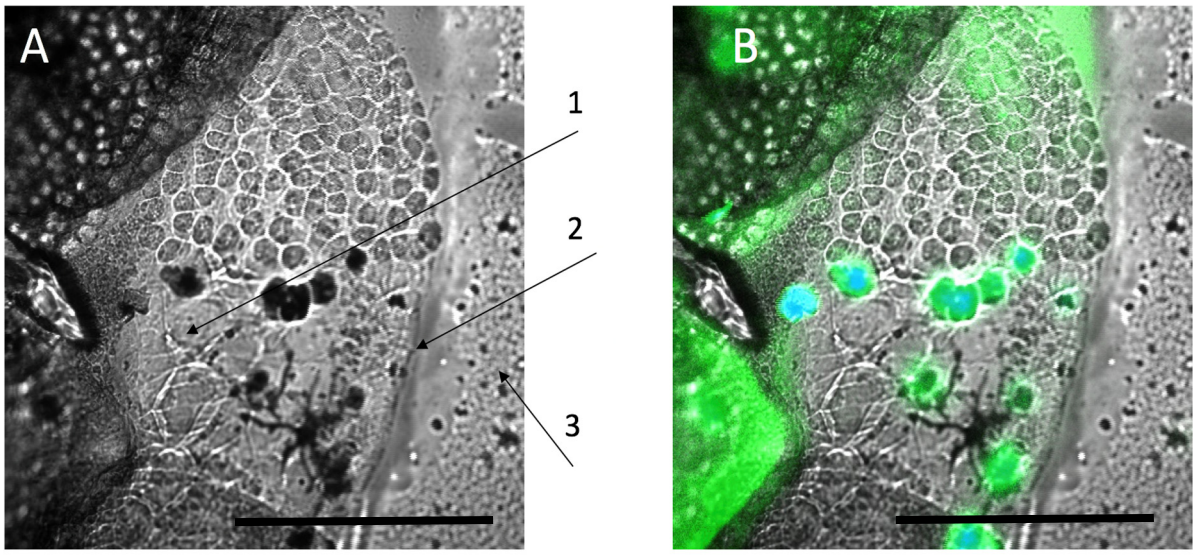

Figure 9.8 Autofluorescence in a zebrafish heart

A: Brightfield confocal image of zebrafish heart. 1: dissolving cell structure, 2: pericardium 3: dissolved cells integrating into solution medium, B: fluorescent confocal image of A.. Scale bar 100 µM

Artificial fluorescence and samples contaminated with autofluorescence existed also without abnormal anatomy. These samples had to be eliminated from the analysis, too, not alter the results (Becker and Hickl, 2015). The first step was to evaluate the confocal picture for a non-specific (auto) fluorescent layer (see “A” in Fig. 9.9). The second and objective step was to use the FLIM analysis program SPCImage to detect artificial and altered probes: If the long lifetime component (number 2 in “B” in Fig. 9.9) exceeded 2500, the sample was not in the physiological range of the sensor, and subsequently not included into the data acquisition.

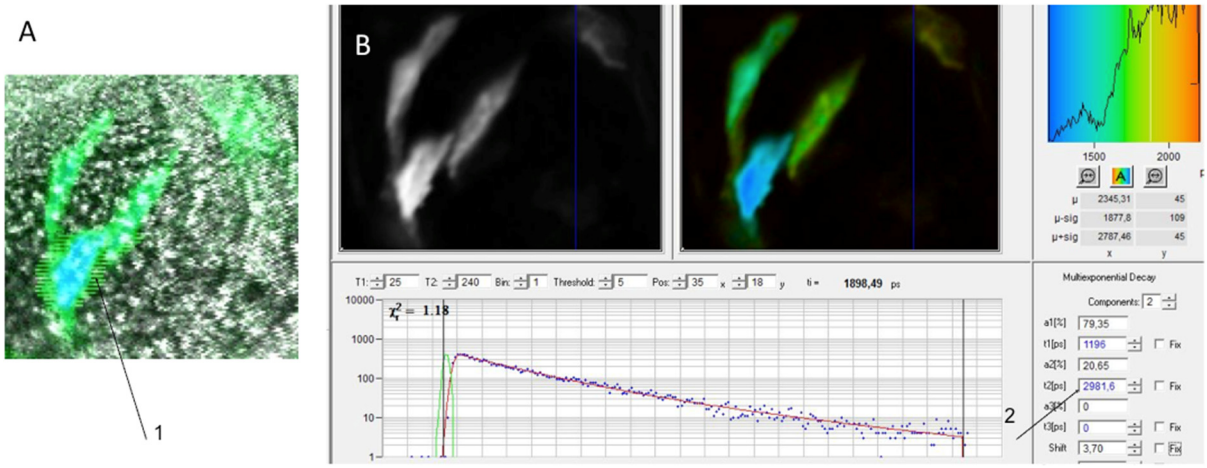

Figure 9.9 The detection of artificial fluorescence

A: confocal image 1: oversaturation indicating artificial fluorescence B: Picture of A analyzed with the FLIM software SPCImage. 2: long lifetime component furthermore indicates artificial fluorescence

9.6 THE EFFECT OF DMSO ON THE FLUORESCENT LIFETIME TI

In order to immobilize the heart, I incubated the zebrafish in a 200 µM blebbistatin solution. blebbistatin was dissolved in 100% DMSO, which can be toxic for the fish, because it disrupts lipid bilayers of cell membranes. During experiments that involved drug treatment, the DMSO percentage I had further increased, because the drugs (forskolin and SNAP, see 5.6) were also dissolved in 100% DMSO. Therefore, I made an experiment evaluating whether an increased DMSO percentage influenced the fluorescent lifetime of the FLIM-FRET-measurements. This was not the case (see Fig. 9.10).

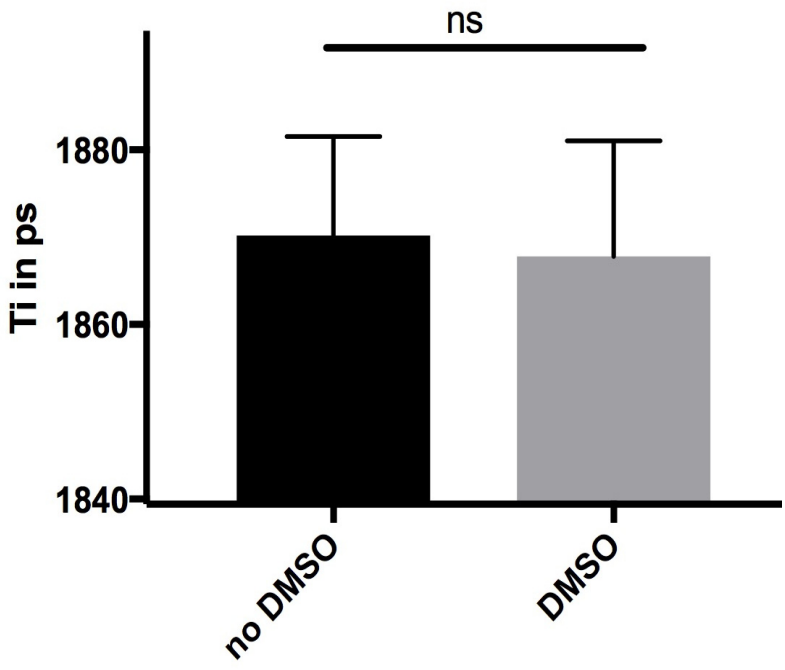

Figure 9.10 The effect of DMSO on the fluorescent lifetime Ti

Graphs show the lifetimes of individual cells expressing the EPAC1-camps sensor. The no DMSP group (n=25 from 8 with was treated with blebbistatin only. The DMSO group (n=15 from 6 fish) was treated with blebbistatin and 100% DMSO in the same amount that was used for 750 µM drug treatment with forskolin/SNAP. Columns show the mean with SEM. Gaussian distribution was checked with the Shapiro-Wilk normality test. The one-way ANOVA Newman-Keuls multiple comparisons test was used for evaluating the significance of the means of the samples. The significance is indicated in the following: ns: not significant.

In the following, I show the results from the FRET-FLIM measurements.

9.7 THE LOCALIZATION OF THE CAMP/CGMP SENSOR IN CARDIOMYOCYTES

Both the EPAC1-camps sensor for tracking cAMP and the cGi500 sensor for tracking cGMP showed mosaic expression in cardiomyocytes of the F_0 generation of the zebrafish. An example is shown in Fig. 9.11. It is important to consider that the images with the confocal microscope indicate that the sensor is expressed throughout the cytosol, but not in the nucleus (see Fig. 9.11 B). Furthermore, as expected in using the *cmlc2* promoter, the sensor is expressed specifically in the myocardium and neither in the epi- nor endocardium (Huang, et al., 2003). Not all cardiomyocytes could appropriately be used for FLIM-FRET. As seen in Fig. 9.12 B/C, sometimes using high resolution confocal microscopy revealed that gene expression was actually weak, although in the fluorescent microscope used for sorting expressing fish cardiomyocytes showed strong expression. Figure 9.13 shows the expression of EPAC1-camps within the different planes of one cardiomyocyte.

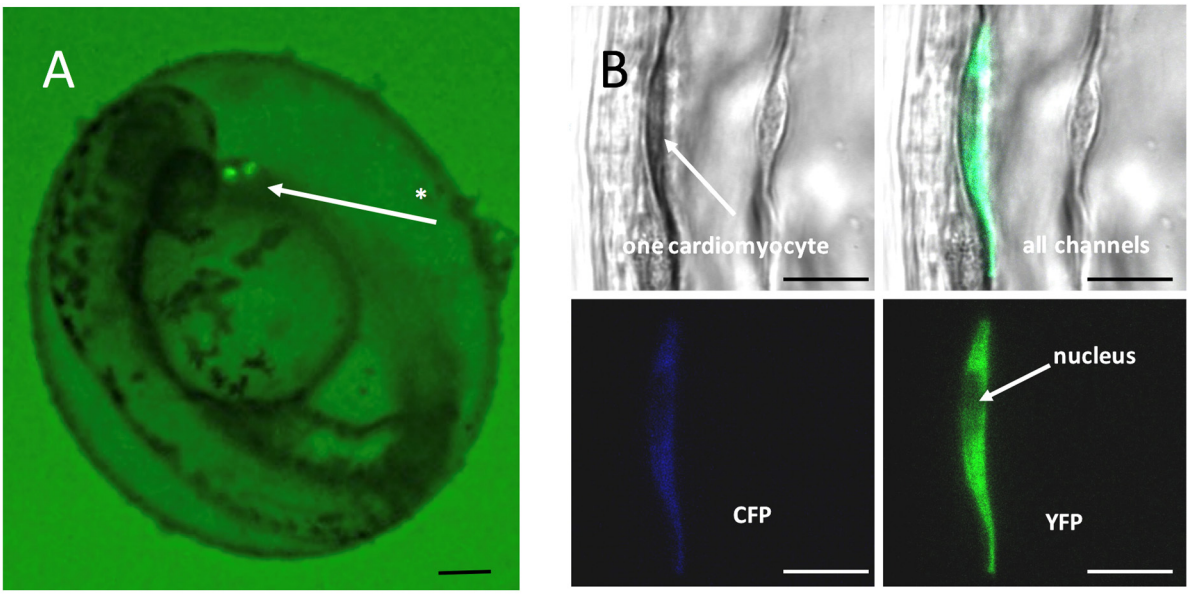

Figure 9.11 EPAC expressed in one cardiomyocyte

A shows an 48 hpf embryo before dechorionation with two clear expressing cardiomyocytes. The same cardiomyocyte imaged with a confocal microscope reveal all the possibility to distinguish between the fluorophores CFP and YFT. The expression of the sensor throughout the cell represents the shape of the cell, indicating the sensor is poorly localized in the nucleus but retained in the cytosol. Scale bar in A: 200 µM. Scale bar in B: 5 µM

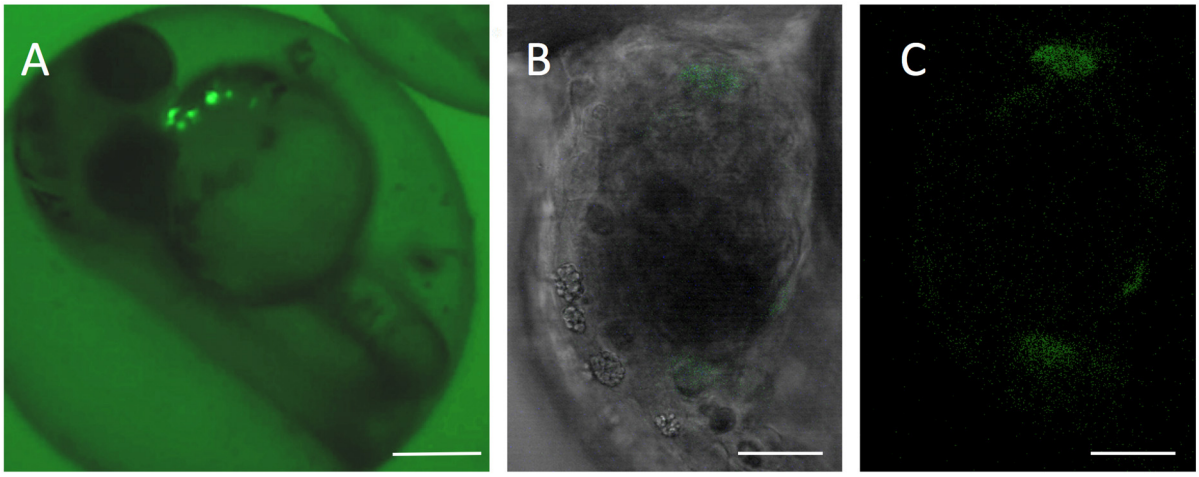

Figure 9.12 cGi500 expressed in cardiomyocytes

A shows an 48 hpf embryo before dechorionation with several clear expressing cardiomyocytes. The same cardiomyocytes imaged with a confocal microscope (B) revealed only diffused expression. In the YFP panel, expression is very weak.

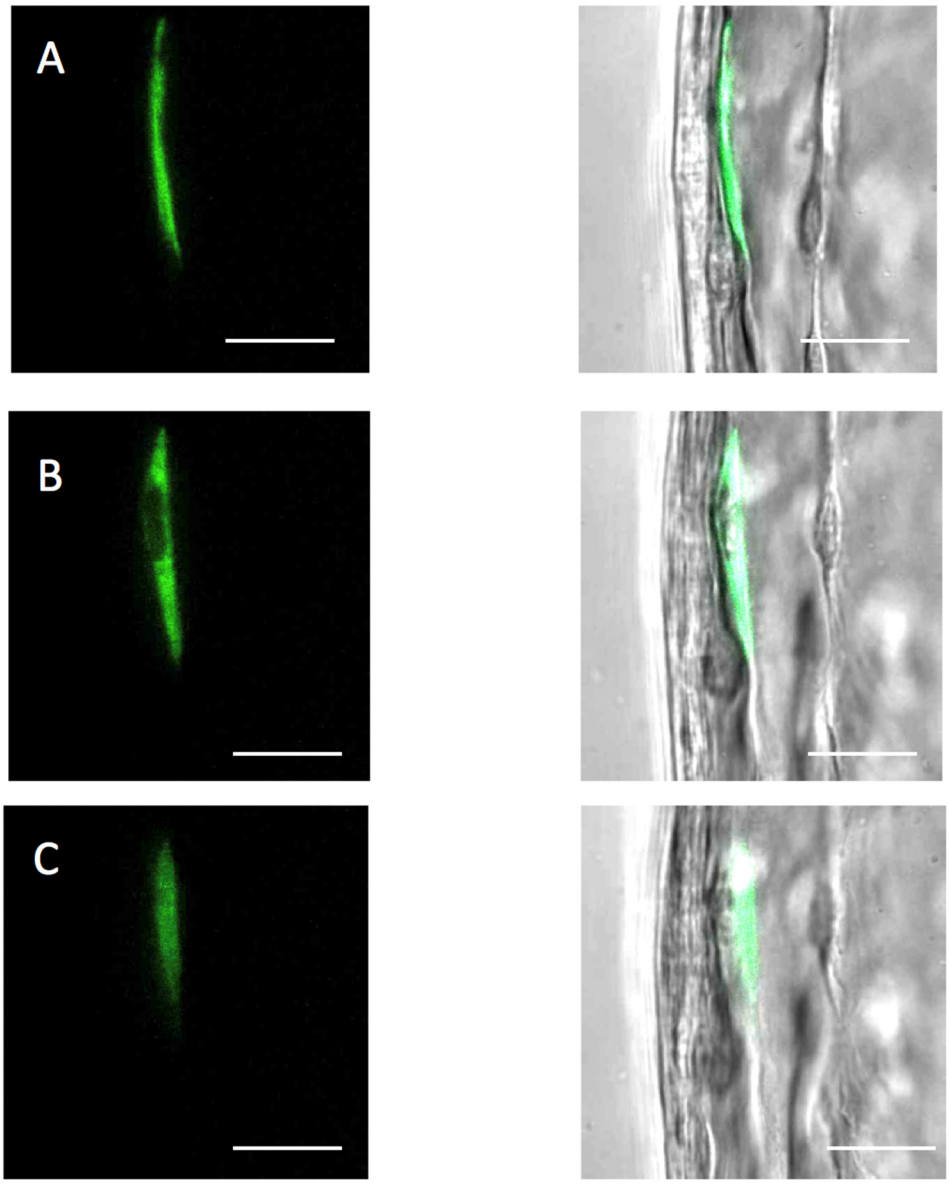

Figure 9.13 A Z-stack of EPAC1-camps expressed in one cardiomyocyte

1-3 show different z-stacks of the same cardiomyocyte with brightfield (on the right) and just the fluorescent channels (on the left). These different planes of the cell show that, depending on the plane, subcellular distributions analyzed in this study come from different areas of the cells. Improvements would involve taking z – stacks from every cell that is imaged, or including localization signals to the cells. Scale bar 2,5 µM.

9.8 CHANGES IN CAMP/CGMP CONCENTRATIONS

A functional characterization includes the evaluation how the fluorescent genetic sensors react to changes in the concentrations of cAMP and cGMP. I treated the fish with increasing concentrations of the cAMP-increasing agent forskolin for EPAC1-camps and the cGMP-increasing agent SNAP (see 5.6 and 8.3).

A preliminary screening showed an increased fluorescent lifetime, Ti, under exposure with forskolin and SNAP for both FLIM-FRET sensors, with best results using a 750 µM solution for incubation (see Fig 9.14 and Fig. 9.15).

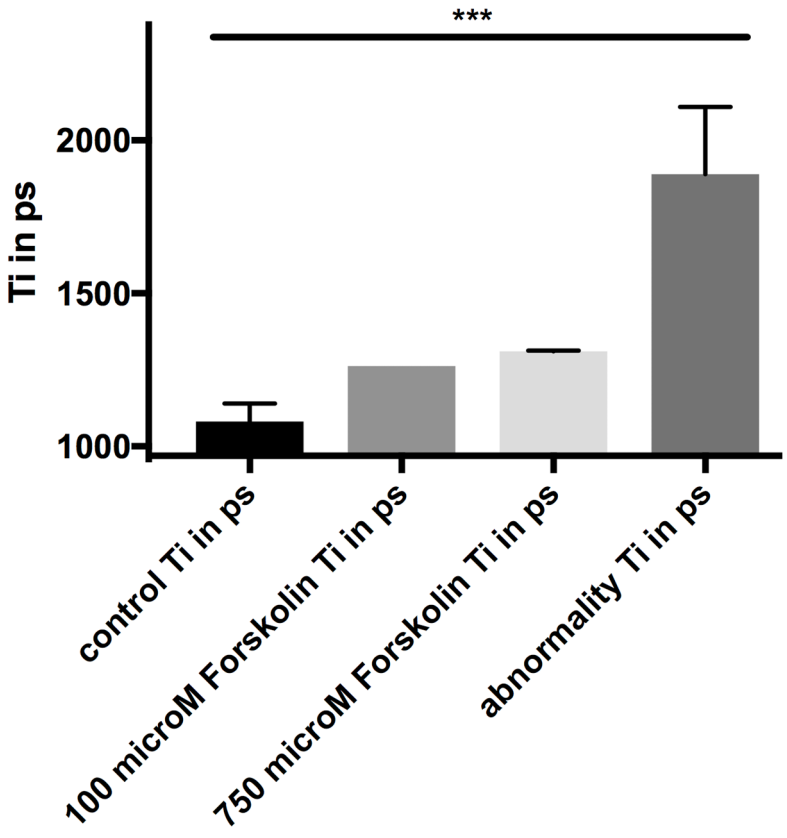

Figure 9.14 EPAC1-camps response to increasing forskolin concentrations

Graphs show the preliminary lifetimes of individual cells expressing the EPAC1-camps sensor under different conditions (control: n=11 from 5 fish, 100 µM forskolin: n=2 from 2 fish, 750 µM forskolin n=4 from 2 fish, abnormality (fish showing abnormal behavior/anatomy or increased autofluorescence): n=11 from 4 fish) Columns show the mean with SEM. Gaussian distribution was checked with the Shapiro-Wilk normality test. The one-way ANOVA Newman-Keuls multiple comparisons test was used for evaluating the significance of the means of the samples. The significance is indicated in the following: ***: p <0.001) Treatment with 750 µM forskolin showed the highest increase in the lifetime. Note that preliminary means that this data was collected in trial-and error experiments and did not strictly fit the mounting and criteria explained in 9.3.1/2.

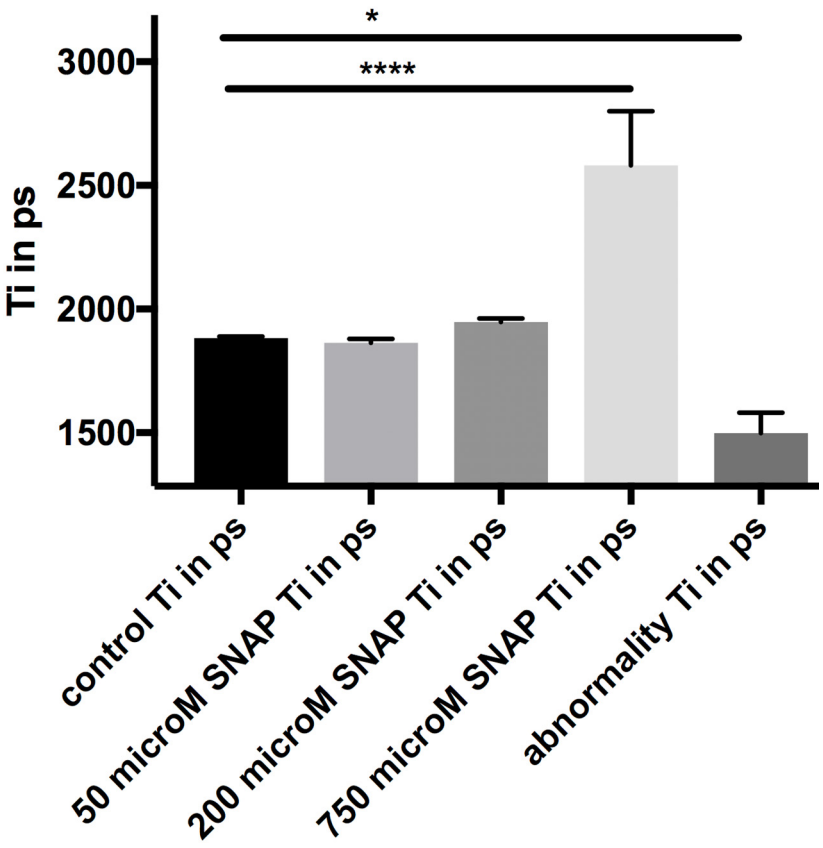

Figure 9.15 The screening results of cGi500 with increasing SNAP concentrations

Graphs show the preliminary lifetimes of individual cells expressing the cGi500 sensor under different conditions (control: n=10 from 10 fish, 50 µM SNAP: n=3 from 2 fish, 200 µM SNAP: n=5 from 4 fish 750 µM forskolin n=5 from 5 fish, abnormality (fish showing abnormal behavior/anatomy or increased autofluorescence): n=6 from 6 fish) Columns show the mean with SEM. Gaussian distribution was checked with the Shapiro-Wilk normality test. The one-way ANOVA Newman-Keuls multiple comparisons test was used for evaluating the significance of the means of the samples. The significance is indicated in the following: *: p <0.05, ****: p <0.0001) Treatment with 750 µM SNAP showed the highest increase in the lifetime. Note that preliminary means that this data was collected in trial-and error experiments and did not strictly fit the mounting and criteria explained in 9.3.1/2.

I further validated the preliminary screening results by applying the criteria and mounting explained in 9.3-4. Both the EPAC1-camps and the cGi500 sensor reacted significantly to an increase of cAMP or cGMP through forskolin and SNAP (both with a concentration of 750 µM) (see Fig. 9.16)

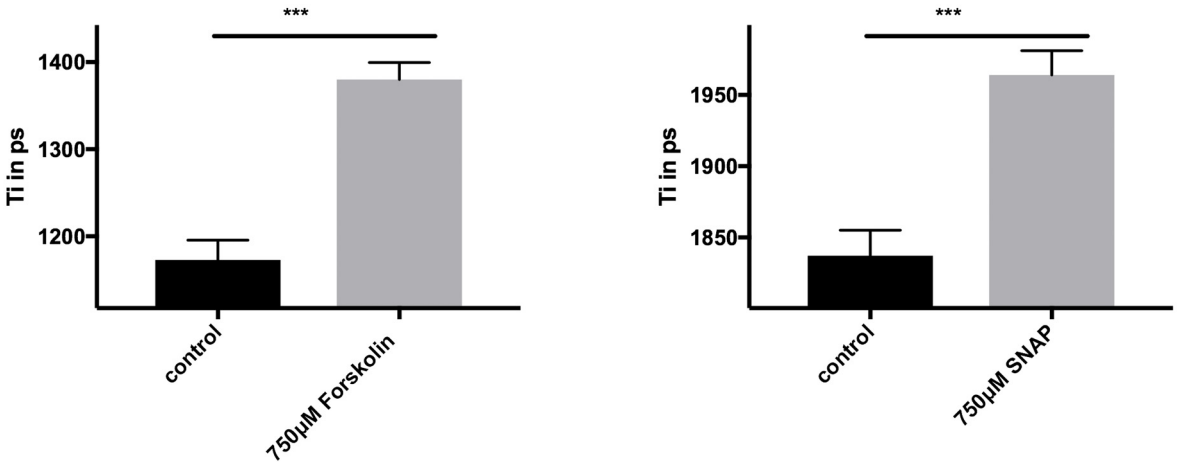

Figure 9.16 The influence of forskolin/SNAP on the fluorescent lifetime Ti

Graphs show the lifetimes of individual cells expressing the EPAC1-camps/cGi500 sensor under different conditions (control EPAC1-camps: n=7 from 4 fish, 750 µM forskolin EPAC1-camps: n=4 from 3 fish/control cGi500 fish n=26 from 6 fish, 750 µM SNAP cGi500 n=29 from 4 fish) Columns show the mean with SEM. Gaussian distribution was checked with the Shapiro-Wilk normality test. The one-way ANOVA Newman-Keuls multiple comparisons test was used for evaluating the significance of the means of the samples. The significance is indicated in the following: ***: p <0.001) Treatment with 750 µM forskolin/SNAP showed a significant increase in the lifetime.

As explained in 9.3-4, fish showing abnormal behaviour/anatomy or increased autofluorescence were excluded from the measurements, because they might show altered physiology and therefore altered cAMP and cGMP levels. Preliminary sceenings, where I seperately measured data from fish showing abnormalities confirm that these fish indeed have altered cAMP and cGMP levels: cAMP concentrations are higher and cGMP concentrations are is lower. For further validation of this phenomenon, I imaged an individual EPAC1-camps and an individual cGi500 expressing cardiomyocyte meeting the criteria for abnormality (abnormal behaviour/anatomy or increased autofluorescence) over a period of one hour. Over extended times the lifetime of the cAMP sensor EPAC1-camps increases (indicating a higher concentration of cAMP) and the lifetime of the cGMP sensor cGi500 decreases (indicating a decreased concentration of cGMP).

9.9 COMPARTMENTALIZATION

Statistical analysis denied a significant difference in the control group of the EPAC1-camps sensor (p value 0,0854). Fig 9.17 shows the distribution of all samples around the mean. In the following, a pseudo-colored map of selected cells that represent the numerical pattern in Fig 9.18 are shown.

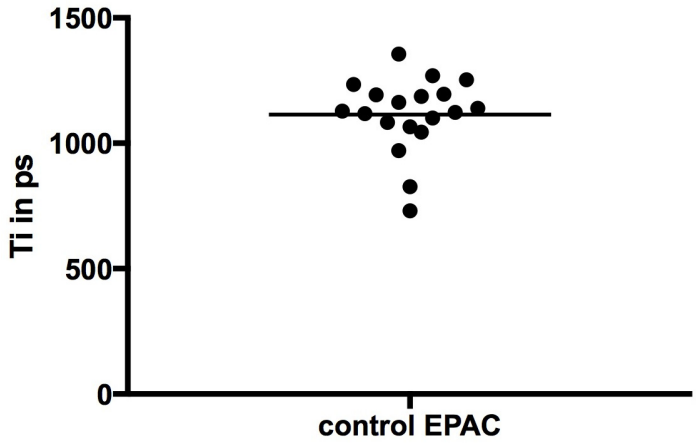

Figure 9.17 The distribution of the lifetimes of control EPAC1-camps expressing cells around the mean

Graph shows the lifetimes of individual cells expressing the EPAC1-camps sensor. n=19 from 14 fish. The mean is indicated with a horizontal bar. Statistical analysis did not confirm a significant difference within the individual lifetimes.

Figure 9.18 shows individual cells that are representative for the data collected. A-C show control cardiomyocytes. Low cAMP concentrations are shown in blue, high cAMP concentrations in orange/red (see legend of Fig. 9.18). The pictures indicate that cAMP is not uniformly distributed in the cell, instead local pools of high cAMP exist. Due to the threshold (see 9.5), not all pixels of the cardiomyocytes were included into the measurements. Under forskolin treatment, the heterogeneous distribution of cAMP was kept, however, the cardiomyocytes show an overall increased cAMP concentration (see D, E in Fig 9.18). In the situation of abnormality (abnormal behavior/anatomy or increased autofluorescence, see 9.3), cardiomyocytes showed significantly higher cAMP concentrations, but cAMP remained to be heterogeneously distributed (F, G in Fig 9.18).

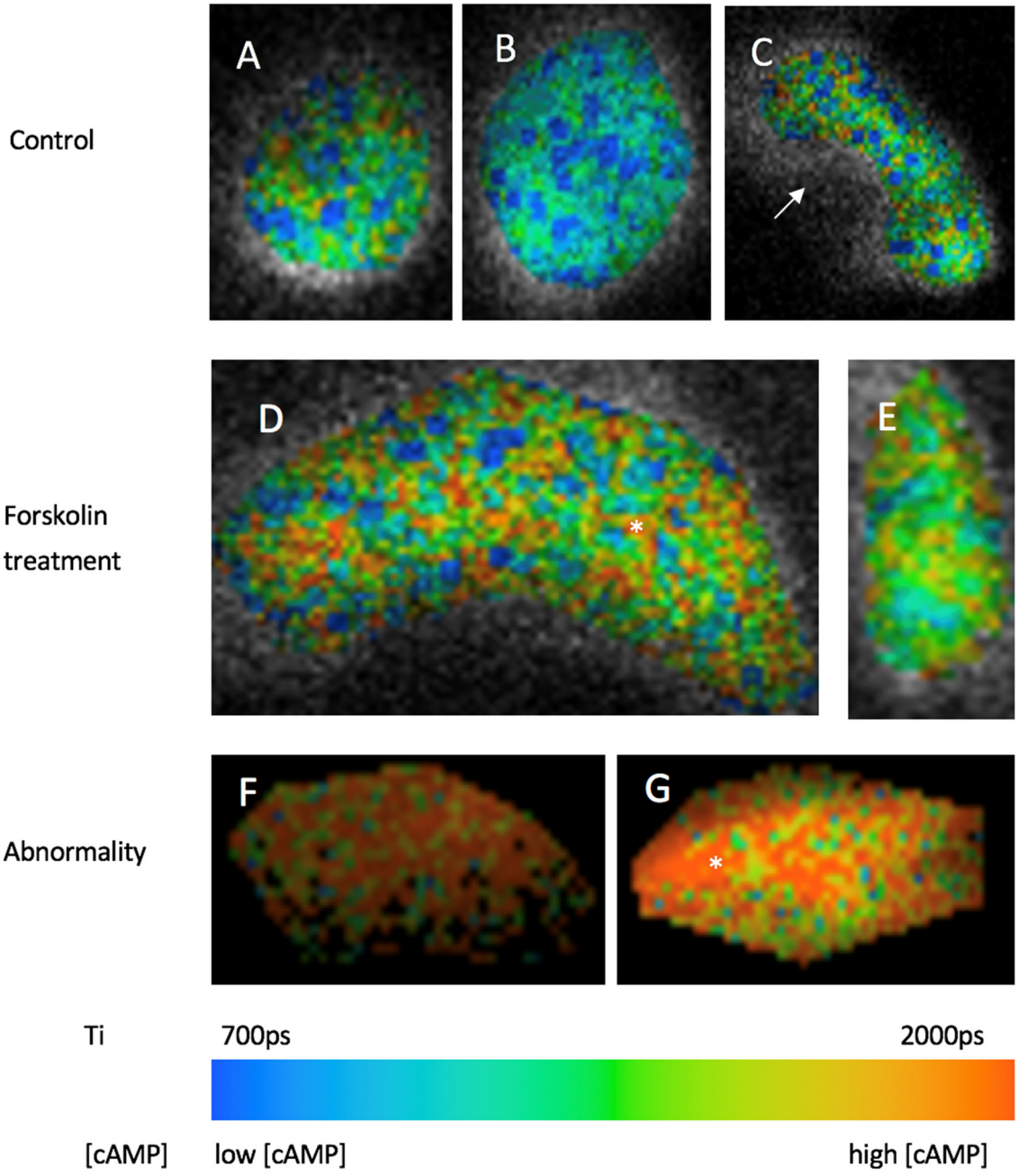

Figure 9.18 EPAC1-camps expressing cells in different conditions

A, B, C: control cardiomyocytes, blue: area of low cAMP, orange/red: area of high cAMP. C, D: cardiomyocytes of fish that had forskolin treatment, arrow: area below threshold (see 9.5) F, G: cardiomyocytes of fish showing signs of abnormality. Every cell shows compartmentalized cAMP.

Statistical analysis also denied a significant difference in the control group of the cGi500 sensor (p value 0,7754). Fig 9.19 shows the distribution of all samples around the mean. In the following, a pseudo-colored map of selected cells that represent the numerical pattern in Fig 9.19 are shown.

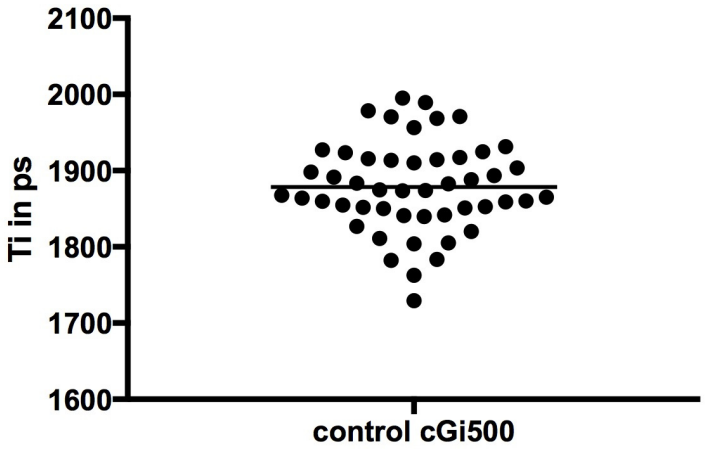

Figure 9.19 The distribution of the lifetimes of control cGi500 expressing cells around the mean

Graphs show the lifetimes of individual cells expressing the cGi500 sensor. n=49 from 21 fish. The mean is indicated with a horizontal bar. Statistical analysis did not confirm a significant difference within the individual lifetimes.

Figure 9.20 shows individual cells that are representative for the data collected. A-E show control cardiomyocytes. Low cGMP concentrations are shown in blue, high cGMP concentrations in orange/red (see legend of Fig. 9.20). The pictures show that cGMP is not uniformly distributed in the cell, instead local pools of high cGMP exist. Due to the threshold (see 9.5), not all pixels of the cardiomyocytes were included into the measurements. Under SNAP treatment, the heterogeneous distribution of cGMP was kept, however, the cardiomyocytes show an overall increased cGMP concentration (see F, G in Fig 9.20). In the situation of abnormality (abnormal behavior/anatomy or increased autofluorescence, see 9.3), cardiomyocytes showed significantly lower cGMP concentrations. Although cGMP remained to be heterogeneously distributed (H, I in Fig 9.20), cGMP seemed to be more homogeneously distributed than in the control or SNAP-treated fish.

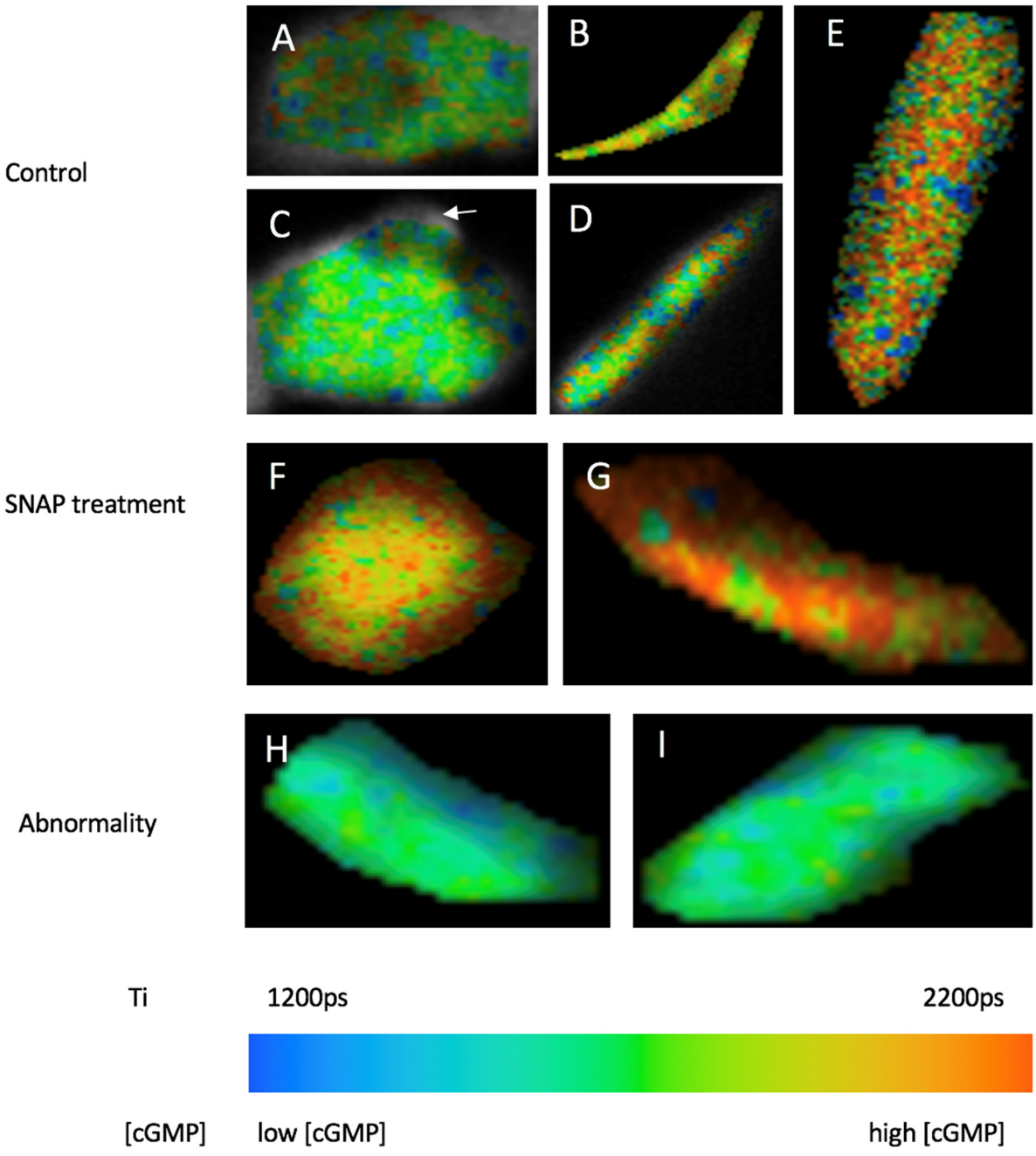

Figure 9.20 cGi500 expressing cells in different conditions

A, B, C, D, E control cardiomyocytes, blue: area of low cGMP, orange/red: area of low cGMP, arrow: area below threshold (see 9.5). F, G: cardiomyocytes of fish that had forskolin treatment, H, I: cardiomyocytes of fish in abnormality. Every cell shows compartmentalized cGMP.

9.10 CALCIUM

I used two different approaches to track Ca^{2+} *in vivo* with fluorescent sensors. The first was to use a genetic sensor, GCaMP6. The second was to use the dye Fluo-4 AM (see 5.7.1).

9.10.1 GCaMP6F

In order to assess subcellular Ca^{2+}, I mounted the zebrafish as described in 8.3. For the imaging, I used confocal microscopy and an Argon laser to detect the fluorescence of the GFP fluorophore of the GCaMPF sensor. As it can be seen in Fig. 9.21, the cardiomyocytes express the GCaMP6F sensor. Closer images to depict subcellular resolutions have to be done in the future (see 10.5).

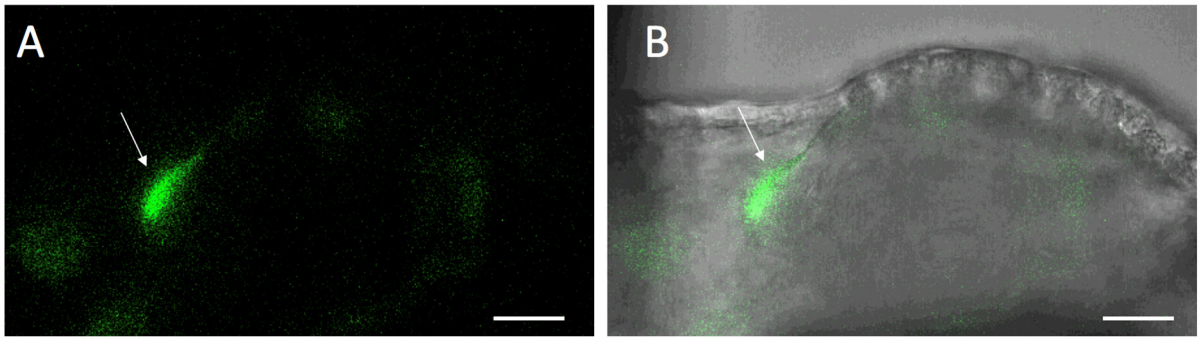

Figure 9.21 GCaMP6F expressed in cardiomyocytes

A: GFP panel. Arrow point towards a cardiomyocyte in focus that expresses the GCaMP6F sensor. B: Brightfield panel with GFP panel. Other cells that are not in focus of the confocal microscope but expressed the sensor are indicated in fuzzy green. The cells are atrial cardiomyocytes. Scale bar: 5 µM

9.10.2 Fluo-4 AM

The aim was to bring the dye Ca^{2+} sensor Fluo-4 AM (see 5.7.1) into larval cardiomyocytes. Fluo-4 AM has been used in cardiomyocytes for a long time in *in vitro* experiments and in perfused zebrafish hearts. All published protocols made use of incubation techniques with the dye at 5-10 µM. However, introducing the dye into the living zebrafish heart revealed some problems. The zebrafish's heart is fully developed after 48h. An early injection of the dye in the form of injections, as done with the plasmid DNA for the genetic sensors, resulted in the degradation of the dye before the heart was developed. A late injection of the dye however was not successful, as individual cardiomyocytes are too small to be individually targeted and were apparently also too thick to allow dye diffusion into the cytosol. A low concentration revealed no or weak results, whereas a high concentration oversaturated the cells and surrounding tissue (see Figure 9.22, A). Incubation in E3 with the dye did not work. Using the injection technique, low volumes did not allow enough dye to approach the cells and a too high volume caused edema in the fish (see Figure 9.22, B). The needle I used for plasmid DNA injections caused too much damage, so I had to bevel it to facilitate entry. Furthermore, I had to figure the appropriate mounting, as the fish did not fit into the molds I used for one-cell stage DNA injections (see 8.3). A summary of the problems I encountered is shown in Table 9.2.

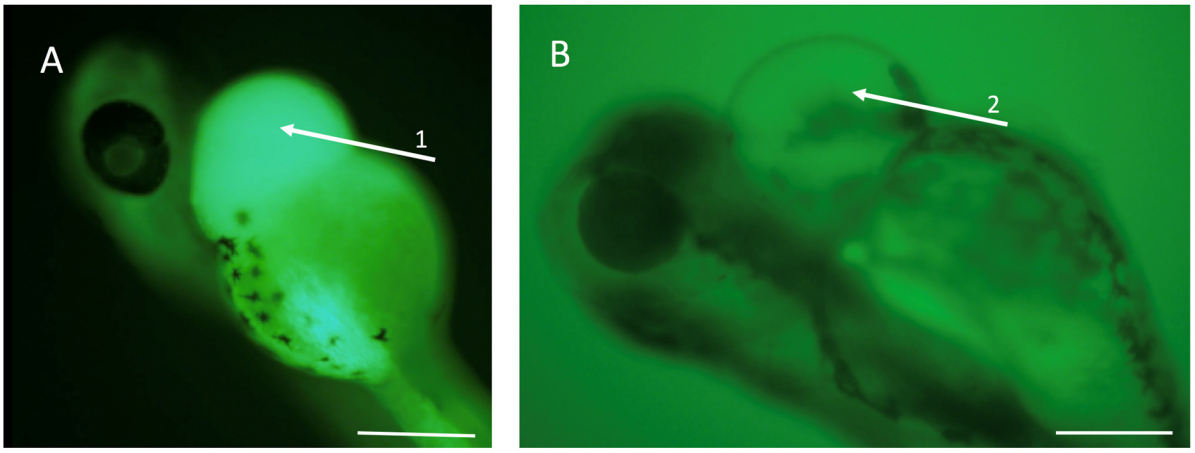

Figure 9.22 Oversaturation and edema caused by Fluo-4 AM treatment

A: A 72hpf zebrafish with 500 µM injected Fluo-4 AM dye. 1 indicates the oversaturated pericardium. Cardiomyocytes are not visible. B: A zebrafish developing edema (2). Scale bar: 100 µM.

Table 9.2 Summary of different approaches for introducing Fluo-4 AM into zebrafish cardiomyocytes *in vivo*

Variable	Experiments	Comments
Time point of injection	One-cell-stage	Dye does not last until heart is developed
	Aiming at heart field, 24hpf	Dye does not last until heart is developed
	48 hpf	1 out of 20 good results
	72hpf	Heart too much developed, dye does not get in anymore
Concentration of Fluo-4 AM	5 µM	Nothing visible
	10 µM	Hardly anything visible
	50 µM	1 out of 20 good results
	500 µM	Oversaturation of dye (Figure 9.25)
	1mM	Development of edema, oversaturation of dye
Injection volume	1nl	Not enough dye flow
	20nl	1 out of 20 good results
	50nl	Too much damage at injection site
Needle	Normal diameter as used in DNA injections	Too much damage at injection site
	Beveled needle	Works much better, smoother gliding into pericardium
Type of injection	One shot	Not enough dye flow
	Multiple perfusions	Enough dye flow
Mounting	Plane agarose petri dish	Fish slip away during injection
	Molded agarose petri dish	Difficult to approach with needle
	Agarose petri dish with lanes	Works nicely

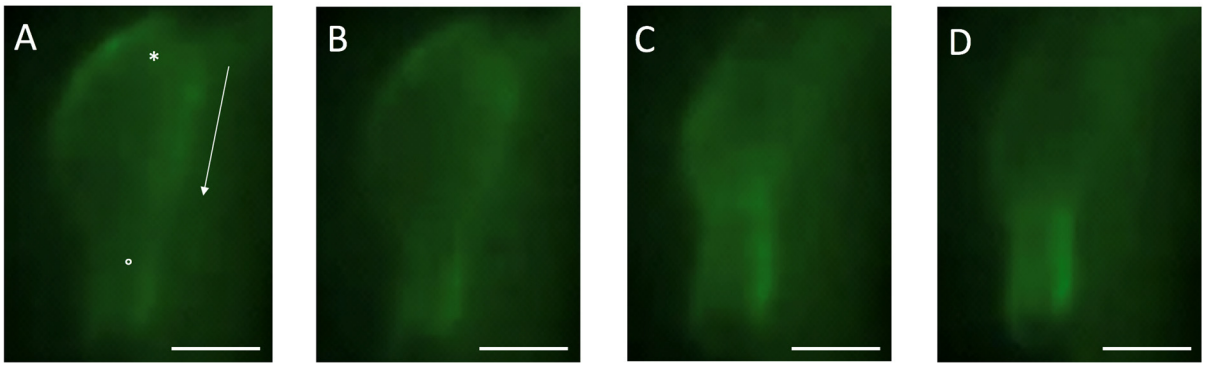

Figure 9.23 Ca^{2+} release detected with Fluo-4 AM during contraction in the sequence of a heart cycle

A-D show one heart cycle. Arrow in A indicates the direction of contraction. *: atrium, °: ventricle. Over the course from A-D, the Fluo-4 AM dye represents Ca^{2+} release to initiate contraction, starting from the atrium to the ventricle (D). Scale bar 25 µM.

Finally, I established a protocol showing satisfactory results (see Fig. 9.23) First, I took 48h old WT embryos of either the AB or WT type and anesthetized them with MESAB (see 7.3.4). I put 5 embryos on the corresponding mold and placed them in a way that their heart points towards the approaching needle. Then, I break through the pericardial sack and guide the needle also out of the pericardium so that there are two small incisions. Finally, I perfused the pericardium with 15 pushes (each 20nl) with the Fluo-4 AM solution (50 µM) (see Fig. 9.24). It is important to perfuse, otherwise the dye is trapped in the pericardium and does not allow the myocardial cells to be distinguished in the microscope.

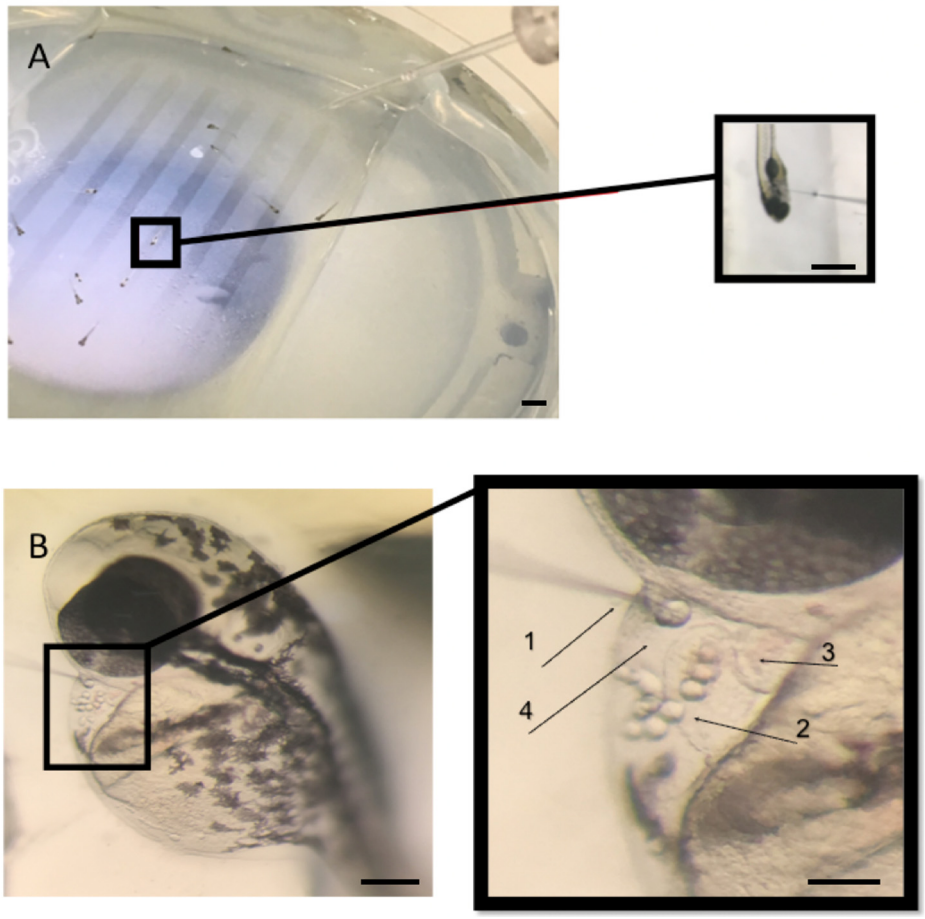

Figure 9.24 Pericardial perfusion with Fluo-4 AM in a 48 hpf embryo

A: Anesthetized 48 hpf zebrafish on the agarose mold. Scale bar: 3mm. The direction for appropriate needle approach is indicated in the black box, which is enlarged in the right (Scale bar: 1mm). B: the injections procedure. Scale bar: 100 µM. Black box is enlarged in the right (Scale bar: 50 µM). 1: the needle. 2: atrium 3: ventricle 4: pericardium

10. DISCUSSION

The methods I developed have potential to learn about subcellular cAMP, cGMP and Ca^{2+} in cardiomyocytes *in vivo*. The sequencing results (see 9.1) showed that the cloning was successful. I thereby provide three new constructs to the scientific community, which allow the tracking of cAMP, cGMP and Ca^{2+} in zebrafish cardiomyocytes via fluorescence. Furthermore, I injected the constructs into zebrafish fertilized embryos and demonstrated for the first time

a.) EPAC1-camps and cGi500 expression in zebrafish cardiomyocytes.
b.) successful Fluo-4 AM *in vivo* application in zebrafish larval heart.

Moreover, in this study, I established a protocol to mount zebrafish for performing FLIM-FRET with both the EPAC1-camps and cGi500 expressing zebrafish. First, all previous studies were performed in intact cardiomyocytes *in vitro* or with dissected samples (such as perfused hearts or mice follicles), not *in vivo*. Second, EPAC1-camps or cGi500 were analyzed by intensity-based FRET in cardiomyocytes before, but not with FLIM-FRET.

10.1 THE ADVANTAGES OF FLIM-FRET

The use of intensity-based FRET in previous studies revealed some problems. The concentration of the sensor, the donor and the acceptor fluorophores varies throughout the sample. Therefore, intensity-based FRET depends on donor-acceptor intensities, which requires calibration measurements with donor-only and acceptor-only samples. Furthermore, the FRET-excited acceptor emission is altered by the overlap of the donor-emitted fluorescent emission into the acceptor-emission band (donor bleedthrough). Acceptor fluorophores can also be excited directly (acceptor signal bleedthrough) (Piston, et al., 2016). Consequently, intensity-based FRET analyses require careful calibration, making it drawn to error. FLIM-FRET is better for analyzing molecular interactions with FRET sensors, because FLIM-FRET does not show the disadvantages of other FRET-analyzing methods and provides more accurate results (Becker and Hickl, 2015; Trautmann, et al., 2013). The advantage of FLIM-FRET over intensity-based FRET analyses is also that the lifetime of the excitation state of the donor fluorophore only depends on whether or not the acceptor fluorophore is in close proximity. This enables concentration independent measurements. Additionally, FLIM-FRET provides better accuracy than intensity-based FRET for a given efficiency of the optical system and detector and a given excitation power (Pelet, et al., 2006). This is due to the fact a FRET sensor can have two different conformations (see also Figure 5.2).

1. In the absence of the molecule (non-interacting sensor) FRET occurs, the lifetime of the donor fluorophore is short
2. In the presence of the molecule (interacting sensor) FRET cannot occur, the lifetime of the donor fluorophore is long

FLIM-FRET can distinguish between 1. and 2. by using a double-exponential fitting model applied to the collected data to determine the fluorescent lifetime. Because intensity-based FRET can only evaluate absolute fluorescent intensities, information about how many sensors are interacting and contributing to the fluorescent signal cannot be included into the analysis. Furthermore, by showing the different lifetime components of 1. and 2., FLIM-FRET provides the possibility to exclude measurements of fluorescence from artifacts or autofluorescence (which would show significant longer lifetimes, see 9.5 Figure 9.9).

10.2 cAMP/cGMP SENSOR CHARACTERIZATION

My data shows that the cAMP and cGMP sensor represent elevations of cAMP and cGMP levels after treatment with cAMP-increasing (forskolin) and cGMP-increasing (SNAP) drugs, indicating the sensors are fully functional. In addition, I was able to achieve higher subcellular resolution for cAMP and cGMP measurements than previously reported (see Fig. 10.1, compare “B” to other panels). Therefore, the *in vivo* FLIM-FRET method that I developed has the potential to greatly improve the temporal and spatial detection of where and how much these second messengers accumulate in cardiomyocytes *in vivo*.

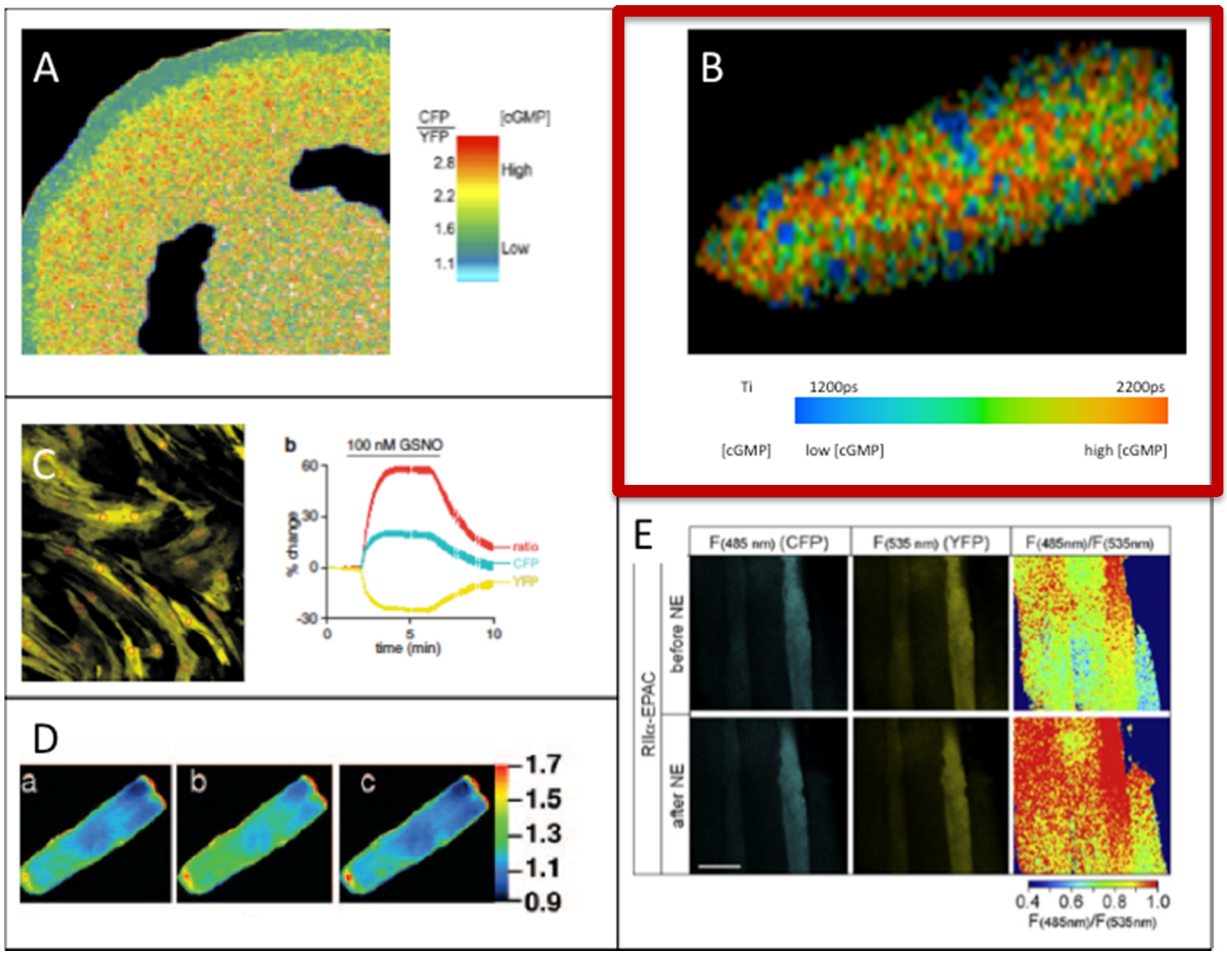

Figure 10.1 Different studies using FRET-based sensors

A. (Shuhaibar, et al., 2015) cGMP diffusion through gap junctions in live mice follicle. B. A zebrafish cardiomyocyte expressing the cGMP sensor cGi500 that I analyzed with FLIM FRET. C: (Thunemann, et al., 2013a) live YFP fluorescence of the cGi-600 sensor and CFP/YFP ratio values S after treatment with Nitrosoglutathione (GSNO, stimulates soluble guanylyl cyclases) D: (Leroy, et al., 2008) mice cardiomyocyte before (a) after (c) and during ISO treatment, pseudo-colored picture depicting CFP/YFP ratio, of an EPAC sensor E: (Röder, et al., 2009) cAMP in skeletal muscle mice fibers shown as 1 with the CFP, 2 YFP panel of the used PKA based FRET sensor and 3. A pseudo-colored image showing CFP/YFP ratio.

It can be argued that data of the EPAC1-camps sensor might be altered due to the fact that three mutations appeared in comparison to the original EPAC1-camps gene on addgene. However, the same mutations were in the original sensor that Dr. Nikolaev kindly provided to me, and he showed in his publications that these mutations don't have a significant effect (Perera, et al., 2015; Shuhaibar, et al., 2015; Sprenger, et al., 2015). Still, the further characterization of the sensors applied in zebrafish larvae should be done in the future. This would include the determination of minimal and maximal lifetimes when the sensors are fully saturated with the molecule or when no molecule is interacting with the sensor. This would also help to evaluate fluctuations in control measurements on different experiments with the same sensor expressed by different fish. Moreover, an important step in the future is to check whether the fish that I raised harbor the genetic sensors. In this case, a new transgene line would have been introduced into the zebrafish community. Working with transgenes

would also increase the number of experiments significantly, as the time-consuming process of DNA injection and subsequent screening of the F_0 generation does not have to be done. Drawing data from a higher number of experiments (getting n-numbers higher than 19 for EPAC1-camps and 49 for cGi500) would improve the accuracy of my study, because then the data is more representable for the population the samples are drawn from.

10.3 SCIENTIFIC CONTEXT

My data complements previous findings that cAMP and cGMP are not uniformly distributed through the cell (Leroy, et al., 2008; Mika, et al., 2012a; Nikolaev, et al., 2010; Vandecasteele, et al., 2006; Zaccolo, et al., 2002). However, a very important fact in this context is that the zebrafish is lacking T-tubuli (Bovo, et al., 2013). Although the T-tubuli seem to be important for the compartmentalization of cAMP and cGMP signals (see 5.4.1), zebrafish still show compartmentalization of cAMP and cGMP despite the apparent lack of T-tubuli. Even if I pushed the system by forskolin and SNAP, responses were heterogeneous in the cells, indicating that other factors play an important role in cAMP/cGMP compartmentalization. This would include the role of PDEs (Nikolaev and Lohse, 2006). If, as proposed by Mika et al., the different activity of cAMP-PDEs lead to a disorganization of cAMP compartmentalization and subsequent phenotype of cardiac disease (Mika, et al., 2012a), investigation of cAMP/cGMP compartmentalization in cardiac disease in the zebrafish would be a promising model to increase our knowledge about pathologic mechanisms and potentially new (PDE-dependent)-therapeutic targets.

10.3.1 REGENERATION

Apart from investigating cAMP and cGMP distributions in cardiac disease, the zebrafish provides a good model to investigate how cAMP and cGMP signaling changes during regeneration. The big advantage of the zebrafish is that it can regenerate itself. Experiments can be done involving disease, for example after generating cardiac hypertrophy. The human myocardium is not able to regenerate. After injury, such as ischemia, cardiomyocytes are lost and not replaced. Instead, fibroblasts produce fibrotic matrices at the injury site (Chistiakov, et al., 2016; Shinde and Frangogiannis, 2014). Little is known about the involvement of beta-adrenergic signaling and natriuretic signaling in regeneration. Regeneration experiments could also be performed by simply applying a puncture wound with a needle and then do FLIM measurements with the fish expressing the FRET sensors at different times after injury.

10.4 IMPROVING THE MEASUREMENTS

Using the sensors in the zebrafish larvae *in vivo* model revealed some problems: confocal microscopy for achieving high subcellular resolution images required immobile samples, which contradicts the use of investigations of the heart *in vivo* model, because the heart blurs the image with its movement. I overcame that problem by using blebbistatin, which immobilizes the heart without altering action potential morphology or Ca^{2+} currents (Jou, et al., 2010). Therefore, it has to be taken into consideration, that for my protocols, I used a very high concentration of blebbistatin. This might interfere with cardiac physiology, because experiments that have been done stating that blebbistatin uncouple excitation from contraction in the zebrafish heart without altering the action potential morphology/Ca^{2+} currents did not use this high concentration. In general, I solved the problem that zebrafish larvae are not very responsive to drug treatment in simply increasing the concentration of the drug from 1-10 µM (as used by Jou et al.) to 200 µM (blebbistatin, forskolin and SNAP, respectively), but I don't know whether that interfered with their cardiac physiology. Furthermore, the zebrafish organism is very complex and varies between individual organisms. To give an example, eight minutes of incubation time with blebbistatin might immobilized the heart in one zebrafish, but in another fish heart immobilization takes 25min. Additionally, hatches from different parents vary in terms of egg- and embryo quality, and individual fish responded differently to microinjection. Evidently, I found criteria that ensured the well-being of the embryo for data analysis. Fish must not be used for measurements if they showed signs of abnormality, because these fish might have had an altered physiology (and therefore altered levels of intracellular cAMP and cGMP). However, I can not be sure to have overcome all subjectivities in judging the fish and classifying them as "normal". To overcome this problem, other ways of heart immobilization should be exploited in the future, for example the use of cold water. Although that would also scientifically influence cAMP/cGMP signaling, it can be another way to characterize and find out more about the functionality of the fluorescent sensors and cAMP/cGMP compartmentalization.

The presence of fish showing abnormality (abnormal anatomy/behavior or increased autofluorescence, see 9.3 and 9.5) indicates that the drug treatment and also the injection procedure may have harmed the fish. The data I collected about cAMP/cGMP in the condition of abnormality showed increased cAMP levels and decreased cGMP levels, which is an indication of stress, because stress increases intracellular cAMP via the β-adrenergic pathway (see 5.2). Interestingly, in my study, cGMP levels decreased in the situation of abnormality (Fig. 9.20 H/I). Because previous data indicated that cGMP-signaling is cardioprotective, especially in stress and cardiac disease (see 5.3), it would be interesting to find out whether a stimulation of the cGMP pathway during abnormality (for example by

SNAP) would reduce the signs of abnormality (such as edema/Malformation/increased autofluorescence). I hypothesize that the situation of abnormality means likely a situation of stress for the fish, which results in an increased signaling to adapt to stress (β-adrenergic pathway) and a reduced activation of contra regulatory pathways (the ANP/BNP/NO pathway with cGMP as second messenger). Although I excluded the fish showing abnormality, stress might still have interfered with my cAMP measurements, if it did not show in the form of abnormality. The reason why I think stress might have interfered with my cAMP measurements is because UV light significantly increases the whole body cortisol levels in larval zebrafish heart (Bai, et al., 2016). If UV light has that effect, it is likely that also the exposure to laser light increases body cortisol levels. Cortisol is a stress hormone, which is released together with other stress hormones, such as catecholamines (Lee, et al., 2015), which increases cAMP (see 5.2). Cortisol levels are also generally raised by stress such as mounting the fish for microscopy (Tran, et al., 2014). To exclude alterations by stress from my measurements with the EPAC1-camps sensor it would be an idea to use a beta-blocker in the control and drug-treated experiments, because beta-blockers inhibit the activation of βARs. βARs are activated in stress (see 5.2) and result in the increase of intracellular cAMP. Therefore, the use of beta-blockers inhibits the increase of cAMP during stress.

An future step would also be to not limit the imaging that I did to one plane. Z-stacks and 3D data would greatly improve the precise assessment of the location of cAMP/cGMP/Ca^{2+} at different locations in the cell (see Fig. 9.13). Because my data provides significant evidence that cAMP and cGMP are not uniformly distributed in the cell, it would be an important step to get z-stacks and 3D images to investigate cAMP and cGMP in the whole cell, not just one plane.

In the context of localized assessments cAMP/cGMP/Ca^{2+}, another step in the future would be the inclusion of localization signals with the FRET sensors. This would allow to investigate the specific role of subcellular structures in cAMP/cGMP compartmentalization and heart disease. An example for a localization signal is the use of the Protein Connexin 43 (Cx43). Cx43 is a main part of myocardial gap junctions. Several reasons make Cx43 a localization of interest: Like β_2AR, Cx43 is heterogeneously redistributed in the diseased heart (Magda, et al., 2012), but why remains unclear. Also, Boengler et al. showed that βAR-induced cAMP targets Cx43 (Boengler, 2009). Therefore, assessing cAMP at gap junctions may reveal regulatory mechanisms that are unknown until now. Furthermore, an abnormal distribution of Cx43 can cause electrical dysbalance, because Gap junctions allow the exchange of ions and contributes to electrical propagation (Jalife, et al., 1999), which can be investigated with the Ca^{2+} sensor that I provided with this study.

10.5 INCLUDING CALCIUM

A next step in the future is to relate the distribution patterns of cAMP and cGMP with the ones of Ca^{2+}. This relation enables to include a functional meaning to cAMP and cGMP signaling. Nikolaev and Lohse combined the EPAC1-camps sensor with Fura-2-AM in the context of insulin secretion research (Nikolaev and Lohse, 2006), showing that the combination of genetic sensors with dyes can be successfully performed. In order to combine an analysis of cAMP/cGMP with the Ca^{2+} dye, the Fura-2 AM dye should simply be applied using the Fluo-4 AM protocol I provide in this study. Fluo-4 AM was very useful during the establishment of a protocol that can be used in zebrafish larval heart, because the fluorescence of the dye can be analyzed with an Argon laser that allows fast readouts. However, for generating valuable data the single-wavelength nature of the dye needs the calibration of F/F_0. Errors due to washout and photo-bleaching over the course of longer experiments are likely to happen. Fura-2 AM however is a dye that is ratiometric, thus it has two different excitation wavelengths for the Ca^{2+} unbound or bound state. This dual-excitation with a single emission, and the ratio of fluorescence emitted provides a measure of absolute intracellular Ca^{2+}. Expecting that tissue parameters stay constant, Fura-2 AM fluorescence from different areas in the heart can be directly compared, as can data across different animals. Because the dye is ratiometric, no errors due to indicator leak or photo-bleaching can occur (Venkataraman, et al., 2012).

Also, the GCaMP6F sensor for Ca^{2+} can be combined with cAMP/cGMP assessment, because cAMP/cGMP FRET sensors and the Ca^{2+} sensor GCaMP6F have different fluorophores and can therefore be detected simultaneously with different fluorescent panels. A simultaneous detection of cAMP and cGMP with the sensors I cloned would be difficult, though, because they have the same FRET-fluorophores. However, as Götz et al. used the red GES-DE5 biosensor, which has a cGMP binding domain derived from PDE5 and instead CFP and YFP the green (T-sapphire) and red (Dimer2) Fluorophore for FRET (Götz, et al., 2014), red GES-DE5 might be an alternative that can be used simultaneously with GCaMP6F, given that the devices used can distinguish between the cpGFP and T-sapphire.

Moreover, I not only cloned the GCaMP6F sensor to track contraction but also the GCaMP6M and GCaMP6S sensor to track long lasting responses of Ca^{2+} signaling (see 5.7.1). The use of GCaMP6M/F can be used in the future to connect changes in gene expression with cAMP/cGMP signaling. If used in a disease model with cardiac hypertrophy, it can be investigated how significant cAMP/cGMP compartmentalization is for a long lasting change in sustained Ca^{2+} levels, which can result in changes in gene expression and therefore also hypertrophy (Bers, 2008).

10.6 TRANSFER OF RESULTS DERIVED FROM THE ZEBRAFISH TO HUMANS

It has to be taken into consideration that the physiology of zebrafish differs from the human. Although zebrafish have a high genetic and organ system homology to humans, zebrafish have only a two-chamber heart morphology, different kinetics of various depolarizing and repolarizing ion channels and they lack T-tubuli (Verkerk and Remme, 2012). The calcium signaling in zebrafish differs in such a way that the activation of protein kinase A by forskolin had much different effect in zebrafish compared to mammals, something that is greatly significant to my studies: in zebrafish, an increased Ca^{2+} transient by forskolin was entirely mediated by augmentation of LTCC current, whereas in mammals, Ca^{2+} transients are mainly mediated through Ca^{2+}-induced Ca^{2+} release by RyRs and the SR (Bovo, et al., 2013; Walker, et al., 2014). This is an indication that excitation-contraction coupling in zebrafish cardiomyocytes differs from the mammalian because of such a small contribution of SR Ca^{2+} release to the Ca^{2+} transient. The reason for this a low sensitivity of RyRs to cytosolic Ca^{2+} in zebrafish (Bovo, et al., 2013). Furthermore, the zebrafish shows differences in gene expression: the zebrafish has two genes for the β_2AR (Steele, et al., 2011), whereas mammals have only one. Consequently, results derived from this study should be tested in other animal models and (human) stem cells before drawing conclusions for humans.

10.7 OPEN QUESTIONS AND CONCLUSION

With this study, I present the first FLIM-FRET application for assessing cAMP and cGMP in zebrafish cardiomyocytes *in vivo.* The results of this study include evidence that zebrafish have other mechanisms that lead to cAMP/cGMP compartmentalization than T-tubuli, which keep compartmentalization constant even under extreme cAMP or cGMP increasing drug treatment. Furthermore, my method is promising to allow the investigation of cAMP/cGMP compartmentalization, cAMP/cGMP crosstalk and Ca^{2+} in many different conditions, which provides a new tool to answer the following open questions in the field:

- How do zebrafish ensure cAMP/cGMP compartmentalization without T-Tubuli? Are there unknown mechanisms leading to cAMP/cGMP compartmentalization that we don’t know about?
- Does a change of cAMP compartmentalization lead to the pathological phenotypes of cardiac disease?
- Does a changed compartmentalization of cAMP in cardiac disease influence Ca^{2+} concentrations and therefore contraction?
- Can a changed cAMP compartmentalization in cardiac disease be reduced by cGMP?

- What role does cAMP/cGMP concentrations and subcellular accumulations play in regeneration?
- How do cAMP/cGMP interact at specific subcellular locations, such as gap junctions?

It is important to note that using the zebrafish as a model combined with FLIM techniques, *in vivo*, real-time investigations can be done. Furthermore, the zebrafish`s ability to regenerate heart tissue opens a whole new chapter of what can be researched on in terms of cardiac disease and the role of cAMP/cGMP and Ca^{2+} in cardiac disease, such as heart failure.

11. SUMMARY

Introduction: 23 million patients worldwide suffer from heart failure. These patients depend on cardiac research, because cardiac research enables the development of new therapeutic strategies and –targets. In cardiomyocytes, the compartmentalization of cAMP and cGMP depends on many factors. T-tubuli and PDEs are responsible for the division of cells in microdomains in which localized and specific cAMP and cGMP-signaling occurs. The aim of this thesis was to develop a method to answer the open questions that remain about the physiological and pathophysiological significance of cAMP/cGMP compartmentalization.

Methods: I used the zebrafish as a model, because the transparency of zebrafish larvae enabled non-invasive fluorescent imaging in cardiomyocytes in the living animal. I cloned the Fluorescence Resonance Energy Transfer (FRET) sensors EPAC1-camps for cAMP and cGi500 for cGMP and injected them into zebrafish fertilized embryos. Then I used the F_0 generation for *Fluorescence Lifetime Imaging* (FLIM) -FRET-measurements of cAMP and cGMP. Ca^{2+} is an important downstream mediator of cAMP and cGMP, because Ca^{2+} regulates cardiac contraction. Therefore, I also cloned the Ca^{2+} sensor GCaMP6 and used the dye Fluo-4 AM to include intracellular Ca^{2+} in the imaging.

Results: The cloned sensors for cAMP, cGMP and Ca^{2+} were successfully injected into the zebrafish and showed expression in individual cardiomyocytes. I developed a protocol to mount the living zebrafish embryos and to measure intracellular cAMP and cGMP with FLIM-FRET *in vivo* with high spatial resolution. I characterized the sensors in their functionality by showing that the sensors react to changes in intracellular concentrations of cAMP and cGMP. The results of this study include evidence that zebrafish have mechanisms that lead to cAMP/cGMP compartmentalization in the absence of T-tubuli, and these mechanisms keep compartmentalization constant even under extreme cAMP or cGMP increasing drug treatment. Furthermore, I imaged intracellular Ca^{2+} by confocal microscopy and developed a protocol to use Fluo-4 AM for Ca^{2+} imaging.

Conclusion: The method used in this thesis should allow the investigation of subcellular cAMP/cGMP compartmentalization and Ca^{2+} and to subsequently answer open questions in the field, for example whether a change of cAMP compartmentalization leads to the pathological phenotypes of cardiac disease or if a changed compartmentalization of cAMP in cardiac disease influences Ca^{2+} concentrations and therefore contraction. Additionally, this method can be used to learn more about cAMP, cGMP und Ca^{2+} during regeneration in the heart, because the zebrafish cardiomyocytes can regenerate.

12. ZUSAMMENFASSUNG

Einleitung: Weltweit sind mehr als 23 Millionen unter Herzinsuffizienz leidende Patienten auf die kardiologische Grundlagenforschung angewiesen, da diese die Voraussetzung für eine bessere Versorgung durch adaptierte und neue Behandlungswege schafft. In Kardiomyozyten hängt die Kompartimentierung von cAMP und cGMP von vielen Faktoren ab. T-Tubuli und PDEs werden unter anderem für die Aufteilung der Zellen in Mikrodomänen, in denen lokalisierte und spezifische cAMP- und cGMP-Signalgebung stattfinden kann, verantwortlich gemacht. Das Ziel dieser Arbeit war die Etablierung einer Methode, mithilfe derer offene Fragen bezüglich der physiologischen und insbesondere der pathophysiologischen Relevanz der cAMP- und cGMP Kompartimentierung beantwortet werden können.

Methode: Als Modell diente der Zebrafisch, da die Transparenz von Zebrafisch Embryonen eine nicht-invasive Bildgebung von Fluoreszenz in Kardiomyozyten im lebenden Tier ermöglicht. Dafür klonierte ich die Förster Resonance Energy Transfer (FRET) -Sensoren EPAC1-camps als cAMP-Sensor und cGi500 als cGMP-Sensor und injizierte diese in befruchtete Zebrafisch Embryonen. Anschließend benutzte ich die F_0-Generation für *Fluorescence Lifetime Imaging* (FLIM) -FRET-Messungen von cAMP und cGMP. Da Ca^{2+} als wichtiger *downstream* Mediator von cAMP und cGMP die kardiale Kontraktion reguliert, klonierte ich außerdem den Ca^{2+}-Sensor GCaMP6 und benutzte den Farbstoff Fluo-4 AM, um intrazelluläres Ca^{2+} darzustellen.

Ergebnisse: Die klonierten Sensoren für cAMP, cGMP und Ca^{2+} konnten erfolgreich in den Zebrafisch injiziert werden und zeigten alle Expression in einzelnen Kardiomyozyten. Ich entwickelte ein Protokoll, dass die Fixierung von lebenden Zebrafisch Embryonen und nachfolgender Bildgebung von cAMP und cGMP mit hoher zellulärer Auflösung mit FLIM-FRET *in vivo* erlaubte. Ich konnte eine funktionelle Charakterisierung der Sensoren durchführen, indem ich zeigte, dass sie auf Konzentrationsänderungen von intrazellulärem cAMP und cGMP reagieren sowie zeigen, dass Zebrafische trotz fehlender T-Tubuli eine signifikante cAMP- und cGMP Kompartimentierung aufweisen, auch unter extremen Bedingungen nach Gabe von cAMP/cGMP stimulierenden Substanzen in hoher Dosierung. Ich konnte zudem subzelluläres Ca^{2+} durch konfokale Mikroskopie bildgebend darstellen und entwickelte ein Protokoll, um mit Fluo-4 AM eine schnelle Möglichkeit zu haben, Ca^{2+} mit in die Messungen einzubeziehen.

Ausblick: Die in dieser Arbeit benutzte Methode bietet eine gute Möglichkeit, subzelluläre cAMP- und cGMP-Kompartimentierung und Ca^{2+} zu untersuchen und damit zum Beispiel die Fragen zu beantworten, ob eine veränderte cAMP/cGMP Kompartimentierung zu

Herzkrankheiten wie Hypertrophie führt oder ob eine veränderte cAMP Kompartimentierung den zellulären Ca^{2+} Haushalt und damit die kardiale Kontraktion beeinflusst. Darüber hinaus kann das von mir etablierte Protokoll dazu genutzt werden, mehr über cAMP, cGMP und Ca^{2+} während der Regeneration im Herzen zu lernen, da der Zebrafisch über ausgeprägte Regenerationsfähigkeiten verfügt.

13. REFERENCES

Abi-Gerges A, Richter W, Lefebvre F, Mateo P, Varin A, Heymes C, Samuel JL, Lugnier C, Conti M, Fischmeister R and others. 2009. Decreased expression and activity of cAMP phosphodiesterases in cardiac hypertrophy and its impact on beta-adrenergic cAMP signals. Circ Res 105(8):784-92.

Bacskai BJ, Skoch J, Hickey GA, Allen R, Hyman BT. 2003. Fluorescence resonance energy transfer determinations using multiphoton fluorescence lifetime imaging microscopy to characterize amyloid-beta plaques. J Biomed Opt 8(3):368-75.

Badura A, Sun XR, Giovannucci A, Lynch LA, Wang SS. 2014. Fast calcium sensor proteins for monitoring neural activity. Neurophotonics 1(2):025008.

Bai Y, Liu H, Huang B, Wagle M, Guo S. 2016. Identification of environmental stressors and validation of light preference as a measure of anxiety in larval zebrafish. BMC Neurosci 17(1):63.

Becker, Hickl. 2015. Moldular FLIM Systems for Zeiss LSM 710/780/880 Family Laser Scanning Confocal Microscopes. Berlin: Becker & Hickl GmbH.

Bers DM. 2008. Calcium cycling and signaling in cardiac myocytes. Annu Rev Physiol 70:23-49.

Boengler K. 2009. Stimulation of cardiac β-adrenoceptors targets connexin 43. Br J Pharmacol 158(1):195-7.

Bosch M, Castro J, Saneyoshi T, Matsuno H, Sur M, Hayashi Y. 2014. Structural and molecular remodeling of dendritic spine substructures during long-term potentiation. Neuron 82(2):444-59.

Bovo E, Dvornikov AV, Mazurek SR, de Tombe PP, Zima AV. 2013. Mechanisms of Ca(2)+ handling in zebrafish ventricular myocytes. Pflugers Arch 465(12):1775-84.

Brand M, Granato M, Nüsslein-Volhard C. 2002. Zebrafish : A Practical Approach. Oxford: Oxford University Press.

Brette F, Orchard C. 2003. T-tubule function in mammalian cardiac myocytes. Circ Res 92(11):1182-92.

Bugiel I, König K, Wabnitz H. 1989. Investigation of cells by fluorescence laser scanning microscopy with subnanosecond time resolution. Lasers in the Life Sciences.

Bui AL, Horwich TB, Fonarow GC. 2011. Epidemiology and risk profile of heart failure. Nat Rev Cardiol 8(1):30-41.

Chen T-W, Wardill TJ, Sun Y, Pulver SR, Renninger SL, Baohan A, Schreiter ER, Kerr RA, Orger MB, Jayaraman V and others. 2013. Ultrasensitive fluorescent proteins for imaging neuronal activity. Nature 499:295-300.

Chistiakov DA, Orekhov AN, Bobryshev YV. 2016. The role of cardiac fibroblasts in post-myocardial heart tissue repair. Exp Mol Pathol 101(2):231-240.

Cline J, Braman JC, Hogrefe HH. 1996. PCR fidelity of pfu DNA polymerase and other thermostable DNA polymerases. Nucleic Acids Res 24(18):3546-51.

Coutts CA, Balt LN, Ali DW. 2009. Protein kinase A modulates A-type potassium currents of larval zebrafish (Danio rerio) white muscle fibres. Acta Physiol (Oxf) 195(2):259-72.

Di Benedetto G, Zoccarato A, Lissandron V, Terrin A, Li X, Houslay MD, Baillie GS, Zaccolo M. 2008. Protein kinase A type I and type II define distinct intracellular signaling compartments. Circ Res 103(8):836-44.

Feil R, Lohmann SM, de Jonge H, Walter U, Hofmann F. 2003. Cyclic GMP-dependent protein kinases and the cardiovascular system: insights from genetically modified mice. Circ Res 93(10):907-16.

Fu Q, Kim S, Soto D, De Arcangelis V, DiPilato L, Liu S, Xu B, Shi Q, Zhang J, Xiang YK. 2014. A long lasting beta1 adrenergic receptor stimulation of cAMP/protein kinase A (PKA) signal in cardiac myocytes. J Biol Chem 289(21):14771-81.

Gao T, Puri TS, Gerhardstein BL, Chien AJ, Green RD, Hosey MM. 1997. Identification and subcellular localization of the subunits of L-type calcium channels and adenylyl cyclase in cardiac myocytes. J Biol Chem 272(31):19401-7.

Gee KR, Brown KA, Chen WN, Bishop-Stewart J, Gray D, Johnson I. 2000. Chemical and physiological characterization of fluo-4 Ca(2+)-indicator dyes. Cell Calcium 27(2):97-106.

Götz KR, Sprenger JU, Perera RK, Steinbrecher JH, Lehnart SE, Kuhn M, Gorelik J, Balligand JL, Nikolaev VO. 2014. Transgenic mice for real-time visualization of cGMP in intact adult cardiomyocytes. Circ Res 114(8):1235-45.

Haj Slimane Z, Bedioune I, Lechêne P, Varin A, Lefebvre F, Mateo P, Domergue-Dupont V, Dewenter M, Richter W, Conti M and others. 2014. Control of cytoplasmic and nuclear protein kinase A by phosphodiesterases and phosphatases in cardiac myocytes. Cardiovasc Res 102(1):97-106.

Hoffmann LS, Chen HH. 2014. cGMP: transition from bench to bedside: a report of the 6th International Conference on cGMP Generators, Effectors and Therapeutic Implications. Naunyn Schmiedebergs Arch Pharmacol 387(8):707-18.

Holz GG, Kang G, Harbeck M, Roe MW, Chepurny OG. 2006. Cell physiology of cAMP sensor Epac. J Physiol 577(Pt 1):5-15.

Huang CJ, Tu CT, Hsiao CD, Hsieh FJ, Tsai HJ. 2003. Germ-line transmission of a myocardium-specific GFP transgene reveals critical regulatory elements in the cardiac myosin light chain 2 promoter of zebrafish. Dev Dyn 228(1):30-40.

Jalife J, Morley GE, Vaidya D. 1999. Connexins and impulse propagation in the mouse heart. J Cardiovasc Electrophysiol 10(12):1649-63.

Jou CJ, Spitzer KW, Tristani-Firouzi M. 2010. blebbistatin effectively uncouples the excitation-contraction process in zebrafish embryonic heart. Cell Physiol Biochem 25(4-5):419-24.

Kawakami K. 2005. Transposon tools and methods in zebrafish. Dev Dyn 234(2):244-54.

Kawakami K, Asakawa K, Muto A, Wada H. 2016. Tol2-mediated transgenesis, gene trapping, enhancer trapping, and Gal4-UAS system. Methods Cell Biol 135:19-37.

Kawakami K, Shima A, Kawakami N. 2000. Identification of a functional transposase of the Tol2 element, an Ac-like element from the Japanese medaka fish, and its transposition in the zebrafish germ lineage. Proc Natl Acad Sci U S A 97(21):11403-8.

Konantz J, Antos CL. 2014. Reverse genetic morpholino approach using cardiac ventricular injection to transfect multiple difficult-to-target tissues in the zebrafish larva. J Vis Exp(88).

Landa LR, Harbeck M, Kaihara K, Chepurny O, Kitiphongspattana K, Graf O, Nikolaev VO, Lohse MJ, Holz GG, Roe MW. 2005. Interplay of Ca2+ and cAMP signaling in the insulin-secreting MIN6 beta-cell line. J Biol Chem 280(35):31294-302.

Lee DY, Kim E, Choi MH. 2015. Technical and clinical aspects of cortisol as a biochemical marker of chronic stress. BMB Rep 48(4):209-16.

Lee S, Vinegoni C, Feruglio PF, Fexon L, Gorbatov R, Pivoravov M, Sbarbati A, Nahrendorf M, Weissleder R. 2012. Real-time in vivo imaging of the beating mouse heart at microscopic resolution. Nat Commun 3:1054.

Leroy J, Abi-Gerges A, Nikolaev VO, Richter W, Lechêne P, Mazet JL, Conti M, Fischmeister R, Vandecasteele G. 2008. Spatiotemporal dynamics of beta-adrenergic cAMP signals and L-type Ca2+ channel regulation in adult rat ventricular myocytes: role of phosphodiesterases. Circ Res 102(9):1091-100.

Li C, Meng Q, Yu X, Jing X, Xu P, Luo D. 2012. Regulatory effect of connexin 43 on basal Ca2+ signaling in rat ventricular myocytes. PLoS One 7(4):e36165.

Magda F, Toon vV, Jacques B, Harold vR. 2012. Functional consequences of abnormal Cx43 expression in the heart ☆. 1818(8):2020–2029.

McConkey DJ, Orrenius S. 1997. The role of calcium in the regulation of apoptosis. Biochem Biophys Res Commun 239(2):357-66.

Mies F, Spriet C, Héliot L, Sariban-Sohraby S. 2007. Epithelial Na+ channel stimulation by n-3 fatty acids requires proximity to a membrane-bound A-kinase-anchoring protein complexed with protein kinase A and phosphodiesterase. J Biol Chem 282(25):18339-47.

Mika D, Leroy J, Vandecasteele G, Fischmeister R. 2012a. PDEs create local domains of cAMP signaling. J Mol Cell Cardiol 52(2):323-9.

Mika D, Leroy J, Vandecasteele G, Fischmeister R. 2012b. [Role of cyclic nucleotide phosphodiesterases in the cAMP compartmentation in cardiac cells]. Biol Aujourdhui 206(1):11-24.

Mironov SL, Skorova E, Taschenberger G, Hartelt N, Nikolaev VO, Lohse MJ, Kügler S. 2009. Imaging cytoplasmic cAMP in mouse brainstem neurons. BMC Neurosci 10:29.

Mongillo M, McSorley T, Evellin S, Sood A, Lissandron V, Terrin A, Huston E, Hannawacker A, Lohse MJ, Pozzan T and others. 2004. Fluorescence resonance energy transfer-based analysis of cAMP dynamics in live neonatal rat cardiac myocytes reveals distinct functions of compartmentalized phosphodiesterases. Circ Res 95(1):67-75.

Murray KN, Dreska M, Nasiadka A, Rinne M, Matthews JL, Carmichael C, Bauer J, Varga ZM, Westerfield M. 2011. Transmission, diagnosis, and recommendations for control of Pseudoloma neurophilia infections in laboratory zebrafish (Danio rerio) facilities. Comp Med 61(4):322-9.

Nemtsas P, Wettwer E, Christ T, Weidinger G, Ravens U. 2010. Adult zebrafish heart as a model for human heart? An electrophysiological study. J Mol Cell Cardiol 48(1):161-71.

Nikolaev VO, Bünemann M, Hein L, Hannawacker A, Lohse MJ. 2004. Novel single chain cAMP sensors for receptor-induced signal propagation. J Biol Chem 279(36):37215-8.

Nikolaev VO, Bünemann M, Schmitteckert E, Lohse MJ, Engelhardt S. 2006. Cyclic AMP imaging in adult cardiac myocytes reveals far-reaching beta1-adrenergic but locally confined beta2-adrenergic receptor-mediated signaling. Circ Res 99(10):1084-91.

Nikolaev VO, Lohse MJ. 2006. Monitoring of cAMP synthesis and degradation in living cells. Physiology (Bethesda) 21:86-92.

Nikolaev VO, Moshkov A, Lyon AR, Miragoli M, Novak P, Paur H, Lohse MJ, Korchev YE, Harding SE, Gorelik J. 2010. Beta2-adrenergic receptor redistribution in heart failure changes cAMP compartmentation. Science 327(5973):1653-7.

Nishikimi T, Maeda N, Matsuoka H. 2006. The role of natriuretic peptides in cardioprotection. Cardiovasc Res 69(2):318-28.

Oni-Orisan A, Lanfear DE. 2014. Pharmacogenomics in heart failure: where are we now and how can we reach clinical application? Cardiol Rev 22(5):193-8.

Pelet S, Previte MJ, So PT. 2006. Comparing the quantification of Forster resonance energy transfer measurement accuracies based on intensity, spectral, and lifetime imaging. J Biomed Opt 11(3):34017.

Perera RK, Sprenger JU, Steinbrecher JH, Hübscher D, Lehnart SE, Abesser M, Schuh K, El-Armouche A, Nikolaev VO. 2015. Microdomain switch of cGMP-regulated phosphodiesterases leads to ANP-induced augmentation of β-adrenoceptor-stimulated contractility in early cardiac hypertrophy. Circ Res 116(8):1304-11.

Piston DW, Dickinson ME, Davidson MW. 2016. FRET Microscopy with Spectral Imaging. Zeiss Microscopy.

Ponsioen B, Zhao J, Riedl J, Zwartkruis F, van der Krogt G, Zaccolo M, Moolenaar WH, Bos JL, Jalink K. 2004. Detecting cAMP-induced Epac activation by fluorescence resonance energy transfer: Epac as a novel cAMP indicator. EMBO Rep 5(12):1176-80.

Röder IV, Lissandron V, Martin J, Petersen Y, Di Benedetto G, Zaccolo M, Rudolf R. 2009. PKA microdomain organisation and cAMP handling in healthy and dystrophic muscle in vivo. Cell Signal 21(5):819-26.

Shinde AV, Frangogiannis NG. 2014. Fibroblasts in myocardial infarction: a role in inflammation and repair. J Mol Cell Cardiol 70:74-82.

Shuhaibar LC, Egbert JR, Norris RP, Lampe PD, Nikolaev VO, Thunemann M, Wen L, Feil R, Jaffe LA. 2015. Intercellular signaling via cyclic GMP diffusion through gap junctions restarts meiosis in mouse ovarian follicles. Proc Natl Acad Sci U S A 112(17):5527-32.

Sperelakis N. 1994. Regulation of calcium slow channels of heart by cyclic nucleotides and effects of ischemia. Adv Pharmacol 31:1-24.

Sprenger JU, Perera RK, Steinbrecher JH, Lehnart SE, Maier LS, Hasenfuss G, Nikolaev VO. 2015. In vivo model with targeted cAMP biosensor reveals changes in receptor-microdomain communication in cardiac disease. Nat Commun 6:6965.

Stangherlin A, Gesellchen F, Zoccarato A, Terrin A, Fields LA, Berrera M, Surdo NC, Craig MA, Smith G, Hamilton G and others. 2011. cGMP signals modulate cAMP levels in a compartment-specific manner to regulate catecholamine-dependent signaling in cardiac myocytes. Circ Res 108(8):929-39.

Stangherlin A, Zaccolo M. 2012. cGMP-cAMP interplay in cardiac myocytes: a local affair with far-reaching consequences for heart function. Biochem Soc Trans 40(1):11-4.

Steele SL, Yang X, Debiais-Thibaud M, Schwerte T, Pelster B, Ekker M, Tiberi M, Perry SF. 2011. In vivo and in vitro assessment of cardiac beta-adrenergic receptors in larval zebrafish (Danio rerio). J Exp Biol 214(Pt 9):1445-57.

Suster ML, Kikuta H, Urasaki A, Asakawa K, Kawakami K. 2009. Transgenesis in zebrafish with the tol2 transposon system. Methods Mol Biol 561:41-63.

Thunemann M, Fomin N, Krawutschke C, Russwurm M, Feil R. 2013a. Visualization of cGMP with cGi biosensors. Methods Mol Biol 1020:89-120.

Thunemann M, Wen L, Hillenbrand M, Vachaviolos A, Feil S, Ott T, Han X, Fukumura D, Jain RK, Russwurm M and others. 2013b. Transgenic mice for cGMP imaging. Circ Res 113(4):365-71.

Tran S, Chatterjee D, Gerlai R. 2014. Acute net stressor increases whole-body cortisol levels without altering whole-brain monoamines in zebrafish. Behav Neurosci 128(5):621-4.

Trautmann S, Buschmann V, Orthaus S, Koberling F, Ortmann U, Erdmann R. 2013. Fluorescence Lifetime Imaging (FLIM) in Confocal Microscopy Applications: An Overview. Berlin: PicoQuant GmbH.

Vandecasteele G, Rochais F, Abi-Gerges A, Fischmeister R. 2006. Functional localization of cAMP signalling in cardiac myocytes. Biochem Soc Trans 34(Pt 4):484-8.

Venkataraman R, Holcomb MR, Harder R, Knollmann BC, Baudenbacher F. 2012. Ratiometric imaging of calcium during ischemia-reperfusion injury in isolated mouse hearts using Fura-2. Biomed Eng Online 11:39.

Verkerk AO, Remme CA. 2012. Zebrafish: a novel research tool for cardiac (patho)electrophysiology and ion channel disorders. Front Physiol 3:255.

Wachter SB, Gilbert EM. 2012. Beta-adrenergic receptors, from their discovery and characterization through their manipulation to beneficial clinical application. Cardiology 122(2):104-12.

Walker MA, Williams GS, Kohl T, Lehnart SE, Jafri MS, Greenstein JL, Lederer WJ, Winslow RL. 2014. Superresolution modeling of calcium release in the heart. Biophys J 107(12):3018-29.

Wallukat G. 2002. The beta-adrenergic receptors. Herz 27(7):683-90.

Weber M, Huisken J. 2015. In vivo imaging of cardiac development and function in zebrafish using light sheet microscopy. Swiss Med Wkly 145:w14227.

Weber S, Meyer-Roxlau S, Wagner M, Dobrev D, El-Armouche A. 2015. Counteracting Protein Kinase Activity in the Heart: The Multiple Roles of Protein Phosphatases. Front Pharmacol 6:270.

Westermann BA, Meissl H. 2008. Nitric oxide synthase in photoreceptive pineal organs of fish. Comp Biochem Physiol A Mol Integr Physiol 151(2):198-204.

Wilson JM, Bunte RM, Carty AJ. 2009. Evaluation of rapid cooling and tricaine methanesulfonate (MS222) as methods of euthanasia in zebrafish (Danio rerio). J Am Assoc Lab Anim Sci 48(6):785-9.

Yang J, Drazba JA, Ferguson DG, Bond M. 1998. A-kinase anchoring protein 100 (AKAP100) is localized in multiple subcellular compartments in the adult rat heart. J Cell Biol 142(2):511-22.

Zaccolo M. 2006. Phosphodiesterases and compartmentalized cAMP signalling in the heart. Eur J Cell Biol 85(7):693-7.

Zaccolo M, Magalhães P, Pozzan T. 2002. Compartmentalisation of cAMP and Ca(2+) signals. Curr Opin Cell Biol 14(2):160-6.

Zaccolo M, Movsesian MA. 2007. cAMP and cGMP signaling cross-talk: role of phosphodiesterases and implications for cardiac pathophysiology. Circ Res 100(11):1569-78.

Zaccolo M, Pozzan T. 2002. Discrete microdomains with high concentration of cAMP in stimulated rat neonatal cardiac myocytes. Science 295(5560):1711-5.

Zhao CY, Greenstein JL, Winslow RL. 2016. Roles of phosphodiesterases in the regulation of the cardiac cyclic nucleotide cross-talk signaling network. J Mol Cell Cardiol 91:215-27.

14. ERKLÄRUNGEN

14.1 ERÖFFNUNG DES PROMOTIONSVERFAHRENS

1. Hiermit versichere ich, dass ich die vorliegende Arbeit ohne unzulässige Hilfe Dritter und ohne Benutzung anderer als der angegebenen Hilfsmittel angefertigt habe; die aus fremden Quellen direkt oder indirekt übernommenen Gedanken sind als solche kenntlich gemacht.

2. Bei der Auswahl und Auswertung des Materials sowie bei der Herstellung des Manuskripts habe ich Unterstützungsleistungen von folgenden Personen erhalten:

   - Prof. Dr. Antos, PhD
   - Prof. Dr. med. Ali El-Armouche

3. Weitere Personen waren an der geistigen Herstellung der vorliegenden Arbeit nicht beteiligt. Insbesondere habe ich nicht die Hilfe eines kommerziellen Promotionsberaters in Anspruch genommen. Dritte haben von mir weder unmittelbar noch mittelbar geldwerte Leistungen für Arbeiten erhalten, die im Zusammenhang mit dem Inhalt der vorgelegten Dissertation stehen.

4. Die Arbeit wurde bisher weder im Inland noch im Ausland in gleicher oder ähnlicher Form einer anderen Prüfungsbehörde vorgelegt.

5. Die Inhalte dieser Dissertation wurden in folgender Form veröffentlicht:

   Als **Präsentation** im Rahmen des Seminars “Biopolis Dresden Imaging Platform (BioDIP) Winter Seminar on FLIM - Fluorescence Lifetime Imaging Microscopy” im Max-Planck-Institut für molekulare Zellbiologie und Genetik am 17.01.2017

6. Ich bestätige, dass es keine zurückliegenden erfolglosen Promotionsverfahren gab.

7. Ich bestätige, dass ich die Promotionsordnung der Medizinischen Fakultät der Technischen Universität Dresden anerkenne.

8. Ich habe die Zitierrichtlinien für Dissertationen an der Medizinischen Fakultät der Technischen Universität Dresden zur Kenntnis genommen und befolgt.

14 Erklärungen

Dresden, den

(Julia Annika Janßen)

14.2 Einhaltung der aktuellen gesetzlichen Vorgaben im Rahmen der Dissertation

Hiermit bestätige ich die Einhaltung der folgenden aktuellen gesetzlichen Vorgaben im Rahmen meiner Dissertation:

1. Das zustimmende Votum der Ethikkommission bei Klinischen Studien, epidemiologischen Untersuchungen mit Personenbezug oder Sachverhalten, die das Medizinproduktegesetz betreffen:
   Aktenzeichen der zuständigen Ethikkommission: **entfällt**

2. Die Einhaltung der Bestimmungen des Tierschutzgesetzes:
   Aktenzeichen der Genehmigungsbehörde zum Vorhaben/zur Mitwirkung: **entfällt**

3. Die Einhaltung des Gentechnikgesetzes
   Projektnummer: **AZ.: 55-8811.72/46**

4. Die Einhaltung von Datenschutzbestimmungen der Medizinischen Fakultät und des Universitätsklinikums Carl Gustav Carus.

Dresden, den

(Julia Annika Janßen)

17. SUPPLEMENT

17.1 EPAC1-CAMPS CLONING

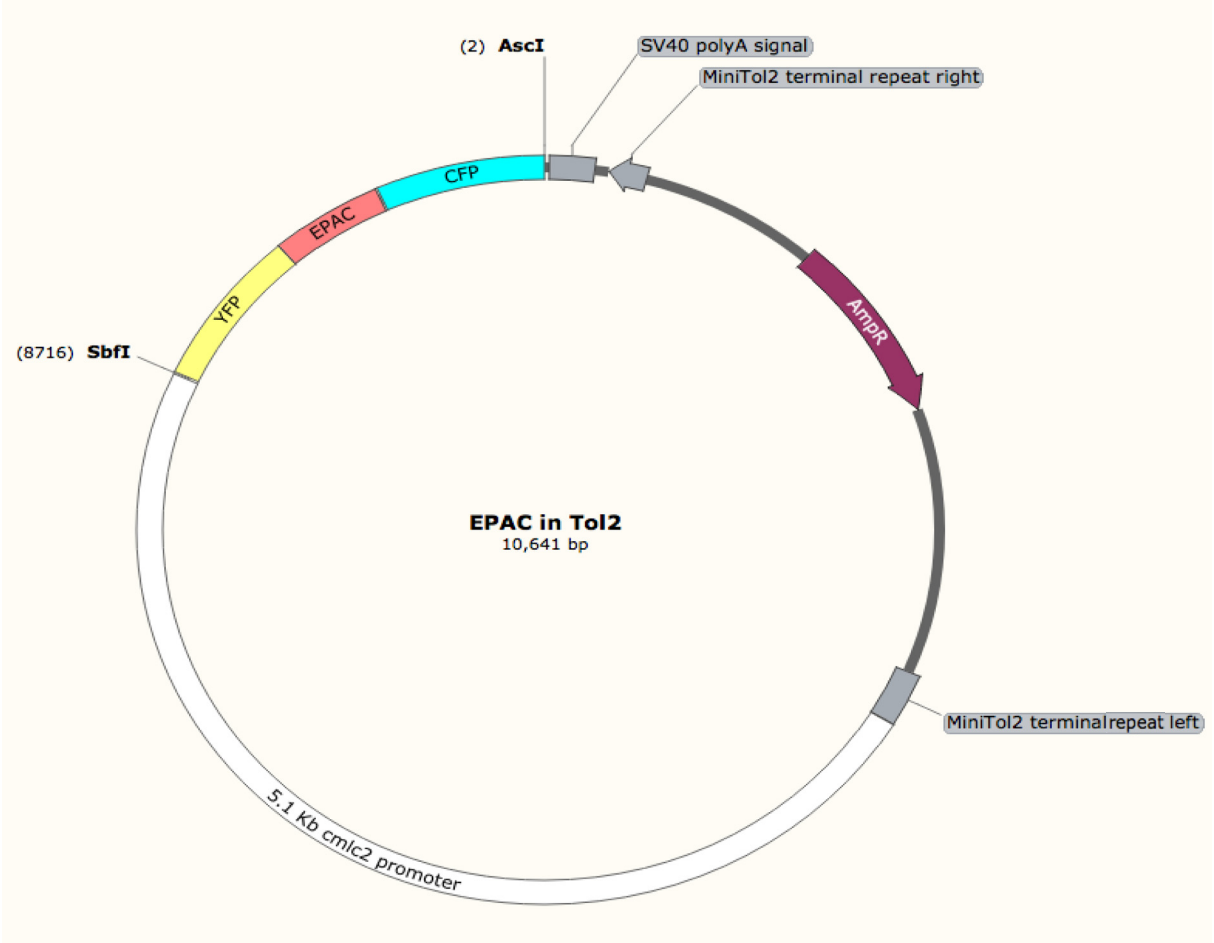

Figure 17.1 The EPAC1-camps gene in the Tol2 vector

The double stranded DNA plasmid with the fluorescent sensor for cAMP, EPAC1-camps, is shown. The EPAC1-camps gene consists of a cAMP binding site, which is labeled “EPAC” and indicated in red. The FRET-fluorophores (yellow for CFP, blue for YFP) are located left and right from EPAC. EPAC1-camps is embedded by the restriction sites used for cloning, SbfI and AscI. The cmlc2 promoter in front of EPAC1-camps ensures cardiomyocyte-specific expression. The two grey MiniTol2 sites define the area in between which is incorporated to the zebrafish when injected into the one-cell stage fertilized embryo. EPAC1-camps is equipped with a PolyA signal, which is important for nuclear export and translation of the protein. The Ampicillin resistance, labeled in dark red, is important for the cloning process. The Ampicillin resistance ensures, that only bacteria carrying the plasmid grow during ampicillin treatment.

The DNA sequence of the EPAC1-camps gene in the Tol2 vector

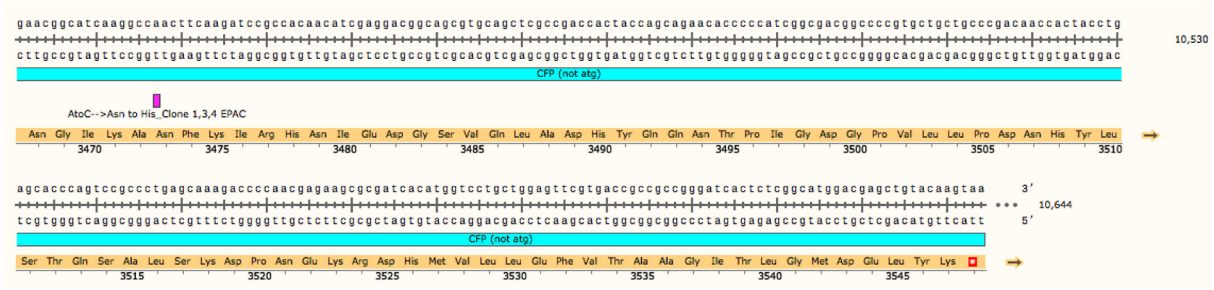

Figure 17.2 The DNA sequence of the EPAC1-camps gene in the Tol2 vector

The DNA sequence of EPAC1-camps in the Tol2 vector is shown. The EPAC1-camps gene consists of an cAMP binding site, which is labeled “EPAC” and indicated in red. The FRET-fluorophores (yellow for CFP, blue for YFP) are located 5’ and 3’ from EPAC. EPAC1-camps is embedded by the restriction sites used for cloning, SbfI and AscI. The 3 Mutations that the sequencing revealed are marked and explained in purple.

17.2 cGi500 CLONING

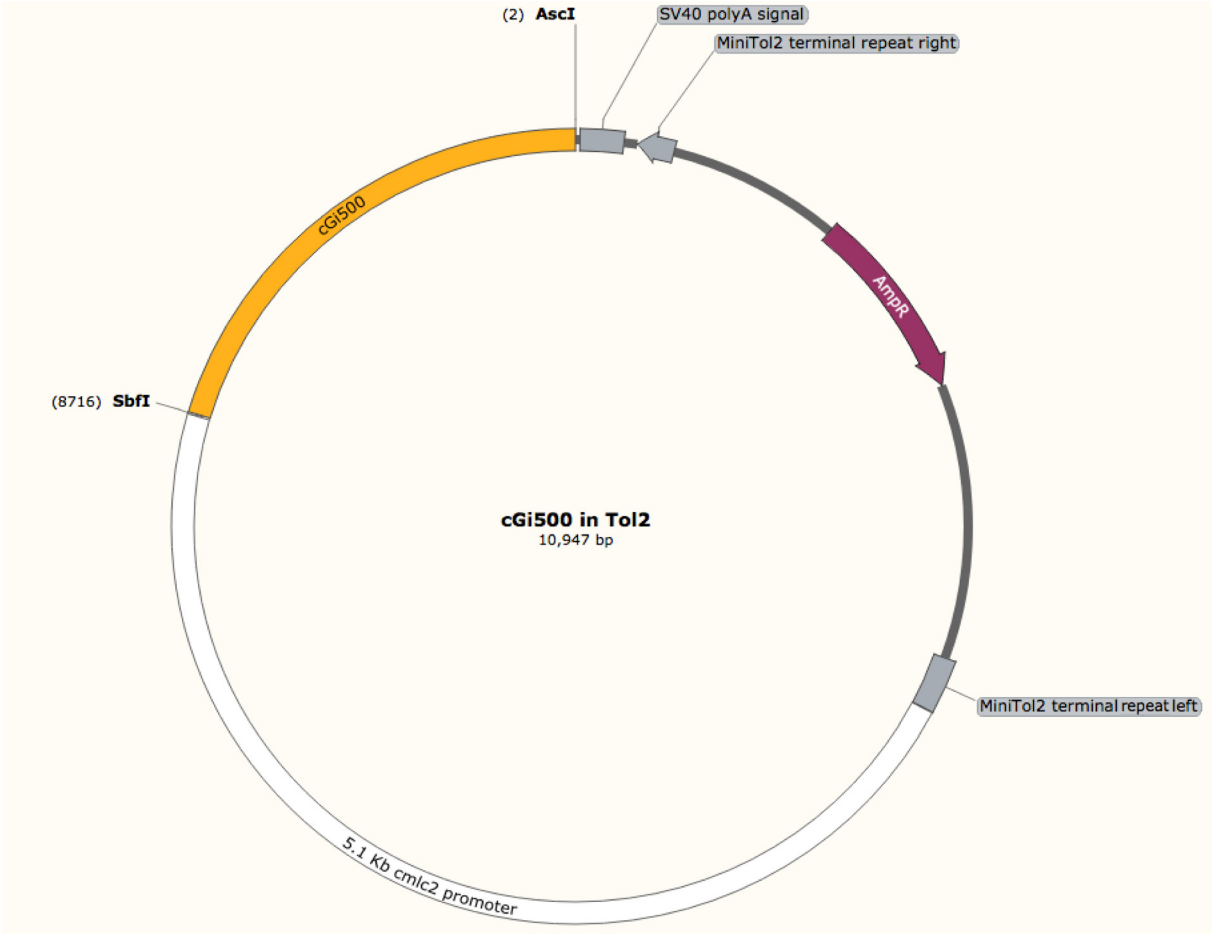

Figure 17.3 The cGi500 gene in the Tol2 vector

The double stranded DNA plasmid with the fluorescent sensor for cGMP, cGi500, is shown. The cGi500 gene is indicated in orange. It is embedded between the restriction sites used for cloning, SbfI and AscI. The cmlc2 promoter in front of cGi500 ensures cardiomyocyte-specific expression. The two grey MiniTol2 sites define the area in between which is incorporated to the zebrafish when injected into the one-cell stage fertilized embryo. cGi500 is provided with a PolyA signal, which is important for nuclear export and translation of the protein. The Ampicillin resistance, labelled in dark red, is important for the cloning process.

The DNA sequence of the cGi500 gene in the Tol2 vector

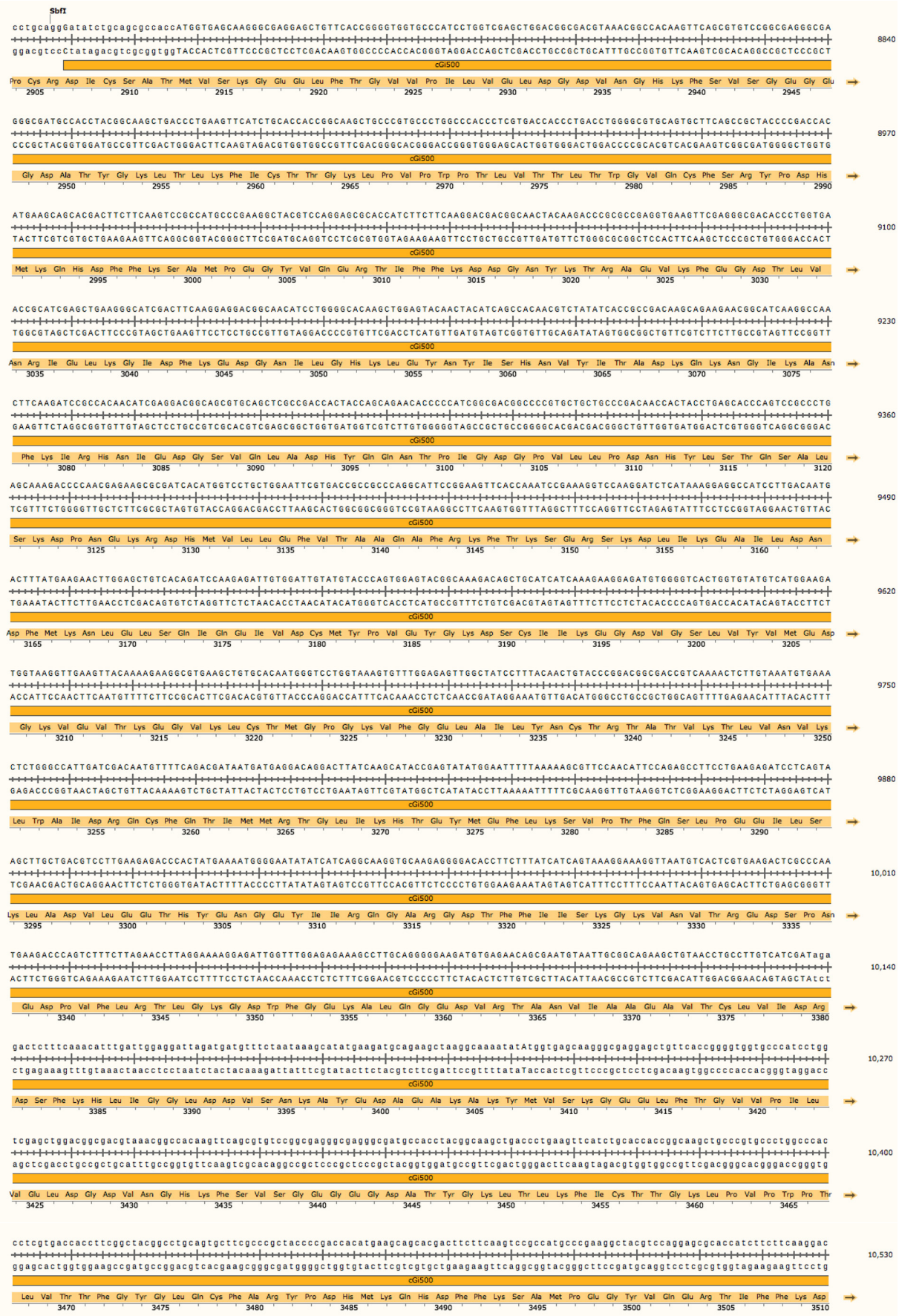

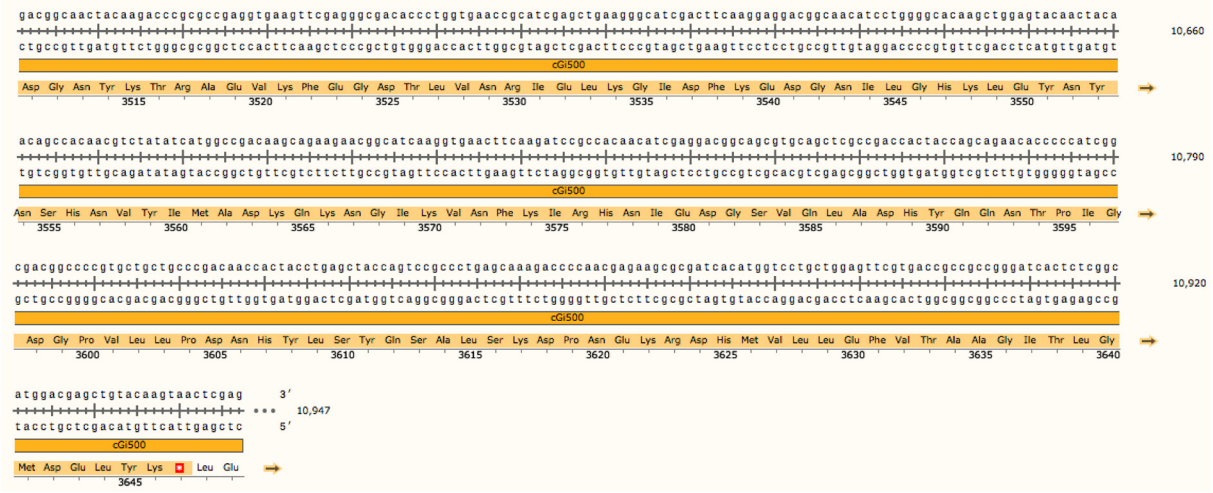

Figure 17.4 The DNA sequence of the cGi500 gene in the Tol2 vector

The DNA sequence of cGi500 in the Tol2 vector is shown. The cGi500 gene is embedded between the restriction sites used for cloning, SbfI and AscI. The sequencing did not reveal any mutations.

17.3 GCaMP6F CLONING

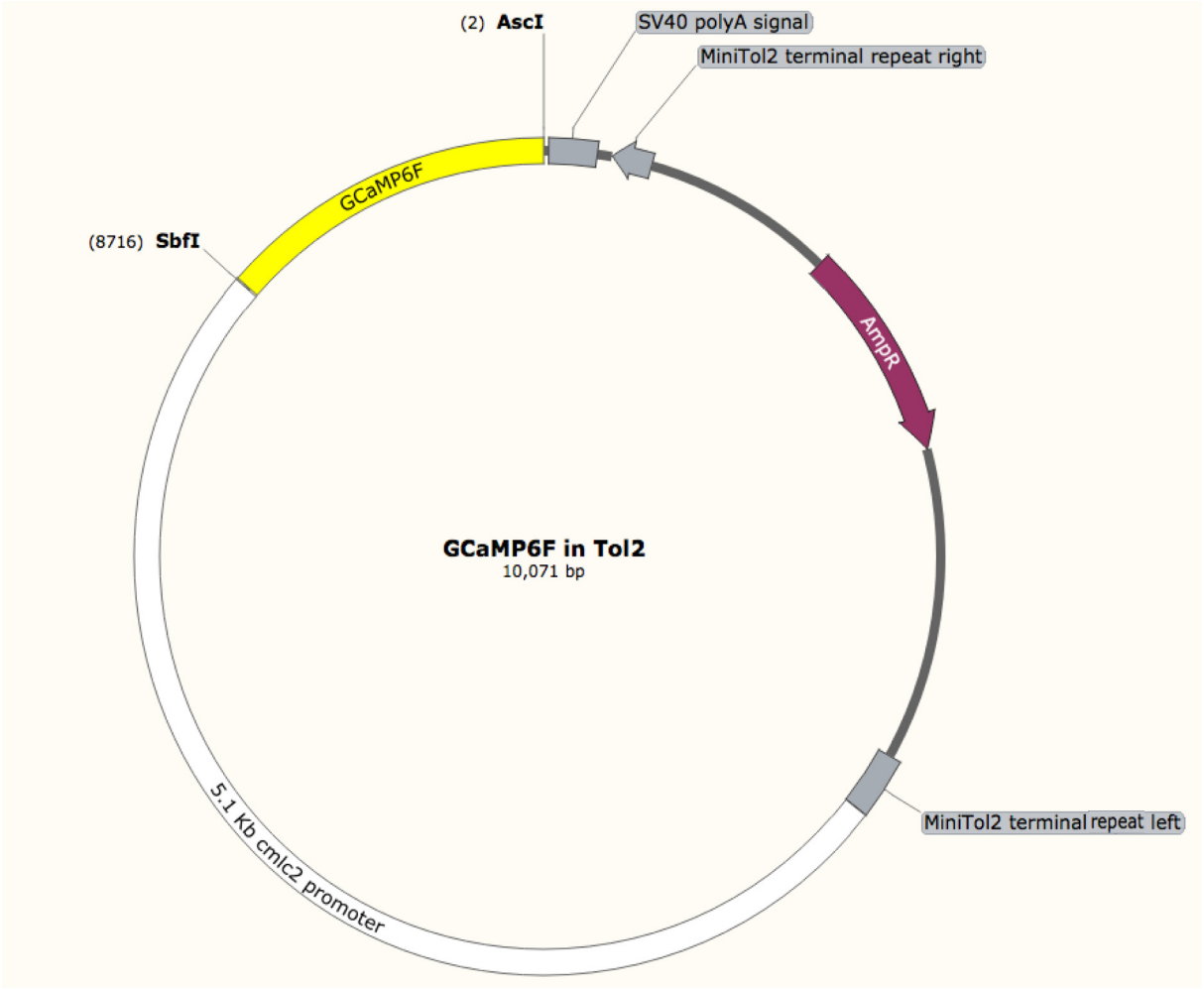

Figure 17.5 The GCaMP6F gene in the Tol2 vector

The double stranded DNA plasmid with the fluorescent sensor for Ca^{2+}, GCaMP6F, is shown. The GCaMP6F gene is indicated in yellow. It is embedded by the restriction sites used for cloning, SbfI and AscI. The cmlc2 promoter in front of GCaMP6F ensures cardiomyocyte-specific expression. The two grey MiniTol2 sites define the area in between which is incorporated to the zebrafish when injected into the one-cell stage fertilized embryo. GCaMP6F is equipped with a PolyA signal, which is important for nuclear export and translation of the protein. The Ampicillin resistance, labelled in dark red, is important for the cloning process.

The DNA sequence of the GCaMP6F gene in the Tol2 vector

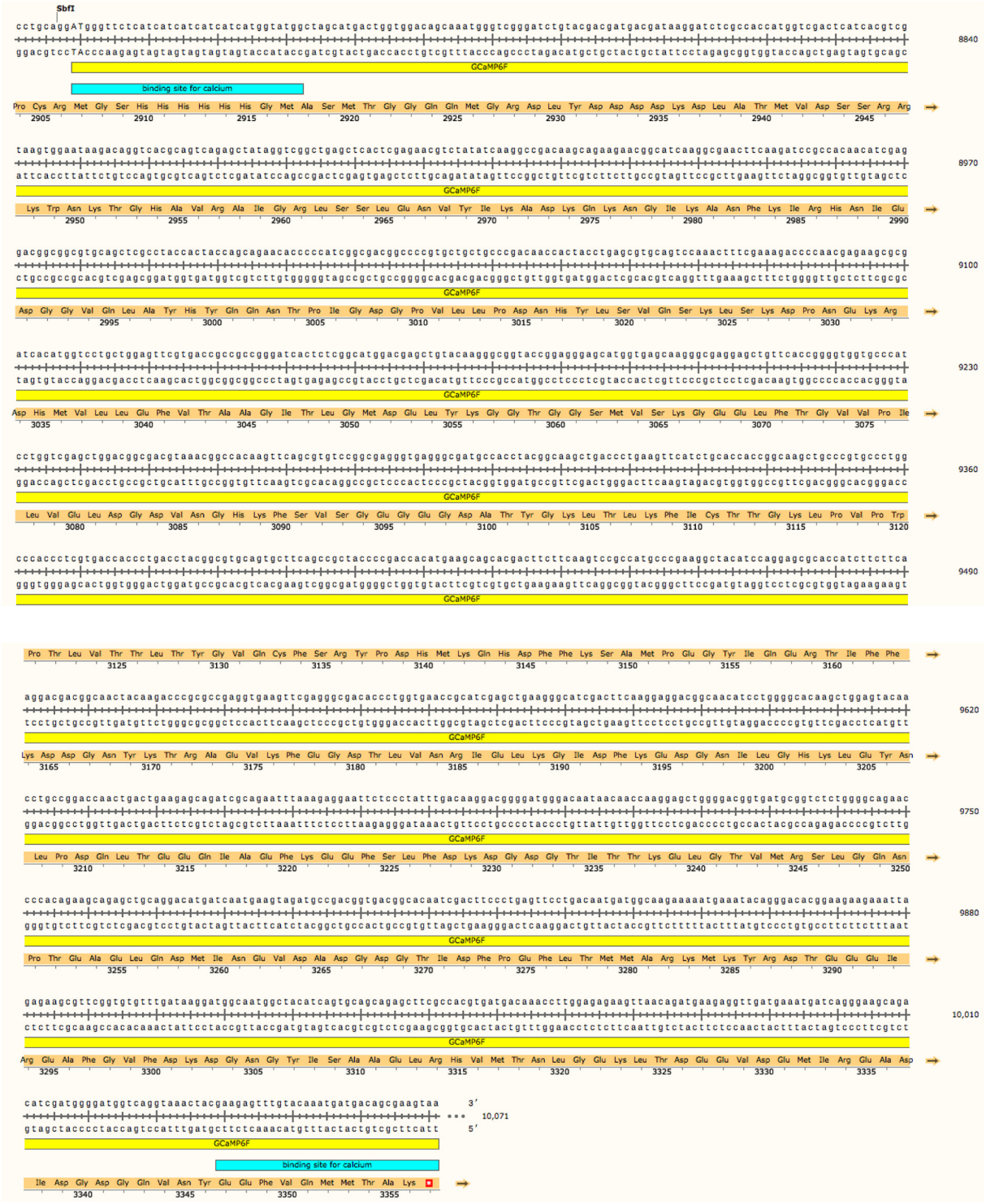

Figure 17.6 The DNA sequence of the GCaMP6F gene in the Tol2 vector

The DNA sequence of GCaMP6F in the Tol2 vector is shown. The GCaMP6F gene is embedded between the restriction sites used for cloning, SbfI and AscI. The sequencing did not reveal any mutations.

17.4 THE DIFFERENT DNA INJECTION CONCENTRATIONS AND THEIR EFFECT ON THE FISH

EPAC1-camps

100ng fish expressing	100ng dead fish	200ng fish expressing	200ng dead fish	250ng fish expressing	250ng dead fish	300ng fish expressing	300ng dead fish
0.10	0.08	0.21	0.10	0.45	0.10	0.40	0.40
0.12	0.09	0.39	0.20	0.44	0.21	0.32	0.50
0.09	0.04	0.15	0.15	0.32	0.15	0.17	0.44
0.05	0.12	0.26	0.18	0.27	0.14	0.50	0.70
0.16	0.04	0.19	0.08	0.12	0.09	0.22	0.54
0.06	0.07	0.20	0.17	0.33	0.11	0.24	0.48

cGi500

100ng fish expressing	100ng dead fish	200ng fish expressing	200ng dead fish	250ng fish expressing	250ng dead fish	300ng fish expressing	300ng dead fish
0.10	0.08	0.21	0.10	0.45	0.10	0.40	0.40
0.12	0.09	0.39	0.20	0.44	0.21	0.32	0.50
0.09	0.04	0.15	0.15	0.32	0.15	0.17	0.44
0.05	0.12	0.26	0.18	0.27	0.14	0.50	0.70
0.16	0.04	0.19	0.08	0.12	0.09	0.22	0.54
0.06	0.07	0.20	0.17	0.33	0.11	0.24	0.48

GCaMP6

100ng fish expressing	100ng dead fish	200ng fish expressing	200ng dead fish	250ng fish expressing	250ng dead fish	300ng fish expressing	300ng dead fish
0.07	0.12	0.15	0.14	0.22	0.34	0.43	0.21
0.08	0.09	0.19	0.18	0.21	0.21	0.33	0.34
0.05	0.05	0.24	0.11	0.28	0.27	0.29	0.33
0.09	0.11	0.22	0.19	0.16	0.26	0.22	0.17
0.10	0.04	0.10	0.27	0.29	0.18	0.34	0.15
0.05	0.18	0.04	0.22	0.34	0.37	0.40	0.18